

See discussions, stats, and author profiles for this publication at: <https://www.researchgate.net/publication/231707987>

Relaxational Dynamics of a Random Heteropolymer

ARTICLE *in* MACROMOLECULES · MAY 1997

Impact Factor: 5.8 · DOI: 10.1021/ma961162b

CITATIONS

6

READS

11

3 AUTHORS, INCLUDING:



Martin J Zuckermann

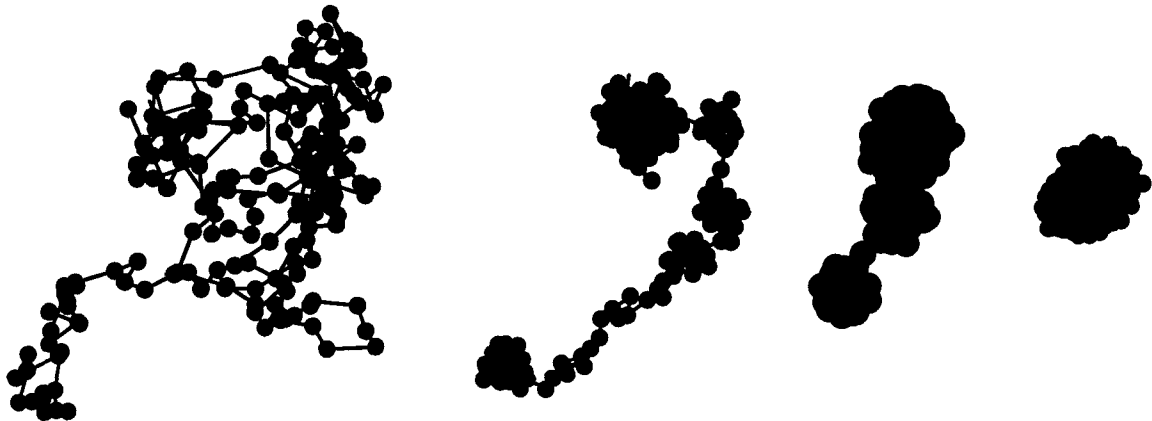
Simon Fraser University

245 PUBLICATIONS 6,282 CITATIONS

SEE PROFILE

Relaxational Dynamics of Random Heteropolymers

Christine Villeneuve
Centre for the Physics of Materials
Department of Physics, McGill University
Montréal, Québec



A Thesis submitted to the
Faculty of Graduate Studies and Research
in partial fulfillment of the requirements for the degree of
Doctor of Philosophy



National Library
of Canada

Acquisitions and
Bibliographic Services

395 Wellington Street
Ottawa ON K1A 0N4
Canada

Bibliothèque nationale
du Canada

Acquisitions et
services bibliographiques

395, rue Wellington
Ottawa ON K1A 0N4
Canada

Your file Votre référence

Our file Notre référence

The author has granted a non-exclusive licence allowing the National Library of Canada to reproduce, loan, distribute or sell copies of this thesis in microform, paper or electronic formats.

The author retains ownership of the copyright in this thesis. Neither the thesis nor substantial extracts from it may be printed or otherwise reproduced without the author's permission.

L'auteur a accordé une licence non exclusive permettant à la Bibliothèque nationale du Canada de reproduire, prêter, distribuer ou vendre des copies de cette thèse sous la forme de microfiche/film, de reproduction sur papier ou sur format électronique.

L'auteur conserve la propriété du droit d'auteur qui protège cette thèse. Ni la thèse ni des extraits substantiels de celle-ci ne doivent être imprimés ou autrement reproduits sans son autorisation.

0-612-78791-5

Canada

*À mamam, papa et frérot,
avec toute ma gratitude.*

CONTENTS

RÉSUMÉ	vii
ABSTRACT	viii
ACKNOWLEDGMENTS	ix
1 INTRODUCTION	1
2 MODELS AND METHODS	7
2.1 Models	7
2.1.1 Hamiltonian	9
2.1.2 Forces	14
2.1.3 Ensemble and boundary conditions	15
2.2 Molecular dynamics methods	18
2.2.1 Langevin dynamics	18
2.2.2 Nosé–Hoover dynamics	21
2.2.3 Physical quantities and parameters	24
3 RANDOM HETEROPOLYMER WITHOUT SOLVENT	32
3.1 Equilibrium considerations	34
3.2 Kinetics of relaxation	37
3.3 Summary	48
4 EQUILIBRIUM STUDY OF A RANDOM HETEROPOLYMER IN SOLVENT	52
4.1 Pure Lennard-Jones solvent	55
4.2 Random monomer-monomer interactions (Model A)	58
4.3 Random monomer-solvent interactions (Model B with a flexible chain)	66
4.4 Effect of chain stiffness (Model B with a semi-flexible chain)	73
4.5 Summary	74
5 COLLAPSE KINETICS OF A RANDOM HETEROPOLYMER IN SOLVENT	79
5.1 Random monomer-monomer interactions (Model A)	83
5.1.1 Temperature–driven random heteropolymer collapse	83
5.1.2 α -driven random heteropolymer collapse	96
5.2 Random monomer–solvent interactions (Model B with a flexible chain)	99
5.3 Effect of chain stiffness (Model B with a semi–flexible chain)	103
5.4 Summary	107
6 DISCUSSION AND CONCLUSION	111
APPENDICES	119
A.1 Langevin equation	119
A.2 Error propagation for t_{50} and t_{90}	128
REFERENCES	130

FIGURES AND TABLES

FIGURES

2.1	Multiple bead–spring model.	9
2.2	Two monomers and a bond modeled by two beads and a spring.	9
2.3	(a) Freely rotating chain and (b) the bending angle.	10
2.4	Lennard–Jones potential.	13
2.5	The random interaction pair potential.	13
3.1	Average radius of gyration versus N for random heteropolymers with (a) $\alpha = 3$ and (b) $\alpha = 6$	36
3.2	T_Θ versus α for $N = 100$	37
3.3	Energy versus time for a random heteropolymer after a temperature quench with parameters $\alpha = 6$, $N = 30$, $T_I = 16$ and $T_F = 10$ (both above the theta point).	39
3.4	Energy as a function of time for a random heteropolymer after a temperature quench with parameters $\alpha = 6$, $N = 100$, $T_I = 16$ (above the theta point) and $T_F = 6$ (below the theta point).	42
3.5	Snapshots of conformations for a random heteropolymer at various times after a temperature quench.	43
3.6	Relaxation curves for quenches across the theta point for $N = 30$	45
3.7	τ as a function $1/\Gamma$	46
3.8	Energy versus time for a random heteropolymer after a temperature quench with parameters $\alpha = 6$, $N = 30$, $T_I = 6$ and $T_F = 4$ (both below the theta point).	47
4.1	Lennard-Jones liquid: (a) P versus ρ for several isotherms. (b) P versus T for several isochores.	56
4.2	Lennard–Jones liquid $P\rho T$ diagram.	57
4.3	$\langle R_{yy}^2 \rangle$ versus T for a Model A type random heteropolymer of length $N = 30$ in an explicit solvent of density (a) $\rho = 0$ for $\alpha = 1, 4, 6$ and (b) $\rho = 0.7$ for $\alpha = 2, 4, 6$	59
4.4	Average number of contacts versus T for a Model A type random heteropolymer of length $N = 30$ in an explicit solvent of density (a) $\rho = 0$ for $\alpha = 1, 4, 6$ and (b) $\rho = 0.7$ for $\alpha = 2, 4, 6$	60
4.5	$\langle R_{yy}^2 \rangle_{coil}$ versus ρ for a Model A type random heteropolymer with $\alpha = 6$ for $N = 30$ and $N = 60$	62
4.6	$\langle R_{yy}^2 \rangle$ versus N for a Model A type random heteropolymer with $\alpha = 6$ in a solvent of density $\rho = 0$ and $\rho = 0.5$	63
4.7	$\varsigma = \frac{\langle R_{yy}^2 \rangle}{6\langle R_{yy}^2 \rangle}$ as a function of solvent density for a Model A type random heteropolymer of length $N = 30$ with $\alpha = 6$	64

4.8	"Phase diagrams" for Model A type random heteropolymer chains of length $N = 30$ with random monomer–monomer interactions and an explicit Lennard–Jones solvent. (a) T_Θ versus α for $\rho = 0$ and $\rho = 0.7$ and (b) T_Θ versus ρ for $\alpha = 6$	65
4.9	Snapshots of conformations of a Model A type random heteropolymer in equilibrium in a solvent of density, $\rho = 0.7$, at various temperatures	67
4.10	$\langle R_{gy}^2 \rangle$ versus T for a Model B flexible random heteropolymer of length $N = 30$ with (a) $\alpha' = 1$ and (b) $\alpha' = 6$	68
4.11	Average number of contacts between monomers versus T for a Model B flexible random heteropolymer of length $N = 30$ with (a) $\alpha' = 1$, and (b) $\alpha' = 6$	69
4.12	Average number of contacts between monomers and solvent particles versus T for a Model B flexible random heteropolymer of length $N = 30$ with (a) $\alpha' = 1$ and (b) $\alpha' = 6$	69
4.13	Snapshots of conformations of a Model B flexible random heteropolymer with $\alpha' = 1$ and $\alpha' = 6$ in equilibrium in a solvent of density $\rho = 0.2$ at $T = 1$	71
4.14	"Phase diagram" for Model B flexible random heteropolymer chains of length $N=30$. T_Θ versus ρ for $\alpha' = 1$ and $\alpha' = 6$	72
4.15	$\langle R_{gy}^2 \rangle$ versus T for a Model B semi–flexible random heteropolymer of length $N = 30$ with $\alpha' = 1$	74
4.16	Average number of contacts between monomers versus T for a Model B semi–flexible random heteropolymer of length $N = 30$ with $\alpha' = 1$. . .	75
4.17	Average number of contacts between monomers and solvent particles versus T for a Model B semi–flexible random heteropolymer of length $N = 30$ with $\alpha' = 1$	75
4.18	"Phase diagrams" for Model B random heteropolymer chains of length $N = 30$. T_Θ versus ρ for $\alpha' = 1$ with and without bending restrictions.	76
5.1	Relaxation curves for a Model A type random heteropolymer with $\alpha = 4$ for various solvent densities: (a) R_{gy} versus t , (b) n_{MM} versus t and (c) T^* versus t	85
5.2	Relaxation curves for a Model A type random heteropolymer with $\alpha = 6$ for various solvent densities: (a) R_{gy} versus t , (b) n_{MM} versus t and (c) T^* versus t	86
5.3	t_{50} and t_{90} as a function of ρ for a Model A type random heteropolymer.	88
5.4	Relaxation curves for a Model A type random heteropolymer at solvent density $\rho = 0$ for various values of α : (a) R_{gy} versus t , (b) n_{MM} versus t , (c) T^* versus t and (d) E versus t	91
5.5	Relaxation curves for a Model A type random heteropolymer at solvent density $\rho = 0.7$ for various values of α : (a) R_{gy} versus t , (b) n_{MM} versus t , (c) T^* versus t and (d) E versus t	92
5.6	Relaxation curves for a Model A type random heteropolymer at solvent density $\rho = 0.9$ for various values of α : (a) R_{gy} versus t , (b) n_{MM} versus t , (c) T^* versus t and (d) E versus t	93
5.7	t_{50} as a function of α for a Model A type random heteropolymer.	94

5.8	t_{90} as a function of α for a Model A type random heteropolymer.	95
5.9	Relaxation curves corresponding to a constant temperature collapse for a Model A type random heteropolymer: (a) R_{yy} versus t , (b) n_{MM} versus t , (c) T^* versus t and (d) E versus t	97
5.10	t_{50} and t_{90} as a function of ρ for the α driven collapse of a Model A type random heteropolymer.	98
5.11	Relaxation curves for a Model B type flexible random heteropolymer: (a) R_{yy} versus t , (b) n_{MM} versus t , (c) T^* versus t and (d) E versus t	100
5.12	t_{50} as a function of ρ for a Model B type flexible random heteropolymer.	101
5.13	t_{90} as a function of ρ for a Model B type flexible random heteropolymer.	101
5.14	Relaxation curves for a Model B type semi-flexible random heteropolymer: (a) R_{yy} versus t , (b) n_{MM} versus t , (c) T^* versus t and (d) E versus t	104
5.15	Comparison of t_{50} as a function of ρ for flexible and semi-flexible chains with random monomer-solvent interactions (Model B).	105
5.16	Comparison of t_{90} as a function of ρ for flexible and semi-flexible chains with random monomer-solvent interactions (Model B).	105

TABLES

3.1	$\langle\beta\rangle$ and $\langle\tau\rangle$ for $N = 30$	41
3.2	$\langle\beta\rangle$ and $\langle\tau\rangle$ for $N = 100$	41
5.1	β and τ for the thermal relaxation of a Model A random heteropolymer with $\alpha = 4$ and $\alpha = 6$	89
5.2	β and τ for the thermal relaxation of a Model A random heteropolymer with $\rho = 0$, $\rho = 0.7$ and $\rho = 0.9$	95
5.3	β and τ for the relaxation of the energy of a Type A random heteropolymer from $\alpha_I = 1$ to $\alpha_F = 6$	98
5.4	β and τ for the thermal relaxation and the relaxation of the energy of a type B flexible random heteropolymer with $\alpha' = 1$	102
5.5	β and τ for the relaxation of the thermostat and the energy of a type B semi-flexible random heteropolymer with $\alpha' = 1$	107

RÉSUMÉ

Nous étudions les propriétés à l'équilibre et la dynamique de relaxation d'hétéopolymères aléatoires en trois dimensions en considérant d'abord un hétéropolymère isolé, c'est-à-dire sans solvant explicite, avant d'étudier différents types d'hétéropolymères dans un solvant. Les données numériques sont obtenues en effectuant des simulations de dynamiques moléculaires hors-réseau. Un "diagramme de phase" est tracé pour chaque système moléculaire, ce qui nous permet de trouver une température caractéristique qui sépare la phase étendue de la phase globulaire. Cette température est une fonction croissante de la force de l'interaction aléatoire ainsi que de la densité de solvant et nous permet de déterminer des températures initiales et finales appropriées pour la trempe d'une conformation étendue à une conformation globulaire. L'écoulement d'un hétéropolymère est un processus en deux régimes temporels distincts, en particulier pour les longues chaînes isolées. C'est deux régimes temporels sont énergétiquement de la forme d'une exponentielle étirée. Nos simulations démontrent la nature du processus de relaxation qui débute par la formation de petits regroupements locaux suivie par l'agrégation globale de ces petits regroupements. Enfin, nous déterminons l'effet d'un solvant explicite sur la dynamique de l'écoulement d'un hétéropolymère aléatoire. Nous comblons l'écart entre un solvant implicite et un solvant explicite en deux étapes. D'abord, nous considérons un hétéropolymère avec une interaction aléatoire entre les monomères en immersion dans un solvant purement répulsif. Nous trouvons que la vitesse d'écoulement augmente avec le force de l'interaction aléatoire mais demeure presqu'indépendante de la densité du solvant pour des valeurs élevées de la force de l'interaction aléatoire. Ensuite, nous examinons un hétéropolymère avec une interaction aléatoire entre les monomères et les particules du solvant et nous observons que la vitesse d'écoulement croît légèrement mais elle est presque constante à faible densité. À densité plus élevée, la tendance change et la vitesse d'écoulement diminue. De plus, lorsqu'une restriction angulaire est ajoutée à la chaîne, une augmentation marquée du temps d'écoulement est observée. Cet effet associé à l'augmentation de la rigidité de la chaîne semble être plus important à des densités plus élevées du solvant car une augmentation de la densité a un effet plus important sur le ralentissement de la dynamique de l'écoulement d'un polymère qui possède des restrictions conformationnelles.

ABSTRACT

We investigate the equilibrium properties and the relaxational dynamics of random heteropolymers in three dimensions. We proceed by studying an isolated random heteropolymer without an explicit solvent before studying different types of random heteropolymers in a monomeric solvent. Both equilibrium and relaxational data were obtained by performing extensive off-lattice molecular dynamics simulations. An equilibrium “phase diagram” is determined in all cases which facilitates the determination of a characteristic temperature separating extended states from collapsed states of the heteropolymer. This temperature is an increasing function of the strength of the random interactions and of the solvent density. It allows us to determine the appropriate initial and final temperatures to be used for the quenches from an extended coil to a collapsed globule. In particular for long isolated chains the heteropolymer collapse is a process which involves two distinct time regimes; both are energetically of stretched exponential form. Our simulation clearly shows the nature of the relaxation process where the formation of locally collapsed clusters takes place first followed by a global aggregation of the local blobs leading to the two collapse time regimes. Finally, we determine the effect of an explicit solvent on the collapse dynamics of a random heteropolymer. We bridge the difference between implicit and explicit solvents in two steps. First, we consider a heteropolymer with random interaction between the monomers, immersed in a purely repulsive solvent and we find that the rate of collapse increases with the strength of the random interaction but remains almost independent of the solvent density for higher values of the strength of the random interaction. Secondly, we look at a random heteropolymer with random interaction between the monomers and the solvent particles and we find that the rate of collapse increases slightly with density but is almost constant at low densities. At higher densities, the trend is reversed and the rate of collapse starts to decrease. Adding a bending restriction to the fully flexible chain results in a marked increase in the collapse time. Furthermore, the effect related to an increased stiffness of the chain seems to be most pronounced at higher solvent density since an increase in the density has a considerably stronger effect on the slowing down of the collapse dynamics of a conformationally restricted polymer chain.

ACKNOWLEDGMENTS

I want to thank Martin Zuckermann and Hong Guo for sticking by me all these years. They never gave up on me even when I was having doubts about being a physicist. When I failed to see anything interesting in my results, Martin and Hong could always point out something that made the effort that I put into the research worthwhile. I also appreciated all their wise suggestions.

During the last two years, I have benefited enormously from the presence of James Polson in the department. He was always a source of good advice and encouragement. I am convinced that he will make an excellent supervisor. He also had the generosity to read my thesis carefully which I greatly appreciated. James and his wife Beth have become good friends and I enjoyed all the social time that I spent with them. I shall miss them. Chris and Mikko have always been there for stimulating discussions. I also thank all my colleagues who have been great office mates, coffee or wine drinking friends and lunch partners.

I am also grateful to Paula, Rachel and Linda for making all the horrible administrative stuff more tolerable. I must mention Martin Lacasse who wrote the nice L^AT_EX package which I used to write my thesis. Juan was an indispensable resource which I used profusely in the past few months. I admire his knowledge, his patience and his kindness. My Ph.D. would have been much more difficult without him. I would also like to thank the NSERC, the Carl Reinhardt Foundation and the Walter C. Sumner Foundation for their financial support over these years.

My family and friends were of great help on a personal level. My parents and my brother always believed in me and were a great source of encouragement. My friend May gave me a lot of support via email. Nicolas rescued me during rough times and brought a lot of happiness to my life. Sonya was an exemplary roommate and a great friend. Lise is the best friend I could ask for. She has shown me that it is possible to have it all; boyfriend, children, friends and career. Julia, my god-child (yes, the one I always talk about), has been a source of constant joy in my life for the past four years. I hope that one day she will be a “lover of science and poetry” (Reeves [93]). The last but not the least, Neil, the man who makes me happy on a daily basis.

Relaxational Dynamics of Random Heteropolymers

... There is a never ending interest
in the definite mathematical problem
of a set of points endowed with inertia
and mutually acting upon one another
with any given force.

Sir William Thomson
Baltimore Lectures on Molecular Dynamics
and the Wave Theory of Light (1884)

INTRODUCTION

It is well known that natural proteins fold into their native structures remarkably easily in spite of the enormous number of possible physical configurations (Creighton [92]; Levinthal [68]). It is believed (Go and Abe [81]; Shakhnovich et al. [91]; Wolynes, Onuchic and Thirumalai [95]) that protein sequences are “optimized” such that there is not only a stable and unique structure for the ground state, but also a funnel-like energy landscape which leads to efficient folding kinetics (Go and Abe [81]; Sali, Shakhnovich and Karplus [94]). A principle of minimal frustration was proposed (Bryngelson and Wolynes [87]) to enforce a selection of the interactions between monomers such that as few energetic conflicts as possible occur and thus folding can take place efficiently. It has also been suggested that such folding takes place as a two step process: a rapid folding to a “molten globule” intermediate configuration which is partially folded but more expanded than the compact native configuration and then a slow folding to the native configuration itself.¹ The rapid folding is mainly controlled by environmental influences such as the presence of water (hydrophobic interaction) and the slow folding depends on the specific sequence of the chain. Among other research work in this field, considerable theoretical effort has been devoted to constructing appropriate models for protein folding and investigating various sequencings which lead to fast folding kinetics. Due to the immense complexity of the protein folding problem, much of our understanding and intuition have been obtained from various computer simulations based on lattice models (Honeycutt and Thirumalai [90]; Honeycutt and Thirumalai [92]; Shakhnovich and Gutin [90]).

Protein folding is a complex process, but it has been postulated that the initial stages of this process can be described qualitatively by heteropolymer collapse. In

¹For a discussion of the molten globule model, see the contribution of Baldwin [94].

this dissertation, we use numerical simulation to study heteropolymer collapse by examining both their equilibrium properties and their collapse kinetics via temperature quenches. According to Xu [96], a polymer is “a large molecule built up by the repetition of small, simple units, which are linked to each other through covalent bonds”. Furthermore, the structure of a heteropolymer can be represented by multiple repetition of different types of these units (monomers). More specifically, we will study random heteropolymers (RHP) which have a random term in the monomer–monomer or monomer–solvent interaction. It was Shakhnovich and Gutin’s analysis of the relationship between random heteropolymers and protein sequences (Shakhnovich and Gutin [90]) that motivated us to study random heteropolymers. In particular, they pointed out that since there are 20 amino-acids involved in protein sequences, there are 210 different pairwise interactions. Such a large number of interaction parameters gives a motivation for the use of a completely random distribution of mutual interactions between monomers. In fact, according to Pande, Grosberg and Tanaka, sequences of real proteins are close to random since only extremely sensitive statistical tools can detect any correlations present (Pande, Grosberg and Tanaka [00]). Although random heteropolymers fold on a longer time scale than real proteins (Bryngelson and Wolynes [89]), the heteropolymer models themselves are interesting in their own right and also because they may possess similar features to proteins. Indeed, much intuition concerning the equilibrium and kinetic properties of proteins has been obtained by investigating heteropolymers. Furthermore, from a polymer physics point of view, heteropolymers are interesting since they may behave completely differently to homopolymers and most of the theoretical work on polymer collapse has been done on homopolymers. Moreover, even less is known about random heteropolymers since their random nature renders them even more difficult to study.

The first theoretical work on homopolymer collapse is due to de Gennes who used a mean-field approach for dynamics near the Θ -solvent conditions (de Gennes [85]). He proposed that the polymer initially collapsed into a “sausage” shape, after which the effect of diffusion caused a uniform thickening of the “sausage” as the ends contract. Grosberg, Nechaev and Shakhnovich [88] followed de Gennes’ lead and included the

effects of topological constraints on later stages of the collapse in order to improve the original model. Many other analytical approaches have been considered with various degrees of success. Another significant analytical approach that is worth mentioning is the Gaussian Self-Consistent theory proposed by Dawson and his colleagues to describe both the collapse dynamics of homopolymers (Timoshenko, Kuznetsov and Dawson [95]; Kuznetsov, Timoshenko and Dawson [96b]) and heteropolymers (Timoshenko, Kuznetsov and Dawson [98]). In their work on heteropolymer collapse, it becomes apparent that the collapse is driven by a complicated process which is strongly dependent on the sequence of the chain. However, the various theories proposed up to now do not agree in their interpretation of the collapse process nor on the scaling laws related to it.

The experimental picture for polymer collapse is also not clear because of the numerous difficulties encountered in the laboratory. One such difficulty is due to the competition between the collapse of the individual chains and the aggregation of several polymers (*i.e.*, the strong coupling of the intrachain collapse with the inter-chain aggregation) during polymer collapse. In order to successfully study collapse dynamics in dilute solutions of non-interacting polymers, the aggregation time of the polymers must occur on a much longer time scale than the polymer collapse itself. Another difficulty is related to the submillisecond time resolution needed to study chain collapse which is not accessible by conventional experimental techniques. As a result, there are only a few experimental studies of the kinetics of collapse of individual chains (Chu, Ying and Grosberg [95]; Wu and Zhou [96]; Nakata and Nakagawa [97]; Pollack et al. [01]). Chu, Yu and Grosberg looked at the two-stage kinetics of single chain collapse by dynamic light scattering. Wu and Zhou performed the first observation of the molten globule state of a single homopolymer chain by laser light scattering. Nakata and Nakagawa did static light scattering measurements on poly(methyl methacrylate) to look at the coil–globule transition. Pollack very recently observed the collapse of a folding protein by means of small angle x-ray scattering. Furthermore, with the increased activity of the biotechnology industry of the past few years, experimental methods have progressed significantly and we should expect even more interesting experimental results in the field of polymer collapse.

The above considerations show that, in spite of extensive activity in this area, a complete picture of the kinetics of polymer collapse has yet to emerge. The search for such a picture is motivated primarily by the intense current interest in the protein folding question (Creighton [92]; Pande et al. [98]) because early stages of protein folding are thought to proceed in the same way as the collapse of flexible homopolymers. Because of the difficulties related to the theoretical and experimental aspect of the folding kinetics of polymers and the lack of consensus concerning the collapse picture, many physicists and chemists have used numerical simulation methods. We have also chosen some of these methods for our investigation of random heteropolymers. The application of numerical simulation techniques to polymer science has led to a wealth of information regarding both the kinetics of formation and the equilibrium properties of synthetic and biological macromolecules. These techniques include the Metropolis Monte Carlo (MMC) simulations on self-avoiding walks using a variety of algorithms such as the crankshaft algorithm and the bond fluctuation algorithm; direct MMC simulations using physically motivated Hamiltonians such as the Edwards-De Gennes Hamiltonian (Laradji, Guo and Zuckermann [94]; Soga, Zuckermann and Guo [95]; Soga, Guo and Zuckermann [96]; Miao, Guo and Zuckermann [96]); and the Langevin dynamics (LD) and molecular dynamics (MD) methods (Baumgärtner [87]; Grest and Murat [95]; Grest and Murat [93]). MD simulations evaluate forces to determine the acceleration from Newton's second law. Using an integration algorithm, it is possible to obtain atomic positions and atomic velocities. The Langevin equation is a stochastic differential equation in which two force terms have been added to Newton's second law to approximate the effects of neglected degrees of freedom. One term represents a frictional force, the other a random force. We shall discuss LD in more detail in the following chapter. Instead of evaluating forces to determine incremental atomic motions, Monte Carlo simulation simply imposes relatively large motions on the system and determines whether or not the altered structure is energetically favorable at the temperature simulated (using Boltzmann probabilities). The system jumps abruptly from conformation to conformation, rather than evolving smoothly through time, and this only depends on the relative energy of the conformations before and after the jump. Because MC simulation samples conformation

space without a true “time” variable or a realistic dynamics trajectory, it does not in principle provide time-dependent quantities. However, it is sometimes much better than MD in estimating average thermodynamic properties for which the sampling of many system configurations is important. The most interesting aspect for physicists is the use of simple models in conjunction with numerical methods for the understanding of the universal behavior of polymer systems in the limit of $N \rightarrow \infty$, where N is the number of effective monomers per polymer. Another useful technique is the simulated annealing method which is a special case of either MD (“quenched” MD), LD, or MC simulations in which the temperature is gradually reduced during the simulation according to a cooling schedule. Often, the system is first heated and then cooled. Thus, the system is given the opportunity to surmount energetic barriers in a search for conformations with energies lower than the local-minimum energy found by direct energy minimization. This improved equilibration can lead to more realistic simulations of dynamics at low temperature (Steinbach and Brooks [94]).

In this dissertation, we mostly apply a Langevin dynamics computational method to the study of the equilibrium and collapse properties of random heteropolymers which have a random term in the monomer–monomer or monomer–solvent interaction. Some of these random heteropolymers will be isolated while others will be immersed in an explicit solvent. Few comparable simulation studies of polymer collapse dynamics employing explicit-solvent models have been carried out because of the high computational cost related to such a problem.¹ Rather, many techniques have been used in order to reduce the computational demands related with studying the influence of the solvent on the conformation of a polymer. An example is the technique of dissipative particle dynamics (DPD) which consists in coarse graining the description of the fluid (Kong et al. [97]). Other methods include the density

¹The high computational cost associated with a model including an explicit solvent is related to the necessity to consider a large system: One must employ a sufficiently large number of solvent particles to satisfy the two conditions that the solvent density is high (the realistic limit), and that the simulation cell side is large enough to exclude the possibility that the polymer can directly interact with periodic images of itself. Note that this constraint leads to minimum system sizes (see Section 2.1.3) which increase rapidly with polymer length. We also note that it is significantly more difficult to attain the dilute limit in which the polymer does not interact with periodic images of itself via the long-range hydrodynamic forces, a point which has been noted by Dünweg and Kremer [91]. In addition to system size constraints, many runs must be performed and averaged in order to obtain reliable statistics in simulation studies of polymer collapse (see Chapter 5).

functional theory (Takahashi and Munakata [97]) and the polymer–solvent integral equations theory for the correlation functions for the polymer and the solvent (Gan and Eu [98]). Nevertheless, it is important to simulate polymer collapse in an explicit solvent since other studies using an explicit solvent have discovered interesting effects, notably the solvent–induced entropic polymer collapse transition observed in hard–core models.¹ As anticipated, the collapse behavior for models including an explicit solvent usually differs qualitatively from that observed in simulation studies of isolated chain systems, or even from theories which include the effect of hydrodynamic interactions.

In their Monte Carlo study of an isolated heteropolymer composed of 15 monomers with a large degree of quenched disorder, Iori *et al.* ([91]) discovered a stretched exponential relaxation behavior in the collapse kinetics. It is thus interesting to ask if the stretched exponential relaxation behavior discovered by Iori *et al.* is generic and whether the exponent β is dependent on the parameters of the particular system studied or whether β is a universal number. Also what is its precise value? Chapter 3 addresses these generic questions. Furthermore, we examine the effect of an explicit solvent on the equilibrium properties of a random heteropolymer (Chapter 4) and on the collapse of a random heteropolymer (Chapter 5). We study two types of random heteropolymers in a solvent. In the first case, random interactions are imposed between the monomers themselves and in the second case, they are taken to be between the monomers and the solvent particles. We also examine the effect of adding stiffness to the heteropolymer chain by introducing angular restrictions. Chapters 3, 4 and 5 each contain summaries and discussions of their contents. The details of the microscopic models and the molecular dynamics method used for the numerical simulations are presented in Chapter 2. The dissertation is concluded in Chapter 6 with a summary of our results and proposals for new projects.

¹Dijkstra, Frenkel and Hansen [94]; Dijkstra and Frenkel [94]; Frenkel and Louis [92]; Polson [99]; Khalatur, Zherenkova and Khokhlov [98]; van der Schoot [98]; Luna-Bárcena et al. [96]; Suen, Escobedo and Pablo [97]

MODELS AND METHODS

The purpose of this chapter is two-fold. In the first section, the various three-dimensional microscopic models used in this thesis for the numerical simulation of random heteropolymers are described in detail by specifying the interactions involved in our system as well as the environment characterizing it. The molecular dynamics method used for the numerical simulations are presented in the second section.

2.1 Models

All the models used in this thesis are off-lattice in the sense that both the monomers of the polymer and solvent are not constrained to lie on the sites of a crystalline lattice, but rather they can move in a three-dimensional continuum. This assures that no artifacts due to the lattice structure will be introduced. This is particularly important in the case of polymer collapse since collapsed polymers in a bad solvent can encounter ergodicity problems (*i.e.* the polymer chain can become stuck in a given configuration). However, this means that we will not benefit from the advantages of a lattice algorithm which can significantly speed up the simulation since it uses integer arithmetic.

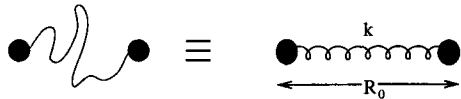
Since we are looking for generic properties of random heteropolymers, we chose a polymer model which does not include specific details of the monomers which represent several chemical groups. Instead the polymer is modeled by the multiple bead and spring model shown in Figure 2.1, and the excluded volume effect is modeled by means of a short range repulsive interaction between monomers. The beads represent the monomers and the harmonic springs model mimics the covalent bonds linking the monomers. In Chapter 3 the polymer is taken to be freely jointed and the properties of random heteropolymers are modeled in the absence of an explicit solvent. Here the

unstretched length of the springs are equivalent to the Kuhn length which is the length scale for angular correlations (see Figure 2.2). The kinetics of this model correspond to Rouse dynamics where hydrodynamic effects are absent. The monomers interact via a repulsive Lennard-Jones potential and an r^{-6} interaction with coefficients which are randomly generated from a Gaussian distribution. The latter interaction can be either repulsive or attractive and it gives rise to the collapse of the random heteropolymer below a characteristic temperature known as the theta point. In Chapters 4 and 5, an explicit solvent is introduced as a set of soft spheres interacting with each other and with the polymer in one of two possible ways. First the model of Chapter 3 for the random heteropolymer is used and the solvent particles interact with each other via uniform Van der Waal's interactions. The monomer–solvent interaction is a repulsive Lennard-Jones potential. We will call this model Model A. In the second model, Model B, the monomers of the polymer interact with one another via uniform Van der Waal's interactions as do the particles of the solvent. The random interactions are introduced via a r^{-6} interaction between the solvent particles and the polymer. This is a more realistic modeling of the hydrophobic effect which is the driving force for protein folding. In Sections 4.4 and 5.3, stiffness is added to the polymer chain by introducing angular restrictions such as bending curvature and torsion as shown in Figure 2.3. This simulates the effect of the side chains of the amino-acid residues of proteins. Furthermore, a longer Kuhn length results from the addition of stiffness. We need to consider the position of three adjacent monomers in order to determine the bending angle and of four adjacent monomers to determine the rotational angle. Note that throughout this dissertation, we refer to Model A to describe any system with a single random heteropolymer with or without an explicit solvent, where random interactions are imposed between the monomers. Furthermore, we refer to Model B to describe any system with a single random heteropolymer which can be either flexible or semi-flexible with or without an explicit solvent, where random interactions occur between the monomers and the solvent particles.

It should be noted that the Kuhn length for the secondary sequences of proteins is of the order of 18 Å which corresponds to 5 – 7 links (Grosberg and Khokhlov [94]). The coil diameter is of order ~ 100 Å, the persistence length is of order ~ 10 Å and



Figure 2.1: Rouse-like multiple bead-spring model.

Figure 2.2: Two monomers and a bond modeled by two beads and a spring with spring constant k and equilibrium length R_0 .

the bond length is of order $\sim 1 \text{ \AA}$. The order of magnitude of the time required for the motion of a segment of Kuhn length is 10^{-8} s and therefore the collapse time of a long polymer is of the order of a few milliseconds which is now accessible by small angle x-ray scattering (Pollack et al. [01]). The Kuhn length and hence the persistence length can be used to describe the degree of polymer chain flexibility (*i.e.*, the distance for which the memory of the direction prevails). Note that these quantities are of the same order of magnitude.

2.1.1 Hamiltonian

In this section we give a general expression for the Hamiltonian which includes all the interactions used in Chapters 3 to 5. This is given by:

$$\mathcal{H} = \mathcal{U}_{MM} + \mathcal{U}_{MS} + \mathcal{U}_{SS} + \mathcal{K}_M + \mathcal{K}_S \quad (2.1)$$

where \mathcal{U}_{MM} is the total potential energy due to the interactions between monomers, \mathcal{U}_{MS} is the total potential energy due to the interactions between monomers and solvent particles, \mathcal{U}_{SS} is the total potential energy due to the interactions between solvent particles, \mathcal{K}_M is the total kinetic energy of the monomers and \mathcal{K}_S is the total kinetic energy of the solvent particles. As in most molecular dynamics simulations, our empirical energy function is developed so as to approximate the potential energy of the system.

Two types of random heteropolymers were studied. In the first case, the random interaction was taken to be between the monomers, while in the second case, it was

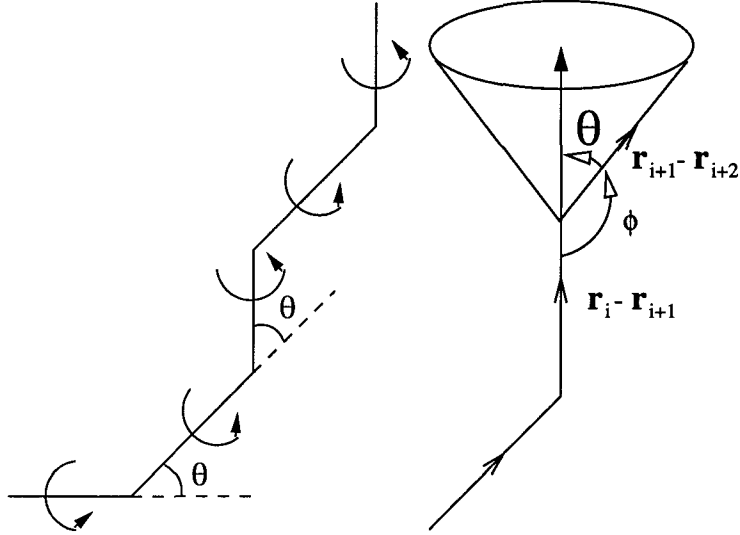


Figure 2.3: (a) Freely rotating chain and (b) the bending angle.

imposed between the monomers and the solvent particles. In some cases, an explicit solvent was present. The general expressions for \mathcal{U}_{MM} , \mathcal{U}_{MS} and \mathcal{U}_{SS} , in Models A and B are as follows:

(1). Model A,

$$\mathcal{U}_{MM} = \sum_{i=1, j=i+1}^{N-1} \mathcal{U}_{Spring}(r_{ij}) + \sum_{i=1}^N \sum_{j>i}^N \mathcal{U}_{RLJ}(r_{ij}) + \sum_{i=1}^N \sum_{j>i}^N \mathcal{U}_{Dis}(r_{ij}, \eta_{ij}) \quad (2.2)$$

$$\mathcal{U}_{MS} = \sum_{i=1}^N \sum_{j'=1}^{N_S} \mathcal{U}_{RLJ}(r_{ij'}) \quad (2.3)$$

$$\mathcal{U}_{SS} = \sum_{i'=1}^{N_S} \sum_{j'>i'}^{N_S} \mathcal{U}_{LJ}(r_{i'j'}) \quad (2.4)$$

(2). Model B,

$$\mathcal{U}_{MM} = \sum_{i=1, j=i+1}^{N-1} \mathcal{U}_{Spring}(r_{ij}) + \sum_{i=1}^N \sum_{j>i}^N \mathcal{U}_{LJ}(r_{ij}) + \sum_{i=1}^{N-2} \mathcal{U}_{Bend}(\theta_i) \quad (2.5)$$

$$\mathcal{U}_{MS} = \sum_{i=1}^N \sum_{j'=1}^{N_S} \mathcal{U}_{RLJ}(r_{ij'}) + \sum_{i=1}^N \sum_{j'=1}^{N_S} \mathcal{U}_{Dis}(r_{ij'}, \eta_{ij'}) \quad (2.6)$$

$$\mathcal{U}_{SS} = \sum_{i'=1}^{N_S} \sum_{j'>i'}^{N_S} \mathcal{U}_{LJ}(r_{i'j'}) \quad (2.7)$$

Here, non-primed indices are used to identify a specific monomer of the polymer chain and primed indices are used to identify a specific solvent particle. Also, $\mathbf{r}_{ij} = \mathbf{r}_i - \mathbf{r}_j$, $\mathbf{r}_{ij'} = \mathbf{r}_i - \mathbf{r}_{j'}$ and $\mathbf{r}_{i'j'} = \mathbf{r}_{i'} - \mathbf{r}_{j'}$ where \mathbf{r}_{ij} is the distance between the i^{th} monomer and the j^{th} monomer, $\mathbf{r}_{ij'}$ is the distance between the i^{th} monomer and the j^{th} solvent particle and similarly $\mathbf{r}_{i'j'}$ is the distance between the i^{th} solvent particle and the j^{th} solvent particle. Furthermore, $r_{ij} = |\mathbf{r}_{ij}|$, $r_{ij'} = |\mathbf{r}_{ij'}|$ and $r_{i'j'} = |\mathbf{r}_{i'j'}|$. N is the number of monomers and N_S is the number of solvent particles.

\mathcal{U}_{Spring} is the harmonic interaction between neighboring monomers on the heteropolymer chain and is given by

$$\mathcal{U}_{Spring}(r_{ij}) = \frac{k}{2}(r_{ij} - R_0)^2, \quad (2.8)$$

where R_0 is the length of the unstretched bond between monomers and k is the spring constant. Here, $j = i + 1$ since only adjacent monomers are linked by springs.

The fluctuations in bond length can be estimated by using the equipartition theorem: $\frac{k}{2} \langle (r_{ij} - R_0)^2 \rangle = \frac{1}{2}k_B T$ therefore $\langle (r_{ij} - R_0)^2 \rangle^{1/2} = \sqrt{\frac{k_B T}{k}}$.

Van der Waal's interactions are due to the fluctuations of the electron cloud of a neutral atom around its positively charged nucleus. The fluctuations in neighboring atoms become correlated, inducing attractive dipole-dipole interactions. The equilibrium distance between two proximal atomic centers is determined by a competition between this attractive dispersion interaction and a core-repulsion interaction that reflects electrostatic repulsion and the Pauli exclusion principle. The Lennard-Jones potential models the attractive interaction as a r^{-6} tail and the repulsive one as r^{-12} :

$$\begin{aligned} \mathcal{U}_{LJ}(r_{ij}) &= 4\epsilon \left[\left(\frac{\sigma}{r_{ij}} \right)^{12} - \left(\frac{\sigma}{r_{ij}} \right)^6 + \left(\frac{\sigma}{r_c} \right)^6 - \left(\frac{\sigma}{r_c} \right)^{12} \right]; & r_{ij} < r_c \\ &= 0; & r_{ij} \geq r_c. \end{aligned} \quad (2.9)$$

The parameter σ is the equilibrium separation distance and ϵ is the well depth (or the coupling constant). What is the origin of this '6-12' form for the van der Waal's interaction? The application of quantum perturbation theory to two well separated

hydrogen atoms in their ground states yields an interaction energy that decays as r^{-6} , and the r^{-12} term is easy to calculate from the r^{-6} term. Lennard-Jones interactions are usually modeled as effectively pairwise additive: the potential energy $\mathcal{U}_{\ell j}^{ABC}$ of three adjacent particles A, B, and C is the sum of the three energies for each particle pair: $\mathcal{U}_{\ell j}^{ABC} = \mathcal{U}_{\ell j}^{AB} + \mathcal{U}_{\ell j}^{BC} + \mathcal{U}_{\ell j}^{AC}$. However, the effective pairwise additivity is only an approximation.¹ By setting $r_c = 2^{1/6}\sigma$, which is the position of the minimum in the Lennard-Jones two-body potential, a purely repulsive Lennard-Jones potential \mathcal{U}_{RLJ} is obtained. \mathcal{U}_{RLJ} is a soft-sphere potential (Figure 2.4) and it is frequently used to model homopolymers in a good solvent (Grest and Murat [93]).

$$\mathcal{U}_{RLJ}(r_{ij}) = \mathcal{U}_{\ell j}(r_{ij}); \quad r_c = 2^{1/6}\sigma \quad (2.10)$$

Setting $r_c = 2.5\sigma$ preserves the long-range attractive tail of the form $(-1/r_{ij}^6)$, a negative well of depth ϵ , and a steeply rising repulsive wall at a distance less than $r \sim \sigma$ (Figure 2.4).

$$\mathcal{U}_{LJ}(r_{ij}) = \mathcal{U}_{\ell j}(r_{ij}); \quad r_c = 2.5\sigma \quad (2.11)$$

The term \mathcal{U}_{Dis} represents a random interaction between each pair of monomers (Figure 2.5).

$$\mathcal{U}_{Dis}(r_{ij}, \eta_{ij}) = \epsilon \left(\frac{\eta_{ij}}{(r_{ij}/\sigma)^6} \right), \quad (2.12)$$

where η is a Gaussian random number with $\langle \eta_{ij} \rangle = 0$ and

$$\langle \eta_{ij} \eta_{k\ell} \rangle = \alpha^2 \delta_{ik} \cdot \delta_{j\ell} \quad (2.13)$$

Hence the “strength” of the random interaction is measured by the parameter α . For clarity, α will be used to represent the strength of the random monomer–monomer interactions while α' will be used to represent the strength of the random monomer–solvent interactions. Iori, Marinari and Parisi [91] point out that, for application to protein folding, η_{ij} represents a series of complex biological interactions such as the

¹In general, the potential energy can be divided into terms depending on the coordinates of individual particles, pairs, triplets *etc.* Since adding non-additive terms in the potential would have a high computational cost, most simulations in the literature are performed with an “effective” pair potential. This pairwise approximation is quite satisfactory for studying the properties of the liquid phase since the average three body effects can be partially included in the “effective” pair potential (see section 1.3.2 of Allen and Tildesley [87]).

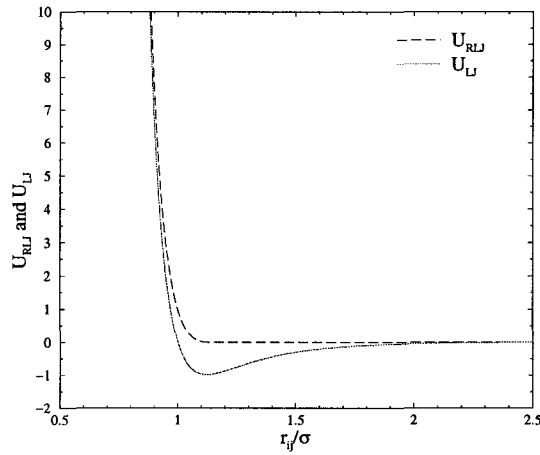


Figure 2.4: The purely repulsive Lennard–Jones potential, \mathcal{U}_{RLJ} and the Lennard–Jones potential truncated at $r_c = 2.5\sigma$, \mathcal{U}_{LJ} .

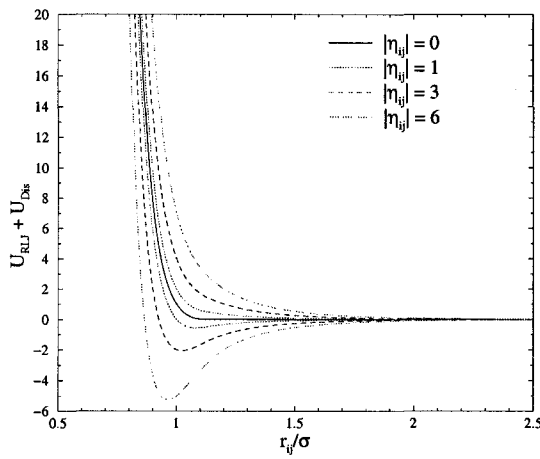


Figure 2.5: The random interaction potential \mathcal{U}_{Dis} for $\eta_{ij} = 0, \pm 1, \pm 3$ and ± 6 .

interactions between different groups of amino-acids and the interactions of these groups with the solvent (*e.g.* an aqueous solution).

\mathcal{U}_{Bend} is the bending potential which is modeled by a harmonic interaction and is given by

$$\mathcal{U}_{Bend}(\theta_i) = \frac{k_\theta}{2}(\phi_i - \phi_0)^2 = \frac{k_\theta}{2}(\theta_i - \theta_0)^2, \quad (2.14)$$

where k_θ is the spring constant, ϕ_i is the angle formed by monomers i, i+1 and i+2 and $\theta_i = \pi - \phi_i$. We choose ϕ_0 and θ_0 as follows based on the angle between C–C bonds in a saturated alkane chain: $\phi_0 \simeq 109.47 \text{ deg} \simeq 1.91 \text{ rad}$ (the tetrahedral angle) and $\theta_0 = \pi - \phi_0$. The value of θ can be calculated by evaluating the following equation and taking the inverse cosine of the following expression.

$$\cos \theta_i = \frac{\mathbf{r}_i - \mathbf{r}_{i+1}}{|\mathbf{r}_i - \mathbf{r}_{i+1}|} \cdot \frac{\mathbf{r}_{i+1} - \mathbf{r}_{i+2}}{|\mathbf{r}_{i+1} - \mathbf{r}_{i+2}|} \quad (2.15)$$

The angular fluctuations can be estimated by the equipartition theorem. The resulting relation is $\langle (\theta_i - \theta_0)^2 \rangle^{1/2} = \sqrt{\frac{k_B T}{k_\theta}}$.

2.1.2 Forces

With the above Hamiltonian, the force acting on the i^{th} monomer/solvent particle due to the j^{th} monomer/solvent particle can be evaluated with the following equation.

$$\mathbf{f}_{ij} = -\nabla_{\mathbf{r}_{ij}} \mathcal{U}(\mathbf{r}_{ij}), \quad (2.16)$$

where \mathcal{U} is the potential energy due to the interaction between particles i and j . The resulting forces are straight-forward to evaluate and are given by

$$\mathbf{f}_{ij}^{Spring} = - \left(\frac{d\mathcal{U}_{Spring}(r_{ij})}{dr_{ij}} \right) \frac{\mathbf{r}_{ij}}{r_{ij}} = -\frac{k}{r_{ij}}(r_{ij} - R_0)\mathbf{r}_{ij} = -k \left(1 - \frac{R_0}{r_{ij}} \right) \mathbf{r}_{ij} \quad (2.17)$$

$$\mathbf{f}_{ij}^{Dis} = -\frac{1}{r_{ij}} \left(\frac{d\mathcal{U}_{Dis}(r_{ij})}{dr_{ij}} \right) \mathbf{r}_{ij} = \frac{6\epsilon}{r_{ij}^2} \left(\frac{\eta_{ij}}{r_{ij}^6} \right) \mathbf{r}_{ij} \quad (2.18)$$

$$\mathbf{f}_{ij}^{\ell j} = -\frac{1}{r_{ij}} \left(\frac{d\mathcal{U}_{\ell j}(r_{ij})}{dr_{ij}} \right) \mathbf{r}_{ij} = \frac{24\epsilon}{r_{ij}^2} \left[2 \left(\frac{\sigma}{r_{ij}} \right)^{12} - \left(\frac{\sigma}{r_{ij}} \right)^6 \right] \quad (2.19)$$

For the bending force, each angle θ_i contributes a force on three monomers, i , $i+1$ and $i+2$.

$$\begin{aligned}\mathbf{f}_i^{Bend} &= -\frac{\partial \mathcal{U}_{Bend}(\theta_i)}{\partial \mathbf{r}_i} \\ &= -\frac{\partial \mathcal{U}_{Bend}(\theta_i)}{\partial \theta_i} \frac{\partial \theta_i}{\partial (\cos \theta_i)} \frac{\partial (\cos \theta_i)}{\partial \mathbf{r}_i} \\ &= \frac{k_\theta(\theta_i - \theta_0)}{\sqrt{1 - \cos^2 \theta_i}} \frac{\partial \cos \theta_i}{\partial \mathbf{r}_i} \\ &= \frac{\mathbf{r}_{i+1} - \mathbf{r}_{i+2}}{|\mathbf{r}_{i+1} - \mathbf{r}_{i+2}| |\mathbf{r}_i - \mathbf{r}_{i+1}|} - \cos \theta_i \frac{\mathbf{r}_i - \mathbf{r}_{i+1}}{|\mathbf{r}_i - \mathbf{r}_{i+1}|^2}\end{aligned}\quad (2.20)$$

$$\begin{aligned}\mathbf{f}_{i+2}^{Bend} &= -\frac{\partial \mathcal{U}_{Bend}(\theta_i)}{\partial \mathbf{r}_{i+2}} \\ &= -\frac{\partial \mathcal{U}_{Bend}(\theta_i)}{\partial \theta_i} \frac{\partial \theta_i}{\partial (\cos \theta_i)} \frac{\partial (\cos \theta_i)}{\partial \mathbf{r}_i} \\ &= \frac{k_\theta(\theta_i - \theta_0)}{\sqrt{1 - \cos^2 \theta_i}} \frac{\partial \cos \theta_i}{\partial \mathbf{r}_{i+2}} \\ &= -\frac{\mathbf{r}_i - \mathbf{r}_{i+1}}{|\mathbf{r}_{i+1} - \mathbf{r}_{i+2}| |\mathbf{r}_i - \mathbf{r}_{i+1}|} + \cos \theta_i \frac{\mathbf{r}_{i+1} - \mathbf{r}_{i+2}}{|\mathbf{r}_{i+1} - \mathbf{r}_{i+2}|^2}\end{aligned}\quad (2.21)$$

By symmetry,

$$\mathbf{f}_{i+1}^{Bend} = -(\mathbf{f}_i^{Bend} + \mathbf{f}_{i+2}^{Bend}). \quad (2.22)$$

This last calculation was also performed by using

$$\mathbf{f}_{i+1}^{Bend} = -\frac{\partial \mathcal{U}_{Bend}(\theta_i)}{\partial \mathbf{r}_{i+1}} \quad (2.23)$$

which gives the same results as Eq. (2.22).

2.1.3 Ensemble and boundary conditions

The natural ensemble for molecular dynamics is the microcanonical ensemble (*NVE*) in which the total energy, volume and particle number are constant parameters. That is, E is fixed and T fluctuates about an average value as energy is exchanged between the kinetic energy and the potential energy. In a conventional molecular dynamics simulation, the Newtonian equations of motions of a system of N particles in a periodic volume V are integrated numerically. In the absence of external perturbations, the total energy E and the total linear momentum p are conserved. Hence, if the

system is ergodic, time averages along a trajectory in phase-space are equivalent to averages in the microcanonical, constant-momentum (NVE,p) ensemble. However, such an ensemble is often not the most convenient for the problem in hand. Since Newton's equations lead naturally to the microcanonical ensemble, any extension to a different ensemble involves some degree of artificiality. Furthermore, there is no well defined way of deriving the modified equations of motion. Various schemes have been proposed by Andersen, Parrinello–Rahman, Nosé–Hoover, Langevin and others, some of which we now summarize.

Andersen (Andersen [80]) introduced one or more degrees of freedom that are additional to the degrees of freedom of the particles of the physical system (extended-system). In the specific case of Andersen, the extra coordinate was the volume V . A change in V corresponds to a homogeneous scaling of all the center-of-mass positions. Associated with the extra coordinate is a new momentum and a new mass. Newton's equations are then solved for the extended system. The conserved quantity is no longer the total energy of the system but a quantity closely related to the total enthalpy H of the system resulting in an (NPH) ensemble. Andersen also used a stochastic method to describe a constant temperature system (NPT).

Parrinello and Rahman [80] proposed a scheme that allows for fluctuations in shape as well as in volume of the periodic cell. This is useful for the study of structural phase transitions of crystalline solids since the periodic boundary conditions (PBC) for one phase could not be used for the other phase. Furthermore, they generalized their method to simulate solids subjected to external stress. They basically generalized Andersen's (NPH) method except that a mass tensor is associated with the dynamics of the unit cell. We, however, have chosen to work in the canonical (NVT) ensemble in which temperature, volume and particle number are constant parameters. There is exchange of energy between the system and a heat bath to keep the average temperature constant at equilibrium. We use two methods for sampling the constant (within fluctuations) temperature ensemble. The first method consists of adding a friction term to the equation of motion which simulates contact with a heat bath. This method is called Langevin dynamics. The second method is an extended-system method which consists of adding a term which represents the heat

bath to the Lagrangian of the system. This is called a Nosé–Hoover thermostat. Both of these methods will be discussed in detail in section 2.2.

The choice of ensemble becomes irrelevant in the thermodynamic limit but this is not always true for the small system sizes used in computer simulations. Most experimental observations are performed in the (*NPT*) ensemble, sometimes in the (μVT) ensemble, in which the chemical potential, the volume and the temperature are constant parameters, and occasionally in the (*NVT*) ensemble. Experiments in the (*NVE*) ensemble are very rare due to the difficulty related to maintaining the energy constant since contact with the outside world is easier if the temperature is kept constant. It is therefore preferable to perform our simulations at constant temperature. Even though constant pressure experiments present no problem in the laboratory, they are more difficult to perform with computer simulations since they involve rescaling the simulation box regularly.

We use two types of boundary conditions in our simulations. For an isolated polymer without an explicit solvent, an infinite system was studied and no boundaries were required. In the case of a polymer in an explicit solvent, a volume had to be determined to contain the system. A box of volume V with periodic boundary conditions was used (Allen and Tildesley [87]). The cubic box used allows us to define a number density $\rho = \frac{(N+N_S)\sigma^3}{V}$ for our system.

In order to overcome surface effects, periodic boundary conditions were chosen. The cubic box is replicated throughout space to form an infinite lattice. As a molecule moves in the original box, its periodic image moves in the same way in the neighbouring boxes. Therefore, as a molecule leaves the central box, one of its images will enter through its opposite face. There are no walls at the boundary of the central box and no surface molecules.

It is important to ask if the properties of an infinite periodic system and the macroscopic system which it represents are the same. This depends both on the range of the intermolecular potential and the phenomenon under investigation. For a fluid of Lennard–Jones particles, it is possible to perform a simulation in a cubic box of side 6σ without a particle being able to sense the symmetry of the periodic lattice (Allen and Tildesley [87]). However, if the potential is long range (*i.e.* $u(r) \sim r^{-\nu}$, $\nu \leq d$

where d is the dimensionality of the system) there will be a substantial interaction between a particle and its own image in neighbouring boxes, and consequently the symmetry of the cell structure is imposed on a fluid which is in reality isotropic. For example, we have $u \sim r^{-1}$ for charged ions and $u \sim r^{-3}$ for dipolar molecules. Even for short-range potentials, the periodic boundary conditions can induce anisotropies in the fluid structure, especially for small systems ($N_S \approx 100$).

The use of PBC inhibits the occurrence of long-wavelength fluctuations. For a cube of side L , the periodicity suppresses any density wave with a wavelength greater than L . Thus it is impossible to simulate a liquid close to the gas–fluid critical point where the range of critical fluctuations are macroscopic. Furthermore, transitions which are known to be first order often exhibit the characteristics of higher order transitions in a small box because of the finite size effect. For the polymer in a box, we have always used $\sim (6\sigma + \max(\text{span}))$ for minimum box size where $\max(\text{span})$ is the maximal length of the polymer in a given direction.

2.2 Molecular dynamics methods

Between the purely stochastic Metropolis Monte Carlo method and the purely deterministic molecular dynamics method, there is a range of methods that have different degrees of stochastic and deterministic characteristics (Slater [93a], Haile [92]). We use two of these methods in this dissertation, the Langevin stochastic dynamics and the Nosé–Hoover deterministic dynamics. Except for special cases, these thermostats give the correct Maxwell–Boltzmann velocity distribution for the canonical ensemble:

$$\mathcal{P}(\mathbf{v}) = \left(\frac{1}{2\pi m k_B T} \right)^{3/2} e^{-\frac{mv^2}{2k_B T}}. \quad (2.24)$$

The equation of motion of the particles is described either by the Langevin phenomenological equation or the Nosé–Hoover equation. The advantage of the more deterministic methods like molecular dynamics and Langevin dynamics is that it allows for a direct study of questions regarding the dynamics of the system.

2.2.1 Langevin dynamics

Most equilibrium and relaxation data were obtained in this work by implementing a Langevin dynamics (LD) method described by Grest and Murat [93] in which each

particle is coupled to a heat bath via a friction coefficient. The Langevin equation is a stochastic differential equation in which two force terms have been added to Newton's second law to approximate the effects of the neglected degrees of freedom. One term represents a frictional force, the other a random force (noise). For example, in the absence of explicit solvent particles, the system being simulated needs to be approximated. To do so, a frictional drag on the solute as well as random kicks associated with the thermal motions of the solvent particles are introduced. Since friction opposes motion, the first additional force is proportional to the velocity of the particle and oppositely directed. Langevin's equation for the motion of particle i is then given by:

$$m \frac{d^2 \mathbf{r}_i}{dt^2} = \mathbf{F}_i - m\Gamma \frac{d\mathbf{r}_i}{dt} + \mathbf{W}_i(t), \quad (2.25)$$

where \mathbf{r}_i is the position of the particle, t is the time, \mathbf{F}_i is the total force acting on particle i by other particles explicitly present in the system, Γ is the friction that couples the particle to the heat bath (collision frequency) and $\mathbf{W}_i(t)$ describes the random force acting on particle i (white noise). The friction coefficient is related as follows to the random force by the fluctuation-dissipation theorem (see Appendix A.1):

$$\langle \mathbf{W}_i(t) \rangle = 0, \quad (2.26)$$

$$\int \langle \mathbf{W}_i(0) \mathbf{W}_j(t) \rangle dt = 6k_B T m \Gamma. \quad (2.27)$$

In simulations it is often assumed that the random force is completely uncorrelated at different times. That is, assuming Gaussian white noise, the above equation takes the form:

$$\langle \mathbf{W}_i(t) \mathbf{W}_j(t') \rangle = 6k_B T m \Gamma \delta_{ij} \delta(t - t'). \quad (2.28)$$

The temperature, T , of the system is maintained via the relationship between $\mathbf{W}_i(t)$ and Γ . On the basis of Eq. (2.28), we generate the random force $\mathbf{W}_i(t)$ with a Gaussian random number generator with width $\sqrt{\frac{2k_B T m \Gamma}{\Delta t}}$, where Δt is the selected time step. From Einstein's relation, the isolated monomer/solvent particle diffusion constant is $D = \frac{k_B T}{m \Gamma}$. The jostling of a solute by a solvent can expedite barrier crossing, and hence Langevin dynamics can search conformations better than Newtonian MD ($\Gamma = 0$). Furthermore, Langevin dynamics is particularly advantageous in the study of isolated heteropolymers like proteins since it mimics the viscous environment of

amino acids in water which makes the motion on the scale of a single amino acid over-damped. A more detailed description of the Langevin equation using kinetic theory can be found in Appendix A.1.

The molecular dynamics simulation proceeds by integrating Eq. (2.25) using a suitable algorithm with an appropriate choice of time step Δt . A well tested algorithm is due to Verlet and uses information from two previous time-steps. This simple yet very stable algorithm has been used for both atoms and molecular liquids and has shown itself to be better or at least the equal of other more complicated algorithm (Ciccotti, Frenkel and McDonald [87]). We begin by evaluating the Taylor series for positions from time t forward to time $t + \Delta t$:

$$\mathbf{r}_i(t+\Delta t) = \mathbf{r}_i(t) + \frac{d\mathbf{r}_i(t)}{dt}(\Delta t) + \frac{1}{2} \frac{d^2\mathbf{r}_i(t)}{dt^2}(\Delta t^2) + \frac{1}{3!} \frac{d^3\mathbf{r}_i(t)}{dt^3}(\Delta t^3) + \mathcal{O}(\Delta t^4), \quad (2.29)$$

and backward to time $t - \Delta t$:

$$\mathbf{r}_i(t-\Delta t) = \mathbf{r}_i(t) - \frac{d\mathbf{r}_i(t)}{dt}(\Delta t) + \frac{1}{2} \frac{d^2\mathbf{r}_i(t)}{dt^2}(\Delta t^2) - \frac{1}{3!} \frac{d^3\mathbf{r}_i(t)}{dt^3}(\Delta t^3) + \mathcal{O}(\Delta t^4). \quad (2.30)$$

Eqs. (2.29) and (2.30) are now added together and the following equation, which has a local truncation error that varies as Δt^4 , is obtained.

$$\mathbf{r}_i(t + \Delta t) = 2\mathbf{r}_i(t) - \mathbf{r}_i(t - \Delta t) + \frac{d^2\mathbf{r}_i(t)}{dt^2}(\Delta t^2) + \mathcal{O}(\Delta t^4) \quad (2.31)$$

The first-order central difference estimate is then used to evaluate the particle velocities.

$$\mathbf{v}_i(t) \approx \frac{\mathbf{r}_i(t + \Delta t) - \mathbf{r}_i(t - \Delta t)}{2\Delta t} \quad (2.32)$$

Eq. (2.25) can be rewritten as follows:

$$\frac{d^2\mathbf{r}_i(t)}{dt^2} = \frac{\mathbf{F}_i(t) + \mathbf{W}_i(t)}{m} - \Gamma \mathbf{v}_i(t). \quad (2.33)$$

From Eqs. (2.31) to (2.33), we obtain the following expression for $\mathbf{r}_i(t + \Delta t)$:

$$\mathbf{r}_i(t+\Delta t) = \frac{1}{1 + \frac{1}{2}\Gamma\Delta t} \left\{ 2\mathbf{r}_i(t) - \left[1 - \frac{\Gamma\Delta t}{2} \right] \mathbf{r}_i(t-\Delta t) + \left[\frac{\mathbf{F}_i(t) + \mathbf{W}_i(t)}{m} \right] \Delta t^2 \right\}. \quad (2.34)$$

Verlet's algorithm is a two-step method because it estimates $\mathbf{r}_i(t + \Delta t)$ from the current position $\mathbf{r}_i(t)$ and the previous position $\mathbf{r}_i(t - \Delta t)$. This algorithm is not self-starting at $t = 0$, and the value of $\mathbf{r}_i(-\Delta t)$ is required.

Molecular dynamics simulations can be speeded up considerably by the use of neighbour lists to evaluate the inter-particle forces. For each solvent particle, a list of neighbours with which it interacts, is defined, and this list is updated periodically. The neighbours of a particular particle are the particles contained within a sphere of radius $r_l = r_c + \Delta r$, where r_c is the potential cutoff distance, and Δr is the thickness of a “safety” buffer. As Δr is increased, the list needs to be updated less often but the number of neighbours becomes larger. The choice of Δr is thus a compromise between CPU time and memory usage.

2.2.2 Nosé–Hoover dynamics

The original Nosé method (Nosé [84]) considers an extended system with an additional degree of freedom, s , which acts like an external reservoir interacting with the system by scaling all the velocities of the particles:

$$\mathbf{v}_i = s\dot{\mathbf{r}}_i = \frac{\mathbf{p}_i}{ms}. \quad (2.35)$$

The Hamiltonian for the extended system is given by:

$$\mathcal{H} = \mathcal{H}_0 + \mathcal{H}_s, \quad (2.36)$$

where \mathcal{H}_0 is the Hamiltonian for the original system and \mathcal{H}_s is the Hamiltonian of the heat-bath with

$$\mathcal{H}_0 = \sum_i \left\{ \frac{\mathbf{p}_i^2}{2ms^2} + \mathcal{U}(\mathbf{r}_i) \right\}, \quad (2.37)$$

$$\mathcal{H}_s = \mathcal{K}_s + \mathcal{U}_s, \quad (2.38)$$

$$\mathcal{K}_s = \frac{p_s^2}{2Q}, \quad (2.39)$$

and

$$\mathcal{U}_s = (g + 1)k_B T \ln s. \quad (2.40)$$

The parameter g is related to the number of degrees of freedom (*d.o.f.*).

$$g = d.o.f. - 1 = 3(N + N_S) + 1 - 1 = 3(N + N_S) \quad (2.41)$$

Q is called the “mass” of the heat bath even though it has the units of (*energy · time²*). A small value of Q corresponds to low inertia of the heat-bath (*i.e.* rapid

temperature fluctuations) and causes a strong perturbation in the dynamics of the system. On the other hand, a large value of \mathcal{Q} will result in little change in the dynamics of the system but it gives rise to a slow response to a temperature jump and the rate of equilibration will be slow. \mathcal{Q} will have an effect on the diffusion constant but it is a much smaller effect than the one that is observed for the Andersen's thermostat which is based on a stochastic collisions scheme which leads to sudden decorrelation of particle velocities. This decorrelation effect will increase the decay of the velocity autocorrelation function which will in turn change the diffusion constant (the time integral of the velocity autocorrelation function). We then conclude that the Nosé–Hoover thermostat is “softer” than the Andersen thermostat. Furthermore, the velocity distribution Eq. (2.24) is independent of the coupling constant \mathcal{Q} . Hamilton's equations for the Nosé–Hoover thermostat are given by:

$$\dot{s} = \frac{\partial \mathcal{H}}{\partial p_s} = \frac{p_s}{\mathcal{Q}} \quad (2.42)$$

$$\dot{p}_s = -\frac{\partial \mathcal{H}}{\partial s} = \frac{1}{s^3} \sum_i \frac{p_i^2}{m} - \frac{(g+1)}{s} k_B T \quad (2.43)$$

$$\dot{\mathbf{r}}_i = \frac{\partial \mathcal{H}}{\partial \mathbf{p}_i} = \frac{\mathbf{p}_i}{ms^2} \quad (2.44)$$

$$\dot{\mathbf{p}}_i = -\frac{\partial \mathcal{H}}{\partial \mathbf{r}_i} = -\frac{\partial U}{\partial \mathbf{r}_i} = \mathbf{F}_i, \quad (2.45)$$

using Eqs (2.36) to (2.40). The following equations of motions, for all variables including s , can be now obtained from these results.

$$\begin{aligned} \ddot{s} &= \frac{\dot{p}_s}{\mathcal{Q}} \\ &= \frac{1}{\mathcal{Q}} \left\{ \frac{1}{s^3} \sum_i \frac{p_i^2}{m} - \frac{(g+1)}{s} k_B T \right\} \\ &= \frac{1}{\mathcal{Q}} \left\{ \sum_i m \dot{r}_i^2 s - \frac{(g+1)}{s} k_B T \right\} \end{aligned} \quad (2.46)$$

and

$$\ddot{\mathbf{r}}_i = \frac{\dot{\mathbf{p}}_i}{ms^2} - \frac{2\mathbf{p}_i \dot{s}}{ms^3} = \frac{\mathbf{F}_i}{ms^2} - \frac{2\dot{\mathbf{r}}_i \dot{s}}{s} \quad (2.47)$$

These equations of motion are not easy to integrate but Hoover was able to simplify them (Hoover [85]). He used $t' = \int_0^t \frac{d\tau}{s}$ so that $dt' = \frac{dt}{s}$ and rewrote Nosé's equations of motion as follows:

$$\frac{d\mathbf{r}_i}{dt'} = s \frac{d\mathbf{r}_i}{dt} = \frac{\mathbf{p}_i}{ms} = \frac{\mathbf{p}'_i}{m} \quad (2.48)$$

$$\frac{ds}{dt'} = s \frac{ds}{dt} = \frac{p_s}{Q} s = \chi s \quad (2.49)$$

$$\frac{d\chi}{dt'} = \frac{s}{Q} \frac{dp_s}{dt} = \frac{s}{Q} \left\{ \frac{1}{s^3} \sum_i \frac{p_i^2}{m} - \frac{g+1}{s} k_B T \right\} = \frac{1}{Q} \left\{ \sum_i \frac{p'_i{}^2}{m} - (g+1)k_B T \right\} = \frac{\Phi}{Q} \quad (2.50)$$

$$\frac{dp'_i}{dt'} = \frac{d}{dt'} \left(\frac{\mathbf{p}_i}{s} \right) = s \frac{d}{dt} \left(\frac{\mathbf{p}_i}{s} \right) = \frac{d\mathbf{p}_i}{dt} + s \mathbf{p}_i \frac{d}{dt} \left(\frac{1}{s} \right) = \mathbf{F}_i - \frac{\mathbf{p}_i p_s}{s Q} = \mathbf{F}_i - \chi \mathbf{p}'_i \quad (2.51)$$

$\chi = \frac{p_s}{Q}$ represents the friction due to the thermostat and $\Phi = Q \frac{d\chi}{dt'}$ is the force acting on the thermostat.

The motion of the system can now be determined without reference to s . The variable $\frac{d\chi}{dt'}$ is a function of \mathbf{p}' only, so the complete description of the system can be given in terms of \mathbf{r} , \mathbf{p}' and real time t' . We have eliminated \mathbf{p} , s , P_s and t . Now let ζ be the coordinates of the thermostat so that $\chi = \frac{d\zeta}{dt'}$. This gives

$$\zeta = \int \chi dt' = \int_0^s \frac{ds}{s} = \ln s. \quad (2.52)$$

In the Hoover representation of the equations of motion, s has been eliminated thus the number of degrees of freedom goes from $3(N + N_S) + 1$ to $3(N + N_S)$ and consequently $g = 3(N + N_S) - 1$. The Hoover Hamiltonian is

$$\mathcal{H}_H = \sum_i \frac{\mathbf{p}'_i{}^2}{2m} + \mathcal{U}(\mathbf{r}) + \frac{1}{2} Q \chi^2 + (g+1)k_B T \zeta \quad (2.53)$$

A good source of information on the Nosé–Hoover thermostat can be found in Toxvaerd [93], Evans and Morriss [90], Martyna et al. [96].

The Nosé–Hoover equations of motion were integrated with a Verlet leap-frog algorithm which is implemented as follows:

(1). Calculate the initial thermostat force from Eq. (2.50)

(2). Perform a full coordinate advance and a velocity half-advance

$$\mathbf{r}_i(t + \Delta t) = \mathbf{r}_i(t) + \mathbf{v}_i(t) \Delta t + \frac{1}{2} \left\{ \frac{\mathbf{F}_i(t)}{m} - \chi(t) \mathbf{v}_i(t) \right\} \Delta t^2 \quad (2.54)$$

$$\mathbf{v}_i \left(t + \frac{\Delta t}{2} \right) = \mathbf{v}_i(t) + \frac{\Delta t}{2} \left\{ \frac{\mathbf{F}_i(t)}{m} - \chi(t) \mathbf{v}_i(t) \right\} \quad (2.55)$$

(3). Similarly, advance the thermostat coordinate and half-advance its friction

$$\zeta(t + \Delta t) = \zeta(t) + \chi(t)\Delta t + \frac{1}{2} \frac{\Phi}{Q} \Delta t^2 \chi\left(t + \frac{\Delta t}{2}\right) = \chi(t) + \frac{1}{2} \frac{\Phi}{Q} \Delta t \quad (2.56)$$

(4). Provisionally advance the velocities and the friction term

$$\mathbf{v}_i^p(t + \Delta t) = \mathbf{v}_i\left(t + \frac{\Delta t}{2}\right) + \frac{\Delta t}{2} \left\{ \frac{\mathbf{F}_i(t)}{m} - \chi\left(t + \frac{\Delta t}{2}\right) \mathbf{v}_i\left(t + \frac{\Delta t}{2}\right) \right\} \chi^p(t + \Delta t) \quad (2.57)$$

$$= \chi\left(t + \frac{\Delta t}{2}\right) + \frac{\Phi}{Q} \frac{\Delta t}{2} \quad (2.58)$$

(5). Evaluate the provisional forces \mathbf{F}_i^p and Φ^p at $t + \Delta t$. After this, the advancement of the velocities and friction needs to be corrected by first evaluating the time derivatives.

$$\dot{\chi} = \frac{\Phi^p}{Q} \dot{\mathbf{v}}_i = \mathbf{F}_i^p - \chi^p \times \mathbf{v}_i^p \quad (2.59)$$

These derivatives are then used to advance the velocities by a half time step.

$$\mathbf{v}_i^p(t + \Delta t) = \mathbf{v}_i\left(t + \frac{\Delta t}{2}\right) + \frac{\Delta t}{2} \dot{\mathbf{v}}_i \chi^p(t + \Delta t) = \chi\left(t + \frac{\Delta t}{2}\right) + \frac{\Delta t}{2} \dot{\chi} \quad (2.60)$$

The whole procedure is repeated until convergence of the velocities and the thermostat friction are achieved.

Note that initial velocities are assigned so as to reflect equilibrium at the desired temperature T (a Maxwellian distribution), without introducing a net translation or rotation of the system. Finally, a good test for this thermostat is to check if the total energy of the extended system is conserved.

2.2.3 Physical quantities and parameters

Fundamental quantities and units

Lennard–Jones units of mass (m), length (σ), energy (ϵ) and time ($\tau_0 = \sigma \sqrt{\frac{m}{\epsilon}}$) are used throughout this work. m is the mass of one Lennard–Jones particle, σ is the distance to zero in $\mathcal{U}_{lj}(r_{ij})$ and ϵ is the energy at the minimum in $\mathcal{U}_{lj}(r_{ij})$. The units will be set so that $m = \sigma = \epsilon = 1$ and consequently $\tau_0 = 1$.

The Lennard–Jones potential was fitted to experimental data for liquid argon and its parameters were evaluated: $\epsilon/k_B \approx 120K$ and $\sigma \approx 0.34nm$ (Haile [92], Allen and Tildesley [87]). Furthermore, the atomic mass of argon is $m \approx 7 \times 10^{-26}kg$ and therefore $\tau_0 \approx 2 \times 10^{-12}s$. Even though our system is not composed of liquid argon, these parameters can still give us an idea of the order of magnitude.

Simulation parameters

Since we work in the (NVT) canonical ensemble, the number of particles (N monomers and N_S solvent particles), the volume of the simulation box, V , and the average temperature, T , of the system are fixed. We can then determine a fixed number density for the system given by $\rho = \frac{(N+N_S)\sigma^3}{V}$.

For all our simulations, we used a time step $\Delta t = 0.005\tau_0$ ($\Delta t \approx 10^{-14}s$ for liquid argon) and checked that this value is compatible with the stability of the integration of the equation of motion. The value of Γ was fixed at $\Gamma = 0.5\tau_0^{-1}$ ($\Gamma \approx 0.25 \times 10^{12}s^{-1}$ for liquid argon).

Physical quantities at time t

(1). System

- (a). The total kinetic energy, $\mathcal{K}(t) = \mathcal{K}_M(t) + \mathcal{K}_S(t)$ where $\mathcal{K}_M(t) = \frac{1}{2}m \sum_{i=1}^N v_i^2(t)$ is the total kinetic energy of the monomers and $\mathcal{K}_S(t) = \frac{1}{2}m \sum_{i'=1}^{N_S} v_{i'}^2(t)$ is the total kinetic energy of the solvent particles.
- (b). The total energy, $E(t) = \mathcal{U}(t) + \mathcal{K}(t)$.
- (c). The temperature at time t , $T^*(t)$ as calculated by the equipartition of kinetic energy theorem. Each component of the average kinetic energy makes the same contribution to the temperature, $k_B T^* = \frac{\mathcal{K}(t)}{3/2(N+N_S)}$, as calculated from the equipartition theorem.

(2). Polymer

- (a). The radius of gyration square: $R_{gy}^2 = \frac{1}{N} \sum_{i=1}^N (\mathbf{r}_i - \mathbf{r}_{CM})^2$ where \mathbf{r}_{CM} is the coordinate of the centre of mass of the polymer.
- (b). The end-to-end distance square: $R_{end}^2 = |\mathbf{r}_N - \mathbf{r}_1|^2$.
- (c). The number of contacts between monomers n_{MM} and monomers and solvent particles n_{MS} . The number of contacts is the number of monomers/solvent particles that are within a distance of 1.5σ of each other.

Statistical quantities monitored in the simulations

Statistical physics usually treats infinite systems ($N \rightarrow \infty$) for which boundary conditions play no role. According to the ergodic hypothesis: given a Hamiltonian $\mathcal{H}(x_i)$ and a physical quantity $A = A(x)$, we have $\bar{A} = \langle A \rangle$ where \bar{A} is the ensemble average and $\langle A \rangle$ is the time average:

$$\bar{A} = \frac{1}{Z} \int_{\Omega} A(x) f(\mathcal{H}(x)) dx, \quad (2.61)$$

$$\langle A \rangle = \lim_{t \rightarrow \infty} \frac{1}{t} \int_0^t A(x(t)) dt. \quad (2.62)$$

Here, Z is the partition function:

$$Z = \int_{\Omega} f(\mathcal{H}(x)) dx, \quad (2.63)$$

$$f(\mathcal{H}(x)) = e^{-\beta \mathcal{H}}. \quad (2.64)$$

However, the partition function is not available from our MD simulations since we follow real dynamics for a long time ($t >$ relaxation time), and we therefore measure the value of A along this natural path. Hence our averages will all be time averages. Since we do not sample continuously in time we need to replace the integral in Eq. (2.62) by a summation:

$$\langle A \rangle = \frac{1}{N_t} \sum_{n=1}^{N_t} A(t_n) \quad (2.65)$$

In practice, we always have $\bar{A} \cong \langle A \rangle$ because the ensemble integral is always approximate and/or the integration over time is not infinite. The initial conditions can also create ergodicity problems, and so we need a sufficiently long warm-up of the system before starting the data collecting process. This information can be found in Slater [93a] [93b] and Haile [92]. We next describe the specific equilibrium and relaxational quantities measured in the simulations.

(1). Equilibrium properties (time average)

We study the equilibrium properties of our random heteropolymer in order to determine a “phase diagram” which allows us to find a characteristic temperature, referred to as the “theta point” T_{Θ} , which separates the extended coil state from the collapsed state. In most models similar to ours, the collapse transition

is driven by a variation in the temperature or by a change in the strength of the hydrophobic force. Such a transition is considered to be second-order-like (or higher) in the limit of long polymers (Zhou et al. [97]). Without a “phase diagram” it would be difficult to perform systematic quenches in order to study the relaxational properties of a random heteropolymer. The following quantities are also calculated in our equilibrium simulations:

- (a). The time average of the temperature $\langle T^* \rangle \approx T$ where T is the temperature parameter from Eq. (2.28).
- (b). $\langle R_{yy}^2 \rangle$ and $\langle R_{yy}^2 \rangle_{coil}$ where $\langle R_{yy}^2 \rangle_{coil}$ is the $\langle R_{yy}^2 \rangle$ of the coil conformation, i.e. the maximal $\langle R_{yy}^2 \rangle$.
- (c). The time average of the end-to-end distance square $\langle R_{end}^2 \rangle$.
- (d). The time average of the number of contacts between monomers $\langle n_{MM} \rangle$ and the number of contacts between monomers and solvent particles $\langle n_{MS} \rangle$.
- (e). The pressure of the system, P , which is calculated from the virial equation:

$$\mathcal{P} = \rho k_B T + \frac{1}{dV} \left\langle \sum_i \sum_{j>i} \mathbf{F}(\mathbf{r}_{ij}) \cdot \mathbf{r}_{ij} \right\rangle \quad (2.66)$$

where d is the dimensionality of the system, $d=3$ throughout this dissertation. The time average quantity is the virial.

- (f). Some equilibrium properties of polymers are known. For example, in the case of a single polymer in a solvent, we have the following asymptotic behavior as $N \rightarrow \infty$:

$$\langle R_{yy}^2 \rangle \propto N^{2\nu} \quad (2.67)$$

where ν is a universal scaling exponent. For a poor solvent $\nu = 1/d$, for a Θ -solvent (a solvent at the theta point) $\nu = 1/2$ and for a good solvent $\nu > 1/2$.

One of the basic properties of an isolated polymer chain is its size and shape under various solvent conditions. In poor solvent the monomers attract one another, and an isolated chain forms a compact globule, roughly spherical in shape, which minimizes the surface area between monomers and solvent.

In a Θ -solvent there is screening of the excluded volume effects and the chain conformation is described by a random walk (RW). For completely flexible chains in good solvent the monomers effectively repel one another, favoring contact with the solvent, and a swollen coil is formed. This is equivalent to a self avoiding walk (SAW) problem which cannot be solved exactly, except in one dimension. Flory obtained the following mean field expression $\nu = \frac{3}{d+2}$ where d is the dimensionality of the system. This result turned out to be exact for $d = 1$, $d = 2$ and $d \geq 4$ (in which case we have a RW). The best simulations in three dimensions give $\nu = 0.588\dots$. Furthermore, the amplitude ratio of the radius of gyration and the end-to-end distance also approach universal value in the limit $N \rightarrow \infty$:

$$\frac{\langle R_{gy}^2 \rangle}{\langle R_{end}^2 \rangle} \cong \frac{1}{(2\nu + 1)(2\nu + 2)}. \quad (2.68)$$

This is valid for two limits, $\nu = 1$ and $\nu = 1/2$. For convenience, we define

$$\varsigma = \frac{\langle R_{end}^2 \rangle}{6 \langle R_{gy}^2 \rangle}. \quad (2.69)$$

For a quasi ideal chain¹ in the limit of infinite chain length, des Cloizeaux and Jannink obtained $\varsigma = 1$ (des Cloizeaux and Jannink [90]). For chains with excluded volume interactions (self-avoiding chains), Sanchez predicted $\varsigma = 1.07$ with a pseudo-Gaussian model (Sanchez [69]). Computer simulation studies show $\varsigma = 1.06$ (Domb and Hioe [69]) and renormalization techniques give $\varsigma = 1.05$ (Witten and Schafer [78]). des Cloizeaux and Jannink predict $\varsigma = 1/3$ for the collapsed state of an isolated chain in a poor solvent (des Cloizeaux and Jannink [90]).

(2). Relaxational properties (ensemble average)

Once the theta point is located, we perform systematic quenches in order to examine the relaxation properties of the random heteropolymer. As with all problems involving stochastic properties, we averaged over several quench runs

¹We have a quasi ideal chain when the second virial coefficient is zero. There is no binary excluded volume interactions (*i.e.* Θ -solvent condition). We say that we have a completely ideal chain when all virial coefficients are zero.

(*i.e.* several random number generator seeds or several “replicas”) for the same initial conditions (*i.e.* same $\{\eta_{ij}\}$) to calculate the thermal average. We also performed averages over different realizations of the random interactions $\{\eta_{ij}\}$ (*i.e.* different random sequences) for a given α . Averages for the following quantities were calculated:

- (a). $\overline{E}(t) = \overline{U}(t) + \overline{K}(t)$
- (b). $\overline{T}^*(t)$
- (c). $\overline{n}_{MM}(t)$
- (d). $\overline{R}_{gy}(t)$
- (e). t_{50} is the time needed for $\overline{n}_{MM}(t)$ or $\overline{R}_{gy}(t)$ to increase/decrease by 50% of its range of values, *i.e.* by 50% $\{\overline{n}_{MM}(0) - \overline{n}_{MM}(t \rightarrow \infty)\}$ or 50% $\{\overline{R}_{gy}(0) - \overline{R}_{gy}(t \rightarrow \infty)\}$.
- (f). t_{90} is calculated similarly to t_{50} but in this case, we consider 90% of the range of values.

Note that in the context of temperature quenches, we will drop the bar to indicate the ensemble average to facilitate the writing of the labels on graphics.

Error analysis

In our work, there are both systematic errors mostly due to the simulation techniques used and statistical errors which are mostly related to the time limitations for computing the data. The systematic errors affect the accuracy of our results while the statistical errors affect their precision.

(1). Systematic errors

The most obvious source of systematic error is the finite size-effect. Thermodynamic properties of macroscopic size systems are defined in the limit of large systems (large number of degrees of freedom). Fortunately, this effect usually decreases as the inverse of the number of molecules and can be reasonably easily included within the statistical uncertainty.

As we have mentioned previously, the use of the Verlet algorithm contributes a local truncation error that varies as $(\Delta t)^4$. Furthermore, a round-off error can be associated with the implementation of this algorithm. These errors are affected by the number of significant digits kept at each stage of the calculation and by the order in which the calculation is performed. Smaller values of Δt reduces the error accumulated over the entire calculation but it increases the accumulation of round-off errors and vice-versa. It is important to choose the time step wisely.

The periodic boundary conditions can induce anisotropies in the fluid structure for small systems. Therefore we have made sure that our system was much larger than the recommended size of $N_S \approx 100$ (Allen and Tildesley [87]). Our system has at least 1000 solvent particles except for the very low density cases. Due to the short-range nature of our interactions, we did not have to consider other possible effects related to the periodic boundary conditions.

We have verified that the choice of our thermostat was not important to study the equilibrium of our system. Nevertheless, it does influence the kinetics of relaxation in some instances. We shall discuss this matter more deeply in Chapters 4 and 5 .

(2). Statistical errors

(a). Calculation of averages

In order to avoid serial correlations in our time averages, we performed our statistical sampling by coarse graining the computed phase-space trajectory into segments whose durations are longer than the relaxation time for the property that we are concerned with. This random sampling scheme can therefore be described by the Gaussian error distribution from which we can calculate the standard deviation σ .

$$\sigma_{n-1} = \sqrt{\sum_{i=1}^n \frac{(x_i - \bar{x})^2}{n-1}} \quad (2.70)$$

where x_i is the i^{th} measurement of a given quantity x , \bar{x} is the average of x and n is the number of measurements we performed. The probability of

having a given measurement fall within σ of the mean value is about 68% and the probability of having a given measurement fall within 2σ is 95%. As a convention we will always describe the uncertainties on our statistical measurements as being σ ($x_i \pm \sigma$). Furthermore, the standard error of the mean is $\frac{\sigma}{\sqrt{n}}$ ($\bar{x} \pm \frac{\sigma}{\sqrt{n}}$).

(b). Curve fits

We used the least-squares fitting method which minimizes the weighted sum of the squares of the deviations, χ^2 . We will not describe this method in detail since we used commercial graphics programs to fit our curves. A good description of this method including the uncertainty calculations on the parameters of the fitted function can be found in Bevington and Robinson [92].

3

RANDOM HETEROPOLYMER WITHOUT SOLVENT

Various studies of the collapse kinetics of short random heteropolymers as a model for protein folding kinetics can be found in Iori, Marinari and Parisi [91]; Iori et al. [92], Struglia [95] and Fugugita, Lancaster and Mitchard [92]. One motivation for studying random heteropolymers is that while homopolymers exhibit a coil and a collapsed or globule phase, random heteropolymers exhibit an additional glassy phase just like proteins. They found that the properties of this glassy phase are completely different from the globule phase resulting from the homopolymer coil-globule transition. Furthermore, according to Iori, Marinari and Parisi [91] the globular phase of a homopolymer has no particular shape, whereas the glassy phase of a random heteropolymer has a definite frozen shape which is a “closed globule”. It is possible to make an analogy between the glassy phase of random heteropolymers and the unique native conformation of proteins in that the number of corresponding energy levels are few and have considerably lower energy than the globular states of homopolymers.

Iori *et al* also investigated the collapse kinetics using Monte Carlo simulations of a heteropolymer model composed of 15 monomers with a large degree of quenched disorder. The internal energy of the system as a function of Monte Carlo time was monitored when the temperature is quenched from a high value to a lower one. It was found that the time course of the internal energy fits very well to a stretched exponential form for quenches to a final temperature which is not too low. The values of the stretched exponent, β , were found to be $\beta \simeq 0.54$ and $\beta \simeq 0.38$ respectively for two sets of the final temperature, with the smaller β corresponding to the lower of the two final temperatures. The same fitting procedure yielded a pure exponential kinetic behavior for the equivalent homopolymer, *i.e.*, $\beta = 1$ if there are no random interactions. Iori et al. [92] also made a Langevin analysis for the relaxation to the

collapsed phase and again found a stretched exponential behavior for the relaxation to the collapsed phase on short time scales (compared to the experimental work on proteins of Iben *et al.* [89] which predicts time scales of the order of seconds).

While the previous calculations give us considerable intuition into the physics of the collapse kinetics of heteropolymers, there are nevertheless many questions which remain unclear. First of all, we expect that the relaxation kinetics of a heteropolymer with random interactions between monomers should depend on the final temperature which can be characterized in several regimes. One can easily imagine that quenching the temperature from above T_Θ but remaining above, from above to below, and from below to below, should lead to different forms of the relaxation. Secondly, from a statistical physics point of view, we believe that the most useful approach to understand the kinetics of protein or heteropolymer collapse is based on the search for universal features in the collapse process. Such universal properties which are generally related to the scaling regime do not depend on details of the chemical nature of the individual monomer groups (de Gennes [79]; Zwanzig [95]). Skorobogatyy, Guo and Zuckermann [97b] made a general study of such features as the dependence of the collapse time on the energy level structure and the level spacing distributions for a simple protein folding model.

In this chapter we use molecular dynamics simulations as described in Chapter 2 to examine in detail the kinetics of formation of random heteropolymer conformations in the absence of an explicit solvent by applying temperature quenches (Villeneuve, Guo and Zuckermann [97]). The Hamiltonian for this case can be obtained directly from Eqs. (2.1) and (2.2) and is given by:

$$\begin{aligned}\mathcal{H} &= \mathcal{U}_{MM} + \mathcal{K}_M \\ &= \sum_{i=1, j=i+1}^{N-1} \mathcal{U}_{Spring}(r_{ij}) + \sum_{i=1}^N \sum_{j>i}^N \mathcal{U}_{RLJ}(r_{ij}) + \sum_{i=1}^N \sum_{j>i}^N \mathcal{U}_{Dis}(r_{ij}, \eta_{ij}) + \mathcal{K}_M.\end{aligned}\quad (3.1)$$

This Hamiltonian is similar to that of Iori *et al.* [91]; [92] and consists of the following interactions: a harmonic term between nearest neighboring monomers of the heteropolymer given by Eq. (2.8), a purely repulsive Lennard–Jones potential between all monomers given by Eq. (2.10) and an additional $1/r^6$ potential whose coupling constant is chosen from a Gaussian distribution of width, α , as given by Eq. (2.12).

This Gaussian represents the degree of quenched random interactions between the monomers.

In order to investigate the collapse kinetics after a temperature quench, we first make a study, in Section 3.1, of the “phase diagram” of the random heteropolymer as a function of both temperature, T , and the strength of the random interaction, α . In particular we calculate the “phase line” between the extended state and the collapsed state which gives the locus of the theta point, T_Θ . Once this “phase line” is located, the relaxation kinetics are studied in Section 3.2 by performing systematic temperature quenches from the extended “phase” to the collapsed “phase” for which two time relaxation regimes were observed. Both relaxation processes were characterizable by stretched exponentials, one of which was found to be generic. Section 3.2 also gives details of the related conformations of the random heteropolymer. Section 3.3 contains a summary and concludes this chapter.

3.1 Equilibrium considerations

In this section we present results obtained from equilibrium simulations for several values of α ranging from 0 to 6. In particular we calculate T_Θ as a function of the strength of the random interactions, α . Since we are primarily interested in the relaxational dynamics and since the location of T_Θ gives us an indication of where temperature quenches should be performed, we calculated values of T_Θ which are accurate enough for our purposes. A precise determination of this quantity requires considerable computer time and is beyond the scope of this work. For a homopolymer, the theta point was located by Grest and Murat [93] by studying the scaling of the radius of gyration, R_{gy} , of the polymer as a function of the polymer length N . The relevant scaling law in the homopolymer case is given by $R_{gy}^2 \propto N^{2\nu}$. Above T_Θ , $\nu = 3/5$; at T_Θ , $\nu = 1/2$; while below T_Θ , $\nu = 1/3$. Here we use the same procedure to locate T_Θ for the random heteropolymer.

In all the calculations reported here, the value of the unstretched bond length was taken to be $R_0 = 1.5\sigma$ and the value of the coupling constant, k , for the harmonic interaction of Eq. (2.8) used in the simulations was chosen as $k\sigma^2/\epsilon = 30$. The number of monomers per heteropolymer used to study the equilibrium conformations

in order to determine an approximate “phase diagram” by locating T_Θ was varied from $N = 30$ to $N = 200$ for values of α ranging from 0 to 6. All quantities described below will be in Lennard–Jones reduced units. Distances are expressed in terms of σ , temperatures in terms of k_B/ϵ , and time in terms of $\sqrt{m\sigma^2/\epsilon}$ where m is the mass of each monomer.

The initial polymer conformation was taken to be a self avoiding random walk for all simulations reported in this chapter. Next molecular dynamics simulations using the Langevin method described in Chapter 2 and involving the interactions given by Eq. (3.1) were performed. The random heteropolymers were equilibrated using 3×10^6 time steps per monomer for $N \geq 100$ and 10^6 time steps per monomer for $N = 30$. Several physical quantities were collected at equal time intervals for time averaging after equilibration. Typically these quantities were saved every 3000 time steps per monomer up to a total of 1000 sets of data.

When $\alpha = 0$, the Hamiltonian of Eq. (3.1) reduces to the Hamiltonian for a homopolymer in a good solvent as described by a repulsive L-J interaction. The theta point in this case is therefore zero. To verify that our simulation method gives the correct scaling in the homopolymer limit, we computed $\langle R_{gy}^2 \rangle$ for $N = 30, 75, 100, 150, 200$ for $\alpha = 0$ and for two temperature values. We found that $\langle R_{gy}^2 \rangle \propto \alpha N^{2\nu}$ with $\nu \approx 0.586$ for $T = 4$, and $\nu \approx 0.607$ for $T = 0.1$, as expected.

Since the theta point is zero for $\alpha = 0$, the existence of a non-zero theta point for $\alpha \neq 0$ for our random heteropolymer model is entirely due to the random interactions. Figure 3.1 (a) shows the logarithm of $\langle R_{gy}^2 \rangle/N$ as a function of N for $\alpha = 3$ and for four different values of T . In this case values of $N = 50, 75, 100, 125, 150, 175$ and 200 were used. The figure shows that the theta point should have a value close to $T \simeq 2$. Figure 3.1 (b) shows the result for $\alpha = 6$. For this and other larger values of α , it is difficult to obtain a precise value of T_Θ due to large fluctuations in the data. However from the figure it is reasonable to assume that it lies in the neighborhood of $T = 8$. For both $\alpha = 3$ and 6 we found that $\langle R_{gy}^2 \rangle \propto \alpha N^{2\nu}$ with $\nu \simeq \frac{3}{5}$ for temperatures above the theta point and that $\nu \simeq \frac{1}{3}$ for temperatures below it, provided that the temperature is not too low (for which case the simulation is hampered by metastable states). Near the theta point, we find that $\nu \simeq \frac{1}{2}$, as expected. The presence of a theta point, T_Θ , is

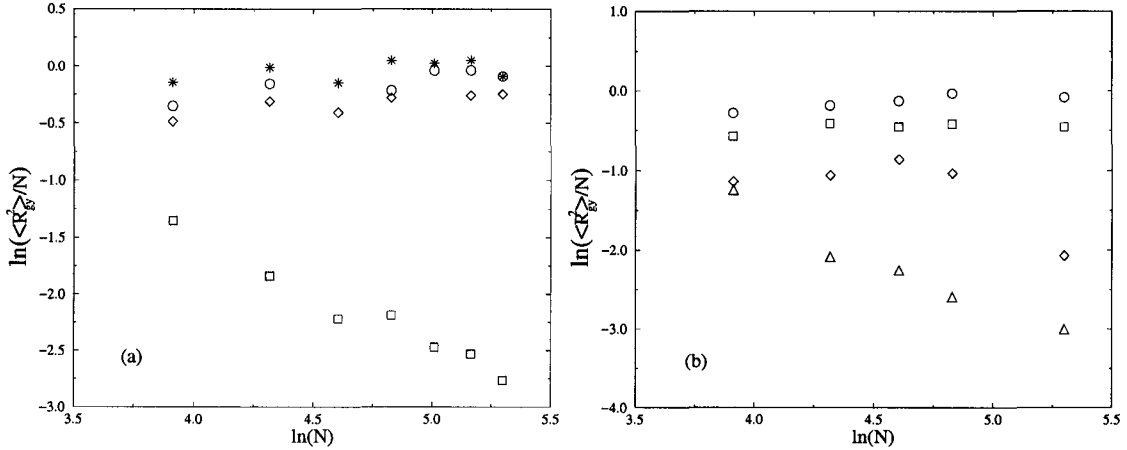


Figure 3.1: (a) Average radius of gyration versus N for random heteropolymers with $\alpha = 3$ for $N = 50$ to 200 and for temperatures $T = 8$ (*), $T = 4$ (○), $T = 3$ (◇) and $T = 2$ (□). $T = 8, 4, 3$ are above T_Θ , where $\langle R_{gy}^2 \rangle \propto N^{2\nu}$ with $\nu \approx 0.59$. $T = 2$ is lower than T_Θ . The theta point lies between $T = 2$ and $T = 3$. (b) Average radius of gyration versus N for random heteropolymers with $\alpha = 6$ for length $N = 30$ to 200, and for temperatures $T = 10$ (○), $T = 8$ (□), $T = 7$ (◇) and $T = 6$ (△). $T = 10$ is above T_Θ with $\langle R_{gy}^2 \rangle \propto N^{2\nu}$ where $\nu \approx 0.57$. $T = 8$ is close to T_Θ with $\nu \approx 0.50$. $T = 7, 6$ are below T_Θ .

also consistent with the behavior of $\langle R_{gy} \rangle$ as a function of temperature. Furthermore we confirmed that in the neighborhood of the theta point, $\langle R_{gy} \rangle$ changes from a small value below T_Θ to a much larger value above T_Θ , indicating a conformation change of the heteropolymer from a compact to an extended structure.

Although it is quite difficult to determine a precise value of T_Θ , it is to be expected that the effective value of T_Θ as determined by our simulation procedure increases considerably with increasing α . This is shown in the inset of Figure 3.2 where $\langle R_{gy} \rangle$ is shown as a function of temperature for several values of α fixing $N = 100$. From this graph we operationally take T_Θ as the temperature at which $\langle R_{gy} \rangle = 6.0$, this being in the mid-point of its values. The values of T_Θ deduced in this manner from the inset of Figure 3.2 are shown in Figure 3.2 which thus serves as a “phase diagram” for the heteropolymer model studied here. The nature of the equilibrium conformation can be examined directly from the final structures of the heteropolymer and we have confirmed that these structures are consistent with the “phase diagram”. Finally, in order to test the stability of our simulations we calculated the average bond length of the polymer as a function of T , N and α . We found that the bond length increases with T in all cases but remains bounded below by 2.0σ up to $T = 10$. Hence the

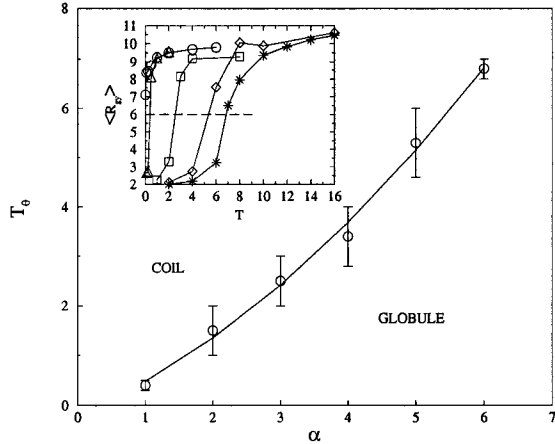


Figure 3.2: T_E versus α for $N = 100$. The values of T_E were measured at the points of inflection of the inset and the error bars were estimated by using Figure 3.1, and related results for $\alpha = 1$ and $\alpha = 5$. This plot serves as an effective “phase diagram”. The solid line is a guide to the eye. Inset: Average radius of gyration as a function of temperature for $N = 100$ and $\alpha = 1$ (Δ), 3 (\square), 5 (\diamond), and 6 ($*$). The horizontal line at $\langle R_{gy} \rangle = 6.0$ corresponds to the point of inflection at which we measured T_E for different values of α . The solid lines are guides to the eye.

average bond length remains reasonably close to its initially chosen value of 1.5σ and exhibits no unusual behavior throughout the entire simulation procedure.

In the next section we study the relaxational dynamics of the heteropolymer after temperature quenches in various regions of the “phase diagram” of Figure 3.2.

3.2 Kinetics of relaxation

The relaxational dynamics of the random heteropolymer described by Eq. (3.1) is investigated by quenching the temperature from an initial value T_I to a final value at T_F , and monitoring the time evolution of the relevant physical quantities. Our “phase diagram” allowed us to examine the relaxation behavior by choosing the temperatures T_I and T_F systematically for the related quenches. The quenches were performed by first bringing the polymer to thermal equilibrium at T_I and then quenching to T_F . To study the relaxational dynamics after a temperature quench, for a given initial equilibrium conformation, 10^5 time steps per monomer were used and the relaxation process was monitored. The results were then averaged over 100 to 500 independent quench runs for the same initial condition. Finally, up to 16 impurity averages for different realizations of $\{\eta_{ij}\}$ for a given α were performed for a given set of the

remaining system parameters.

In the homopolymer case where $\alpha = 0$, exponential relaxation behavior was always observed as expected. For the random heteropolymer case where $\alpha \neq 0$, we examined polymers of length $N = 30$ for $\alpha = 2, 3, 4, 5, 6$ and $N = 100$ for $\alpha = 6$. As mentioned previously, 100 to 500 independent quench runs were averaged for a given $\{\eta_{ij}\}$ to reduce fluctuations in the data since the only difference between each quench run is the thermal noise. The total energy $E(t)$ of the polymer was calculated as a function of time t and was fitted to a stretched exponential form given by

$$E(t) = a_0 e^{-(t/\tau)^\beta} - a_1 \quad (3.2)$$

Here the time t was measured in units of τ_0 . One unit of time is thus equivalent to 200 MD steps. The parameters a_0, β, τ and a_1 were obtained by using a chi-square fit. These values were then impurity averaged¹. For $N = 30$ we performed an impurity average over 8 different realizations of the random interactions $\{\eta_{ij}\}$ for a given α , while 16 such realizations were used for $N = 100$. We found that impurity averaging was vital in determining a reasonably accurate value for the relaxational exponent β .

Exponential relaxation behavior ($\beta = 1$) was always observed when both T_I and T_F were chosen to be in the extended "phase", *i.e.* above the theta point. This is shown in Figure 3.3 for $N = 30$, $\alpha = 6$, $T_I = 16$ and $T_F = 10$. The values of β and τ are tabulated in Table 3.1 and for quenches above the theta point, β is consistently close to unity for all values of α used. We in fact showed that the data for $N = 100$ and $\alpha = 6$ were also well fitted to a pure exponential above the theta point. This behavior is understandable since above the theta point, the heteropolymer in question is extended and thus the random interactions $\{\eta_{ij}/r_{ij}^6\}$ play only a small role because they decay quickly for monomers far away from one another in this case. Under these circumstances the random heteropolymer should therefore behave like a homopolymer.

The quenches of interest for the problem of random heteropolymer collapse are those performed across the line of theta points in the "phase diagram", *i.e.* from the extended to the collapsed states. For this case T_I was chosen to be well above

¹For a given set of random interactions $\{\eta_{ij}\}$, many quench runs were performed in order to obtain the thermal average. The relaxation of the energy $E(t)$ was then averaged over several independent sets $\{\eta_{ij}\}$.

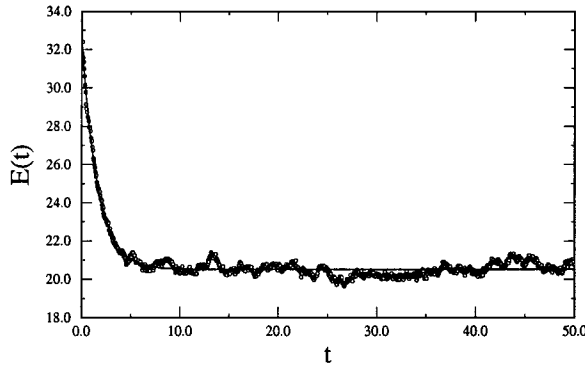


Figure 3.3: Energy versus time for a random heteropolymer after a temperature quench with parameters $\alpha = 6$, $N = 30$, $T_I = 16$ and $T_F = 10$. Both temperatures are above the theta point. From the stretched exponential fit we find $\beta \approx 1.01$ and $\tau \approx 1.63$. Hence this relaxation is a pure exponential. The solid line is the fit to Eq. (3.2).

T_Θ while T_F was below T_Θ . It turned out that if T_F was too low, the simulations were hampered by metastable states and the polymer could not relax to a collapsed equilibrium conformation. Hence we chose the value of T_F to lie not too far below the theta point and monitored the final conformation to ensure that the system was not trapped in an extended metastable state.

We examined the relaxation to equilibrium for quenches over the theta point for long polymers in order to investigate the collapse process in detail. In particular we examined the case of a random heteropolymer of length $N = 100$ in detail for $\alpha = 6$, $T_I = 16$, $T_F = 6$. As before, the energy $E(t)$ was calculated as a function of t and fitted to Eq. (3.2) and the results are summarized in Table 3.2. Out of the 16 realizations of $\{\eta_{ij}\}$, we found that 15 data sets exhibited two relaxational time regimes: a fast relaxation from which partial collapse resulted, followed by a crossover to a considerably slower regime at the end of which the collapse process was complete. The relaxation behavior in both regimes could be fitted to a stretched exponential of the form given in Eq. (3.2). In the first time regime, as shown in Table 3.2, a stretched exponent $\beta \approx 0.7$ with time constant $\tau \sim 1.2$ was determined. These are completely consistent with the values found for $N = 30$ and $\alpha \neq 0$ to be reported below. In the second relaxation regime β was found to be approximately 0.2, a very small value indeed. Figure 3.4 gives relaxation data which showed the two regimes

for one simulation together with the fits using Eq. (3.2).

Why are there two relaxational time regimes? To answer this question we drew typical conformations of the polymer during the relaxation process at various time intervals, as shown in Figure 3.5. At early times, from $t = 0$ to $t = 30$, where the stretched exponent $\beta \approx 0.7$, the conformations show that the collapse is only *local*, where the overall conformation is still extended while locally the monomers collapse into separate “blobs”. If we now calculate $\langle R_{yy} \rangle$ at $t = 30$, its value is still close to that of an extended polymer. By examining all the 15 simulations which exhibit two relaxation regimes, we concluded that the first time regime was due to the local collapse. After the first time regime, the collapse process enters a crossover regime where the local blobs coalesce to form larger blobs, as shown in the figure corresponding to $t = 75$ in Figure 3.5. At this stage the polymer has not completely collapsed but is certainly not extended, and from the point of view of protein folding this may be regarded as being analogous to a molten globule conformation. Finally the collapse process enters the second time regime, which goes approximately from $t = 100$ to the end of our simulation where the polymer is completely collapsed, with an exponent $\beta \approx 0.2$. We conclude that the second relaxation regime, with a small stretched exponent $\beta \approx 0.2$, is due to the collapse of local blobs to the final compact equilibrium state. Clearly, because blobs are much more difficult to move, the collapse of local blobs should be much slower which is reflected by the small value of β . Finally the only one among the 16 simulations which did not exhibit a second time regime appeared to be trapped in the crossover regime. This could be due to anomalous arrangements of the random interactions $\{\eta_{ij}\}$. However, our simulations mostly show that the relaxation during a temperature quench from an extended to a collapsed state is a two stage process in which each process is characterized by a stretched exponential form.

How generic is the value of the stretched exponent? We examined this question by performing temperature quenches over the theta point for a number of values of the strength of the random interactions, $\alpha = 2$ to 6. As the simulations were found to be computationally intensive, we have used shorter chains of $N = 30$. For these shorter heteropolymers we did not always observe two regimes and some relaxations

across the "theta point"	$\alpha = 2, T_I = 4, T_F = 0.5$	$\alpha = 3, T_I = 4, T_F = 1$	$\alpha = 4, T_I = 6, T_F = 1$	$\alpha = 5, T_I = 10, T_F = 4$	$\alpha = 6, T_I = 16, T_F = 6$
$\langle \beta \rangle$	0.75 ± 0.03	0.70 ± 0.02	0.65 ± 0.04	0.68 ± 0.05	0.62 ± 0.06
$\langle \tau \rangle$	1.41 ± 0.04	1.54 ± 0.05	1.54 ± 0.04	1.43 ± 0.06	1.0 ± 0.2
within the extended phase	$\alpha = 2, T_I = 4, T_F = 2$	$\alpha = 3, T_I = 10, T_F = 4$	$\alpha = 4, T_I = 6, T_F = 4$	$\alpha = 5, T_I = 10, T_F = 7$	$\alpha = 6, T_I = 16, T_F = 10$
$\langle \beta \rangle$	0.97 ± 0.02	1.02 ± 0.02	0.88 ± 0.08	0.9 ± 0.2	1.01 ± 0.05
$\langle \tau \rangle$	1.42 ± 0.02	1.51 ± 0.02	1.6 ± 0.1	1.5 ± 0.1	1.59 ± 0.05
within the folded phase	$\alpha = 2, T_I = 1, T_F = 0.5$			$\alpha = 5, T_I = 4, T_F = 2$	$\alpha = 6, T_I = 6, T_F = 4$
$\langle \beta \rangle$	0.38 ± 0.05			0.49 ± 0.07	0.32 ± 0.06
$\langle \tau \rangle$	3 ± 6			7 ± 1	4 ± 1

Table 3.1: $\langle \beta \rangle$ and $\langle \tau \rangle$ resulting from the average over eight realizations of the random interaction $\{\eta_{ij}\}$ for $N = 30$. The first row consists of results from relaxations across the theta point. The second row presents the relaxations within the extended states. The third row results from quenches within the collapsed states. T_I and T_F are the initial and final temperatures respectively.

across the "theta point"	$\alpha = 6, T_I = 16, T_F = 6, t = 0 \text{ to } 30$	$\alpha = 6, T_I = 16, T_F = 6, t = 100 \text{ to } 500$
$\langle \beta \rangle$	0.69 ± 0.02	0.19 ± 0.02
$\langle \tau \rangle$	1.17 ± 0.04	25 ± 5

Table 3.2: $\langle \beta \rangle$ and $\langle \tau \rangle$ resulting from the average over several realizations of the random interaction $\{\eta_{ij}\}$ for $N = 100$. All quenches were performed across the theta point. Times $t = 0$ to $t = 30$ corresponds to the first relaxation regime, and $t = 100$ to $t = 500$ corresponds to the second time regime. $\langle \beta \rangle$ and $\langle \tau \rangle$ were averaged over sixteen realizations for the first relaxation regime and fifteen realizations for the second regime.

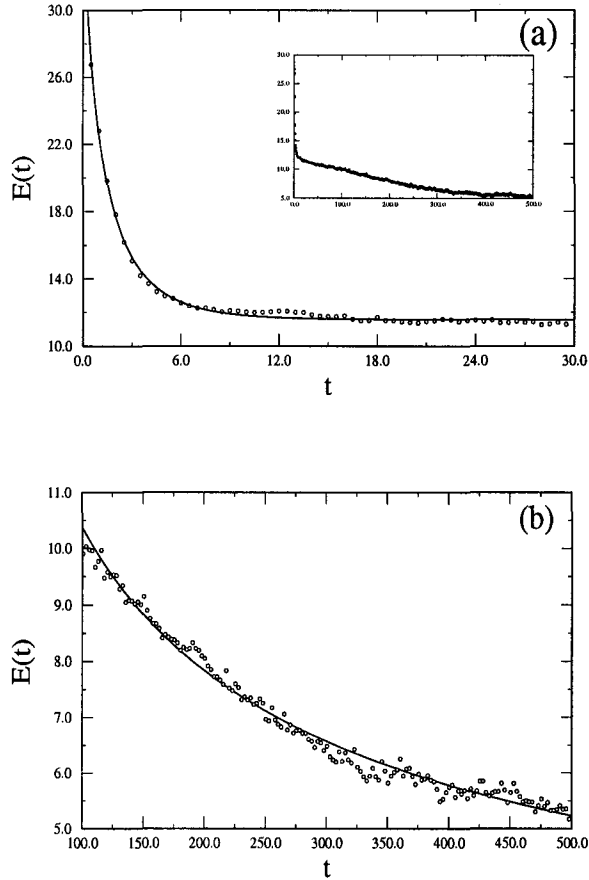


Figure 3.4: Energy as a function of time for a random heteropolymer after a temperature quench with parameters $\alpha = 6$, $N = 100$, $T_I = 16$ (above the theta point) and $T_F = 6$ (below the theta point). Two relaxation regimes are found. (a) First time regime, from $t = 0$ to 30. The stretched exponential fit gives $\beta \approx 0.73$ and $\tau \approx 1.19$. The inset shows the complete relaxation curve from $t = 0$ to 500. (b) Second time regime, from $t = 100$ until the end of the simulation. Fitting to Eq. (3.2) gives $\beta \approx 0.25$ and $\tau \approx 8.71$ for this heteropolymer simulation in the second regime. Solid lines are the fit to Eq. (3.2).

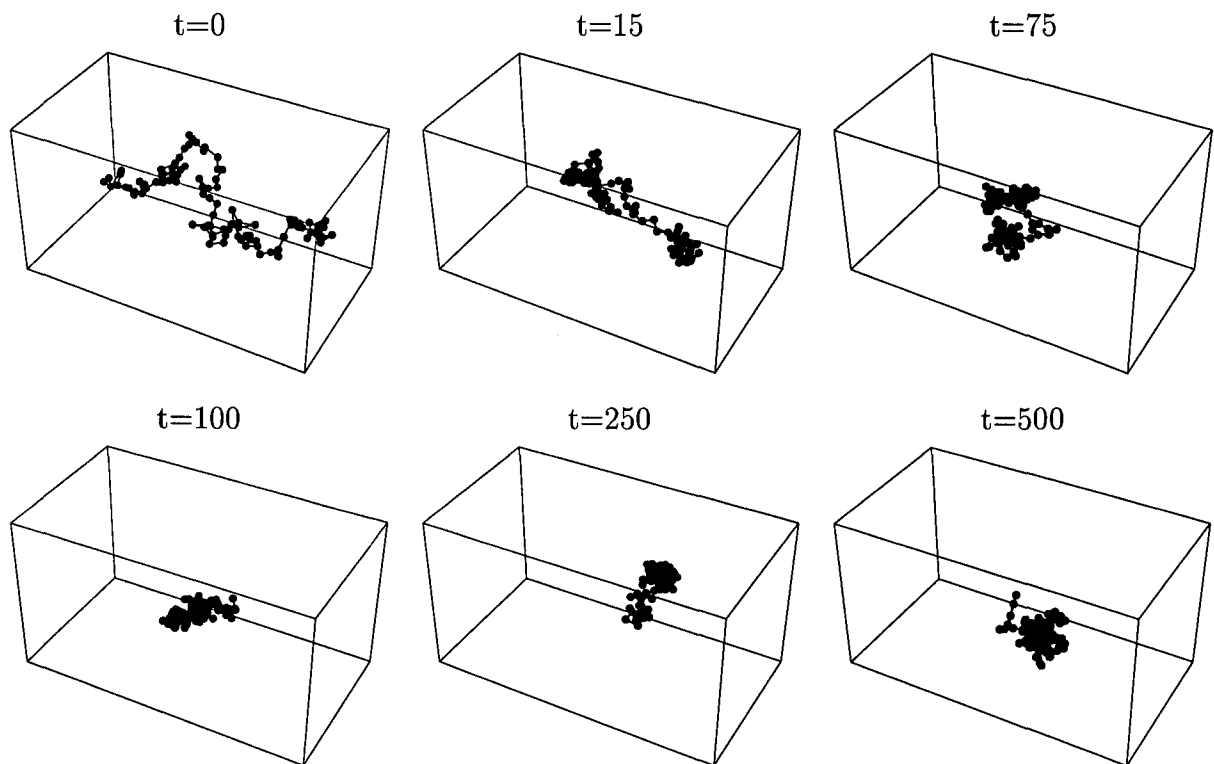


Figure 3.5: Snapshots of conformations for a random heteropolymer (the same polymer as used in Figure 3.4) at various times after a temperature quench, with parameters $\alpha = 6$, $N = 100$, $T_I = 16$ and $T_F = 6$. The first plot labeled $t = 0$ is the equilibrium conformation at $T_I = 16$ which serves as the conformation just before the quench. Other plots represent conformations at different times during the relaxation process. Local collapse is clearly seen before $t = 75$. The polymer is essentially collapsed at $t = 500$.

took place in a single regime. Since the chains are quite short, some of the chains manage to avoid local collapse relax directly to their compact conformations. The results for these simulations are summarized in Table 3.1 which clearly shows that $\beta \approx 0.7$ for all values of α studied for the first time regime. Typical relaxation data are shown in Figure 3.6 which gives $E(t)$ as a function of time for a single simulation and three values of α . The three sets of parameters were $\alpha = 2$, $T_I = 4$ and $T_F = 0.5$; $\alpha = 4$, $T_I = 6$ and $T_F = 1$; and $\alpha = 6$, $T_I = 16$ and $T_F = 6$.

Another question of interest is whether the overall shape of the relaxation curve as given by Eq. (3.2) and the value of the stretched exponent, β , depend on the simulation parameter Γ^{-1} which gives the characteristic time for coupling to the heat bath in the simulation. This question is clearly relevant for the first relaxation regime. To investigate this point, we performed quenches using $N = 30$ and $\alpha = 6$ for several values of Γ , *i.e.* $\Gamma^{-1} = 0.8\tau_0, 1.33\tau_0, 1.0\tau_0$ and $4.0\tau_0$ in addition to $2.0\tau_0$. For all the simulations we found the stretched exponent $\beta \approx 0.7$, independent of Γ . Hence the stretched exponential relaxation has a generic behavior. On the other hand, we expected that the time scale τ of the first relaxation regime would be affected by Γ ; we in fact found τ to be a linear function of Γ^{-1} as shown in Figure 3.7. Finally we found no detectable Γ dependence for the results of the second relaxation regime.

We also examined the second time regime observed in some of the relaxation curves for short chains with $\alpha = 6$ for the simulation shown in Figure 3.6. In this case we found that the relaxation could be characterized by a stretched exponent $\beta \approx 0.45$, in contrast to the case of $N = 100$ where $\beta \approx 0.2$. However we were not able to determine the stretched exponent, β , accurately for the second time regime for short chains, because the second relaxation regime is due to the collapse of local blobs as discussed above. This is because there is only a small number of blobs formed, resulting in a faster relaxation (larger β). For long chains, however, it is possible that the exponent of the second time regime will be determined by the motion of the blobs in a random environment, thus leading to a generic value of β .

Finally, we comment that for extremely short chains such as $N = 15$, the second time regime is not observed as there is essentially no local collapse and the entire chain simply collapses with only one stretched exponent. This behavior was found in

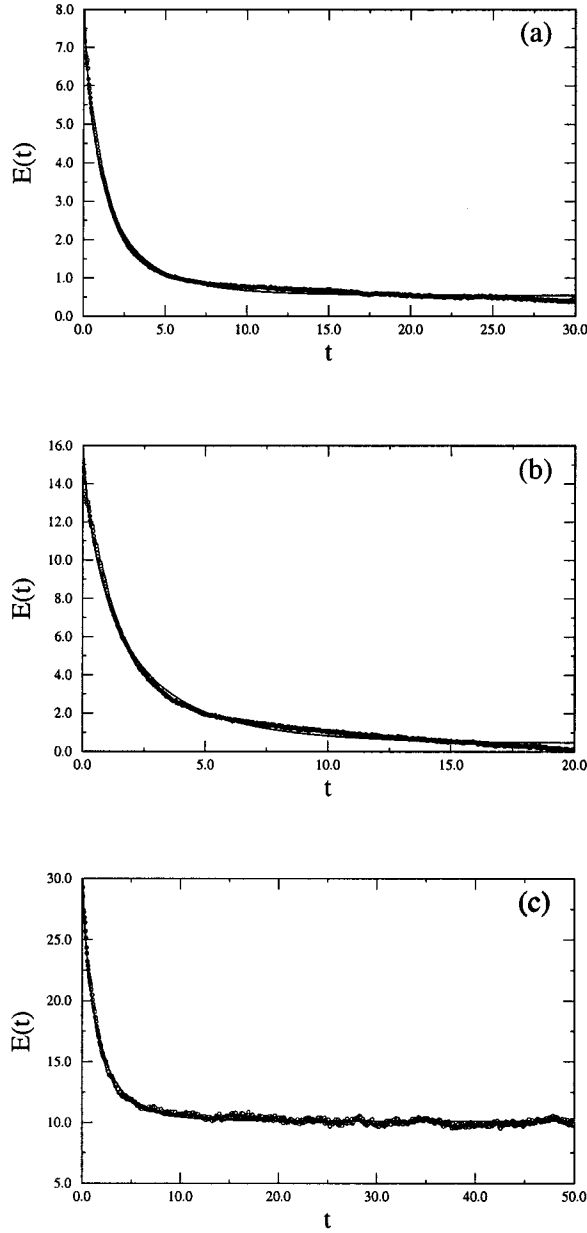


Figure 3.6: Relaxation curves for quenches across the theta point fitted with stretched exponentials for $N = 30$. Only the first relaxation regime is shown. (a) For $\alpha = 2$, $T_I = 4$ and $T_F = 0.5$ we get $\beta \approx 0.69$ and $\tau \approx 1.26$. (b) For $\alpha = 4$, $T_I = 6$ and $T_F = 1$ we get $\beta \approx 0.70$ and $\tau \approx 1.53$. (c) For $\alpha = 6$, $T_I = 16$ and $T_F = 6$; we get $\beta \approx 0.72$ and $\tau \approx 1.41$. Each of these β and τ are only one of the values used to do the averages in Table 3.1. The solid lines are the fit to Eq. (3.2).

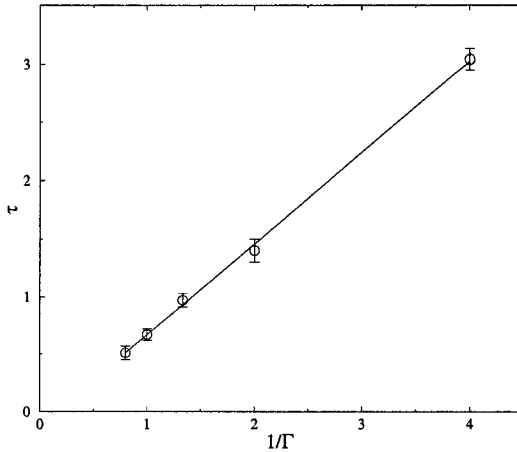


Figure 3.7: τ as a function $1/\Gamma$. The slope of the linear fit is 0.788 ± 0.009 and the intercept is -0.11 ± 0.02 .

the work of Iori *et. al.* [91]. To check this point, we performed MD simulations for random heteropolymers of length $N = 15$ corresponding to the case investigated in Iori, Marinari and Parisi [91]. Using $\alpha = 6$ and averaging 100 quench runs, the data of $E(t)$ was indeed fitted well with a single stretched exponential in agreement with the results of Iori *et al.*. The value of the stretched exponent in this case was found to be consistent with the value reported above for the first time regime for $N = 30, 100$. Thus, as expected, the relaxation to equilibrium was rapid and occurred over 30 time units for these random heteropolymers.

To examine the relaxational dynamics further, we performed temperature quenches entirely below the theta point, *i.e.* with $T_I, T_F < T_\Theta$, using heteropolymer chains with $N = 30$ and $\alpha = 2, 5, 6$. A typical relaxation behavior of the energy is shown in Figure 3.8 for parameters $N = 30, \alpha = 6, T_I = 6$ and $T_F = 4$. In this case there was only one relaxation regime which is understandable since the chain was only changing from an already collapsed state to a more compactly collapsed state. Again the data was well fitted to the stretched exponential form and the results are summarized in Table 3.1. For these ‘below-to-below’ quenches, our data gave $\beta \approx 0.4$ for all values of α used.

How can we interpret relaxation described by a stretched exponential? To examine this question, we turn to the work of Lai [95] who studied the spectrum for the distribution of the relaxation times that leads to the stretched exponential relaxation in the

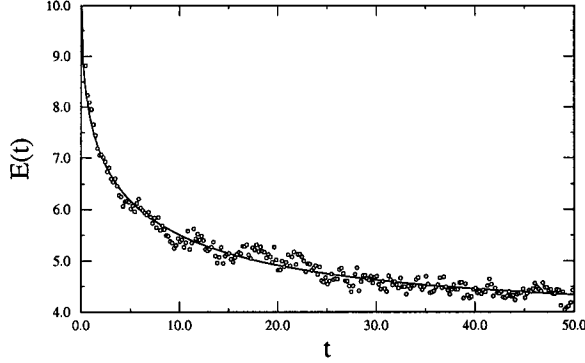


Figure 3.8: Energy versus time for a random heteropolymer after a temperature quench, with parameters $\alpha = 6$, $N = 30$, $T_I = 6$ and $T_F = 4$ (both below the theta point). The stretched exponential fit gives $\beta \approx 0.40$ and $\tau \approx 4.02$ for this polymer.

context of the study of glassy behavior. Lai showed that slow stretched exponential relaxation is due to a wide spectrum of relaxation times. We now follow Lai's analysis to discuss a specific case of interest to us where the relaxation function is the total energy of the system $E(t) = a_0 e^{-(t/\tau)^\beta} - a_1$ and the stretched exponents have values of $\beta \sim 0.7$ and $\beta \sim 0.4$. The value $\beta = 1$ corresponds to the conventional Arrhenius pure exponential relaxation with a single time scale τ . The more complex stretched exponential relaxation can be described as follows by a continuous distribution of possible time scales, $\mathcal{P}(\tau')$, and the presence of parallel relaxation processes:

$$E(t) = \int_0^\infty \mathcal{P}(\tau') e^{-(t/\tau')^\beta} d\tau', \quad (3.3)$$

where $E(t)$ is normalized, *i.e.* $E(0) = 1$. Lai looked for the general form of $\mathcal{P}(\tau')$ analytically for different values of the stretched exponent β as follows. By changing variables in Eq. (3.3), we can write

$$E(t) = E(s) = \int_0^\infty u^{-2} \mathcal{P}\left(\frac{1}{u}\right) e^{-us} du \equiv \mathcal{L}\left[u^{-2} \mathcal{P}\left(\frac{1}{u}\right)\right] = \mathcal{L}\left[\tau'^2 \mathcal{P}(\tau')\right], \quad (3.4)$$

where \mathcal{L} is the Laplace transform with $\mathcal{L}[f(u)] \equiv \int_0^\infty f(u) e^{-su} du$, for some function $f(u)$. Thus we can obtain the distribution function of relaxation times via the inverse Laplace transform.

$$\mathcal{P}(\tau') = \frac{1}{\tau'^2} \mathcal{L}^{-1}[E(t)] = \frac{1}{\tau'^2} \mathcal{L}^{-1}\left[a_0 e^{-(t/\tau)^\beta} - a_1\right]. \quad (3.5)$$

The inverse Laplace transform is difficult to calculate for general values of β . Hence Lai only computed the $\beta = 1$ and $\beta = 1/2$ cases. Nevertheless all the information about $\mathcal{P}(\tau')$ can be computed from its moments.

$$\langle \tau'^n \rangle = \frac{\tau^n}{\beta(n-1)!} \Gamma(1/\beta), n = 1, 2, \dots \quad (3.6)$$

Next, we use Eq. (3.6) to calculate the width of the relaxation spectrum $W = \sqrt{\langle \tau'^2 \rangle - \langle \tau' \rangle^2}$. For $\beta = 1$, $W = 0$, for $\beta = 0.7$, $W \sim 0.9\tau$ and for $\beta = 0.4$, $W \sim 3\tau$. We have also checked to see if $\mathcal{P}(\tau')$ was a Gaussian distribution of time scales using the following expression:

$$\mathcal{P}(\tau') = \frac{1}{W\sqrt{2\pi}} \exp\left\{-\frac{(\tau' - \langle \tau' \rangle)^2}{2W^2}\right\}. \quad (3.7)$$

The values for W and $\langle \tau' \rangle$ were estimated from Eq. (3.6). We evaluated Eq. (3.3) numerically before fitting the resulting curve with Eq. (3.2). For W and $\langle \tau' \rangle$ estimated for $\beta = 0.7$ we obtained a good fit with a stretched exponent $\beta = 0.644 \pm 0.001$ and $\tau = 0.1042 \pm 0.0002$. This indicates that the Gaussian distribution of possible time scales was an appropriate choice. However for $\beta = 0.4$, $\mathcal{P}(\tau)$ could no longer be fitted by a Gaussian distribution.

Since protein denaturation is of great interest (Daggett and Levitt [92]), we also examined the kinetics of “unfolding”. To this end we studied a random heteropolymer with $N = 100$ and $\alpha = 6$. We initiated the polymer in an equilibrium conformation at $T_I = 6$ and abruptly changed the temperature to $T_F = 16$. The energy was then monitored as a function of time and fitted with Eq. (3.2). As expected in the absence of an explicit solvent, the “unfolding” showed an exponential behavior ($\beta = 1.01 \pm 0.06$ and $\tau = 1.7 \pm 0.1$).

3.3 Summary

In this chapter, we first examined the “phase diagram” of a single random heteropolymer in detail. A clear idea of the equilibrium “phase” behavior is necessary for investigating the relaxational dynamics after a temperature quench since the dynamic behavior is different depending on the temperature range. In our model, the random heteropolymer is composed of N monomers connected by harmonic springs. The

monomers mutually interact via a repulsive Lennard-Jones potential and the random interactions between the monomers were included by means of a Van der Waals interaction whose coupling constants are chosen from a Gaussian distribution of width α . First, the “phase diagram” was obtained from MD simulations and two states were identified: a high temperature extended conformation where the random heteropolymer is described in terms of a self-avoiding random walk; and a low temperature collapsed conformation where the polymer takes up a closed compact conformation. The two states are separated by a line of theta points whose temperature increases with increasing α .

Knowledge of the “phase diagram” allowed us to perform systematic studies of random heteropolymer relaxation processes. Relaxation to equilibrium for temperature quenches inside the extended “phase” showed a pure exponential behavior whereas relaxation processes to the collapsed “phase” exhibited a stretched exponential behavior. We found that the relaxation after a quench from above the theta point to below could be characterized by a two-stage process. The first time regime is characterized by a faster stretched exponential relaxation process with exponent $\beta \approx 0.7$. This value does not depend on the values of α and is quite generic. In the first time regime, the chains locally collapse into separate blobs but the entire chain is still quite extended. In the second time regime the local blobs coalesce to form the final compact structure, but with different stretched exponential form and a lower value of the exponent β . For very short chains such as those examined in Iori, Marinari and Parisi [91], the second time regime is absent as no local collapse takes place. Finally for a quench from below the theta point to further below, the relaxation is a one stage process which is also well fitted with a stretched exponential form.

Relaxation to equilibrium for quenches from the extended to the collapsed “phase” are of the most interest to us due to their relation to protein folding. Figure 3.5 shows that typical final polymer conformations for the first time regime (*i.e.* up to $t = 30$) are extended with a few compact blobs along the chain which eventually coalesce at longer time. The development of this growth and coalescence process occurs during the crossover as can be seen from the conformation in Figure 3.5 near time $t = 75$. This conformation shows that the polymer is now more compact but with the blobs

still connected by extended sections. For such short chains, $N = 100$, it is quite difficult to determine if the blobs are distributed randomly along the chain or if they mostly form near the terminal monomers. If the blobs are in fact randomly distributed, this result is in agreement with the Langevin (Kiernan, Green and Dawson [95]) and Monte Carlo (Yu et al. [95]) simulations performed by Dawson and his colleagues to study both the collapse of homopolymers and random copolymers with degrees of polymerization up to $N = 1000$. In these cases, monomer aggregation was reversible. Furthermore Dawson (Kiernan, Green and Dawson [95]) points out that the neglect of hydrodynamics in the early stage of kinetics is justified by the local nature of the cluster growth mechanism. The effect of this approximation on the second time regime is unclear since we need to know how the hydrodynamic modes affect the basic mechanism leading to coarsening. Dawson further states that this should be checked by adding the Oseen tensor, which would be a demanding calculation. On the other hand, if the blobs mostly form near the terminal monomers, we can compare our collapse mechanism to the one proposed by Ostrovsky and coworkers who considered an irreversible aggregation process as the basis for polymer collapse (Ostrovski and Bar-Yam [95]; Crooks, Ostrovski and Bar-Yam [99]). These authors showed by Monte Carlo computer simulations based on cluster diffusion that the collapse of long homopolymers (up to $N = 1000$ in two dimensions and 500 in three dimensions) and certain heteropolymers is dominated by the nucleation and growth of large clusters at the ends of the polymer coupled with the coalescence of smaller clusters inside the polymer. Note that they also included the primary effects of hydrodynamics by applying Stoke's law.

We propose that our relaxation data can be interpreted in terms of the molten globule concept since we found an initial relaxation to an intermediate conformation in the first time regime after a temperature quench from above to below the theta point. We feel that this conformation is analogous to the "compact but extended" structure discussed by Daggett and Levitt [92] for proteins. This relaxation regime is then followed by a slower relaxation to a collapsed conformation¹. Such behavior is analogous to that discussed in the literature for protein folding. Finally we note that

¹For a discussion of the molten globule model, see the contribution of Baldwin [94].

the relaxation process studied here is quite different from that of the *homopolymer* collapse which proceeds via a single exponential.

EQUILIBRIUM STUDY OF A RANDOM HETEROPOLYMER IN SOLVENT

Most simulation studies of polymer collapse dynamics, have been carried out without any explicit solvent. Similar to what was done in Chapter 3, the solvent is most often incorporated in an implicit way into the effective monomer–monomer interaction in order to reduce the computational cost. Such an implicit solvent model can contribute ample information about a given system, but it is important to determine if the presence of an explicit solvent will significantly affect the static properties and the qualitative nature of the collapse dynamics. It is expected that the complicated hydrodynamic interactions between monomers will in fact modify the collapse dynamics. A more thorough discussion on the hydrodynamic effects will be reserved for Chapter 5.

Among the few computational studies of polymers in an explicit solvent, Polson and Zuckermann [00] used molecular dynamics simulations to examine the equilibrium properties and collapse dynamics of fully flexible Lennard–Jones polymer chains in the presence of an explicit Lennard–Jones solvent in two dimensions. Both homopolymers and random copolymers were considered. Furthermore, Polson and Zuckermann [01] have recently repeated this study for three dimensional systems and found that the results were qualitatively consistent with the results for their two-dimensional system. They concluded that the dimensionality of the system does not strongly affect the qualitative behavior of either the equilibrium properties or the collapse dynamics of their system. Comparison with Polson and Zuckermann’s three-dimensional results will be made throughout the next two chapters. The only other study of polymer collapse in an explicit solvent that we are aware of is the work by Chang and Yethiraj [01]. They looked at the effect of an explicit solvent on polymer collapse dynamics by means of systematic comparison between equivalent implicit–solvent and explicit–

solvent systems. We will describe these simulations in more detail in Chapter 5.

In this chapter, we examine the static properties of a random heteropolymer using a three-dimensional model system in which the polymer is immersed in an explicit Lennard-Jones solvent in order to find the effect of such a solvent on its equilibrium properties. The solvent is essentially a monomeric solvent in that the solvent molecules have the same size and mass as the monomers of the random heteropolymer. Three types of random heteropolymer in an explicit solvent were studied. In the first case, the polymeric chain is fully flexible and the random interactions are imposed between monomers (Model A). In the second case, the chain is also fully flexible but there are now random interactions between monomers and solvent particles (Model B with a flexible chain). The third case is similar to the second one, but this time the chain is not fully flexible since angular restrictions are included (Model B with a semi-flexible chain). The simulations are initialized using configuration on a lattice which is allowed to melt at high temperature until all traces of the lattice have vanished. Furthermore, a Gaussian distribution of the initial velocities, which yields the correct initial temperature, was chosen, and the total momentum of the system was set to zero.

The results presented below were obtained from equilibrium simulations for several values of the strength of the random interactions, α , ranging from 0 to 6 and ρ ranging from 0 to 0.9. The polymer length, N , varies between $N = 20$ and $N = 100$; and special attention was paid to the case where $N = 30$. For shorter polymer chains ($N \leq 40$), the number of solvent particles, N_S , was chosen so that $N_S + N = 512$ for low densities and $N_S + N = 1000$ for densities higher than $\rho = 0.3$. Larger values of N_S were used for longer polymeric chains ($N > 40$), *i.e.* $N_S + N = 2197$ for $\rho \leq 0.5$ and $N_S + N = 3375$ for $\rho > 0.5$. The characteristic temperature, T_Θ , was calculated as a function of both the strength of the random interactions, α , and the number density, ρ . As in Chapter 3, we will only be concerned with making a good estimate of T_Θ which will allow us to perform systematic temperature quenches. Since an extensive discussion on the matter of T_Θ was presented in the previous chapter, the emphasis will now be shifted to the effect of the solvent on the value of T_Θ . In all of the calculations reported here the value of the time step is $\Delta t = 0.005\tau_0$, and the

coupling friction between the particles and a heat bath is $\Gamma = 0.5\tau_0$. Furthermore, the unstretched bond length was taken to be $R_0 = \sigma$, and the value of the coupling constant, k , for the harmonic interaction of Eq. (2.8) used in the simulations was chosen as $k\sigma^2/\epsilon = 500$. Note that these parameters are different from the ones used in Chapter 3. In particular, the bond lengths are shorter and stiffer so as to be able to compare with the work of Polson and Zuckermann (Polson and Zuckermann [00] [01]). Since very long simulations are required to obtain accurate measurements of statistical quantities such as $\langle R_{yy}^2 \rangle$, $\langle R_{end}^2 \rangle$, $\langle n_{MM} \rangle$ and $\langle n_{MS} \rangle$, a single random heteropolymer sequence was used for each measurement. Further averaging over various random heteropolymer sequences is not expected to change the qualitative nature of the equilibrium results. This random sequence should be seen as a sequence of N monomers which interact with each other or with the solvent molecules through a random r^{-6} potential. The sequence is defined before starting the simulation by randomly generating the coefficients of the r^{-6} interactions between the pairs of monomers or between the monomers and solvent molecules via a Gaussian random number generator of width α and mean value of zero. All quantities described in the rest of this chapter are given in Lennard–Jones reduced units. Distances will be expressed in terms of σ , temperatures in terms of k_B/ϵ , and time in terms of $\sqrt{m\sigma^2/\epsilon}$, where m is the mass of each monomer and each solvent particle, as discussed in Chapter 2.

Section 4.1, which presents a study of the Lennard–Jones solvent, was included for completeness. This was done in order to convince the reader that our calculations for the pure solvent did indeed reproduce known and accepted results from the literature. The equilibrium results are presented in Sections 4.2 to 4.4. These sections contain “phase diagrams” for the collapsed versus the extended “phase” of the random heteropolymer immersed in a Lennard–Jones solvent over a broad range of temperature T , random interaction strength α , and density ρ . For the results of Section 4.2, the monomers of the heteropolymer interact directly via random interactions in the presence of an explicit solvent As stated in Chapter 2, we refer to this case as Model A. In Sections 4.3 and 4.4, the monomers of the heteropolymer interact with the solvent particles via random interactions. This model will be referred to as Model B as discussed in Chapter 2. Section 4.3 reports simulation results for the case where the

heteropolymer is freely jointed (Model B with a flexible chain) whereas an angular restriction between neighbouring bonds on the heteropolymer has been included in the simulations reported in Section 4.4 (Model B with a semi-flexible chain). Finally, Section 4.5 contains a summary and concludes the chapter.

4.1 Pure Lennard-Jones solvent

For the results reported in this section, the Lennard-Jones solvent is a monomeric solvent where the particles have the same size and mass as the monomers on the polymer. The semi-empirical Lennard-Jones interaction is described by Eq. (2.11) and Eq. (2.9), and can be visualized in Figure 2.4. By setting the cutoff to $r_c = 2.5\sigma$, an attractive tail of the form $(-1/r_{ij}^6)$, a negative well of depth ϵ , and a steeply rising repulsive wall at a distance less than $r \sim \sigma$ can be observed. The simulations were performed for 125 solvent particles ($N_s = 125$). The Lennard-Jones solvent was equilibrated using 10^5 time steps per solvent particle after a warm up of 10^3 time steps for $T < 3.5$, in reduced units, and using 5×10^5 time steps per solvent particle after a warm up of 10^3 time steps for $T \geq 3.5$, in reduced units. Statistical data were calculated at an interval of 10^2 time steps in both cases.

A truncation and a shift were applied to the Lennard-Jones potential since the Lennard-Jones potential is short-range, and the error due to interactions with particles at larger distances was minimized by choosing r_c sufficiently large. There are considerable advantages of a computational nature to such a truncation. If periodic boundary conditions are chosen, and a cutoff is selected so that it is less than half the size of a side of the simulation box, L , only interactions between a given particle i with the nearest periodic image of a second particle j need to be considered. Since the potential is not precisely zero for $r \geq 1.0$, there is the possibility that truncation related systematic errors may occur. If the interaction decays rapidly, a tail contribution can be added to correct the potential. Since the correction is about $1/60^{th}$ of the well depth, and the details of the solvent did not concern us, we opted to further reduce computational time by omitting this correction. Following the truncation of the potential, it is necessary to shift this potential in order to make the potential vanish at the cutoff. In this way, discontinuities in the intermolecular potential can be avoided,

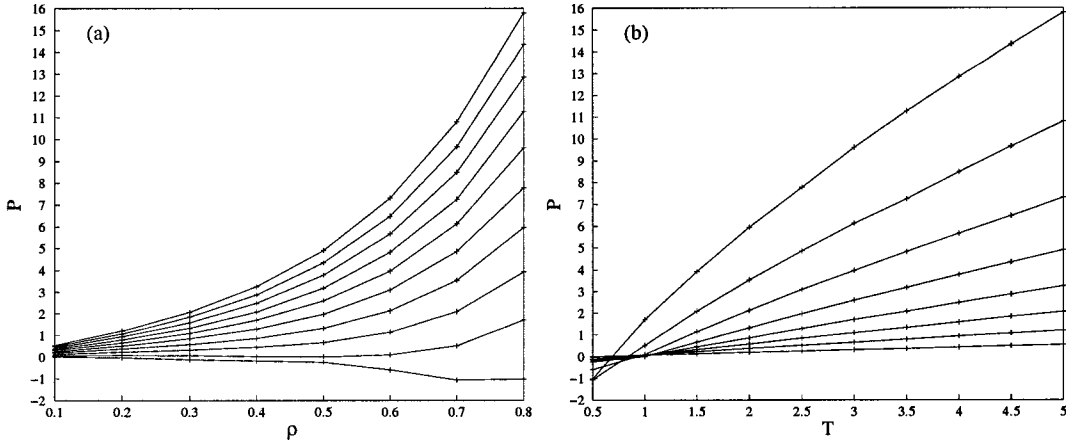


Figure 4.1: Lennard-Jones liquid: (a) P versus ρ for $T = 0.5, 1.0, 1.5, 2.0, 2.5, 3.0, 3.5, 4.0, 4.5, 5.0$ (isotherms) where temperature increases from the lower curve to the upper curve. (b) P versus T for $\rho = 0.1, 0.2, 0.3, 0.4, 0.5, 0.6, 0.7, 0.8$ (isochores) where the density increases from the lower curve to the upper curve.

and hence no impulsive corrections to the pressure are needed. Also, intermolecular forces remain finite which is essential since the Verlet algorithm used to integrate the equations of motion cannot accommodate impulsive forces. The phase diagram is slightly modified by such a truncation and shift, but as long as the system is not close to a critical point, it is straightforward to keep it in the liquid phase. The results for the truncated and shifted Lennard-Jones potential with $r_c = 2.5$ can be found in Smit [92]. In this paper, Smit estimates the critical point at $T_c = 1.085 \pm 0.005$ and $\rho_c = 0.317 \pm 0.006$.

We first verified that the single-component Lennard-Jones solvent displayed the expected behavior by comparing our results to the work of Luna-Bárcena et al. [97] and Cottin and Monson [96]. Figure 4.1, shows (a) several isotherms and (b) several isochores, and Figure 4.2 combines these isotherms and isochores into a three dimensional “ $P\rho T$ ” plot. Furthermore, we were careful to ensure that the solvent remains in the fluid phase by choosing the appropriate values of temperature and density from the well-known temperature-density phase diagram of a single component Lennard-Jones system. This phase diagram can be found in a myriad of books and papers like Frenkel [96] for instance.

The negative pressures seen in Figure 4.1 and Figure 4.2 are related to the fact that the system is in a metastable state at low temperature and high density. Thus, it is in

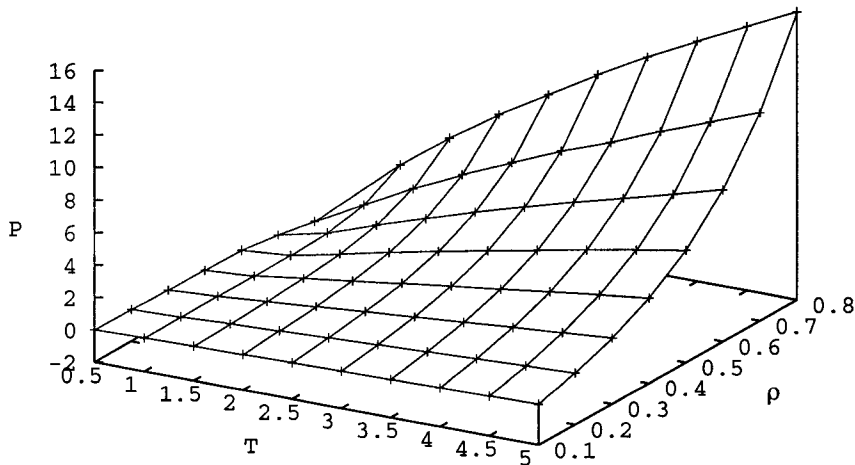


Figure 4.2: Lennard-Jones liquid $P\rho T$ diagram which gives isochores and isotherms on the appropriate axis.

a two-phase (liquid-vapor coexistence) region of the phase diagram. Furthermore, by comparing these results to the Lennard-Jones phase diagram, there are other points with positive pressure that are in the two-phase region. This can be seen for almost the whole range of density at $T = 0.5$ and up to $\rho = 0.6$ for $T = 1.0$. For densities inside the coexistence region, the pressure is expected to be constant and equal to the saturated vapor pressure. However Figure 4.1 (a) shows that the pressure is not constant in the coexistence region. These anomalies were found because molecular dynamics simulations of small systems are not well suited to study coexistence between two phases. This is a well known difficulty which can also be observed in Monte Carlo simulations of finite systems (Frenkel [96]). In a finite system, a relatively large cost in free-energy is associated with the creation of a liquid-vapor interface. This free energy can be so large that for very small systems, it is favorable for the system not to undergo phase separation. Hence, the system becomes metastable. These problems are more important if the system is small, and if the interfacial free-energy is large. This is the reason why standard NVT simulations are not recommended to study the vapor-liquid coexistence region or any other strong first-order phase

transition. However, for our work, using the *NVT* ensemble does not cause problems of this nature since the simulations are performed in the one-phase regions of the phase diagram.

The addition of the polymer does not change the properties of the solvent significantly. This has been verified by our group, and the change in the pressure of the system at a given temperature and density is of the order of a few percent. Therefore, it is safe to refer to the usual Lennard–Jones phase diagram to make sure that the system is in the fluid phase.

4.2 Random monomer-monomer interactions (Model A)

Random heteropolymers similar to the ones of Chapter 3 will be studied in the next three sections but they will now be immersed in a Lennard–Jones solvent identical to the one presented in Section 4.1. The Hamiltonian for this case can be obtained directly from Eqs. (2.1)–(2.4), and is given by:

$$\begin{aligned}\mathcal{H} &= \mathcal{U}_{MM} + \mathcal{U}_{MS} + \mathcal{U}_{SS} + \mathcal{K}_M + \mathcal{K}_S \\ &= \sum_{i=1, j=i+1}^{N-1} \mathcal{U}_{Spring}(r_{ij}) + \sum_{i=1}^N \sum_{j>i}^N \mathcal{U}_{RLJ}(r_{ij}) + \sum_{i=1}^N \sum_{j>i}^N \mathcal{U}_{Dis}(r_{ij}, \eta_{ij}) \\ &\quad + \sum_{i=1}^N \sum_{j'=1}^{N_S} \mathcal{U}_{RLJ}(r_{ij'}) + \sum_{i'=1}^{N_S} \sum_{j'=i'}^{N_S} \mathcal{U}_{LJ}(r_{i'j'}) + \mathcal{K}_M + \mathcal{K}_S\end{aligned}\quad (4.1)$$

Non-primed indices were used to identify a specific monomer of the polymer chain, and primed indices were used to identify a specific solvent particle. This Hamiltonian consists of the following interactions: a harmonic term between nearest neighbor monomers of the heteropolymer given by Eq. (2.8), a purely repulsive Lennard–Jones potential given by Eq. (2.10) and a $1/r^6$ potential whose coupling constant is chosen from a Gaussian distribution of width α , as given by Eq. (2.12), between all monomers. In addition to this, there is a purely repulsive Lennard–Jones interaction between monomers and solvent particles, which is given by Eq. (2.10), and a Lennard–Jones interaction between the solvent particles, Eq. (2.11).

Figure 4.3 shows the temperature dependence of $\langle R_{gy}^2 \rangle$ and Figure 4.4 shows the corresponding temperature dependence of $\langle n_{MM} \rangle$ and $\langle n_{MS} \rangle$ for random heteropolymers of length $N = 30$ as functions of the strength of the random monomer–monomer

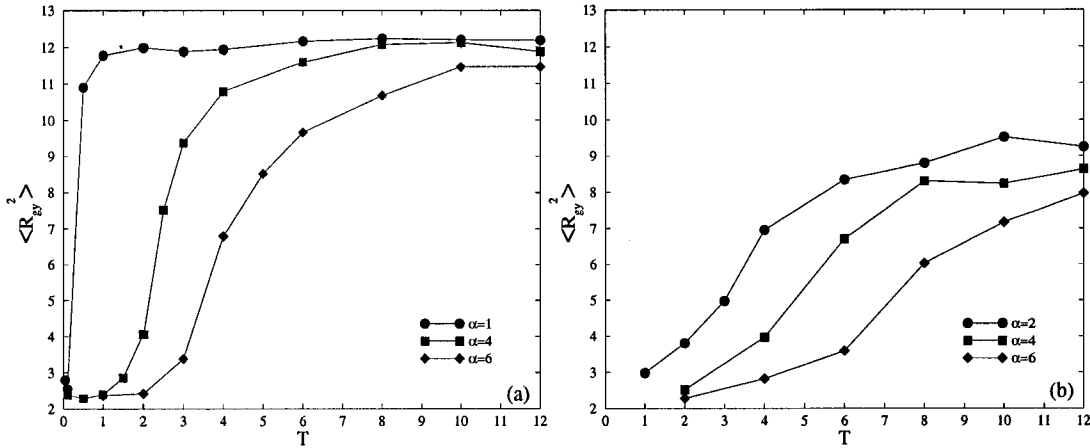


Figure 4.3: $\langle R_{gy}^2 \rangle$ versus T for a Model A type random heteropolymer of length $N = 30$ in an explicit solvent of density (a) $\rho = 0$ and $\alpha = 1, 4, 6$, and (b) $\rho = 0.7$ and $\alpha = 2, 4, 6$.

interactions α at fixed density (a) $\rho = 0$ and (b) $\rho = 0.7$. Many similar calculations were performed for various values of ρ and α , but only a few of these are shown so as to illustrate the general behaviour of these curves. Note that there are no qualitative differences between the results for the two solvent densities shown here. The error bars were not included but a few examples will be presented in order to give a sense of their magnitude. The errors on $\langle R_{gy}^2 \rangle$ for $\rho = 0.7$ and $\alpha = 6$ were of 0.006, 0.03, 0.09 and 0.05 for $T = 2, 6, 8$ and 16 respectively. Sufficiently long runs were performed in order to keep the errors for $\langle R_{gy}^2 \rangle$ below 0.1. Near T_Θ , longer simulation runs were required to lower the errors since the system is less stable and the fluctuations in the measured quantities are larger. The errors for $\langle n_{MM} \rangle$ were 0.1, 0.2, 0.2 and 0.8, and the errors for $\langle n_{MS} \rangle$ were 0.2, 0.3, 0.3 and 0.2, for $T = 2, 6, 8$ and 16 respectively, again for $\rho = 0.7$ and $\alpha = 6$. In both cases, $\langle R_{gy}^2 \rangle$ decreases as the temperature T is lowered. A corresponding increase in $\langle n_{MM} \rangle$ and a corresponding decrease in $\langle n_{MS} \rangle$ were also observed.

At higher T , $\langle R_{gy}^2 \rangle$ approaches a value which will be denoted $\langle R_{gy}^2 \rangle_{coil}$. At these temperatures, the polymer chain forms an extended coil (*i.e.* the good solvent condition), and the number of monomer–monomer contacts is small, whereas the number of monomer–solvent contacts is large. As the temperature is decreased, the value of $\langle R_{gy}^2 \rangle$ drops abruptly until it reaches a plateau $\langle R_{gy}^2 \rangle_{globule}$ at low temperatures. At this point, the polymer chain is collapsed and forms a globule. The value of $\langle n_{MM} \rangle$ is

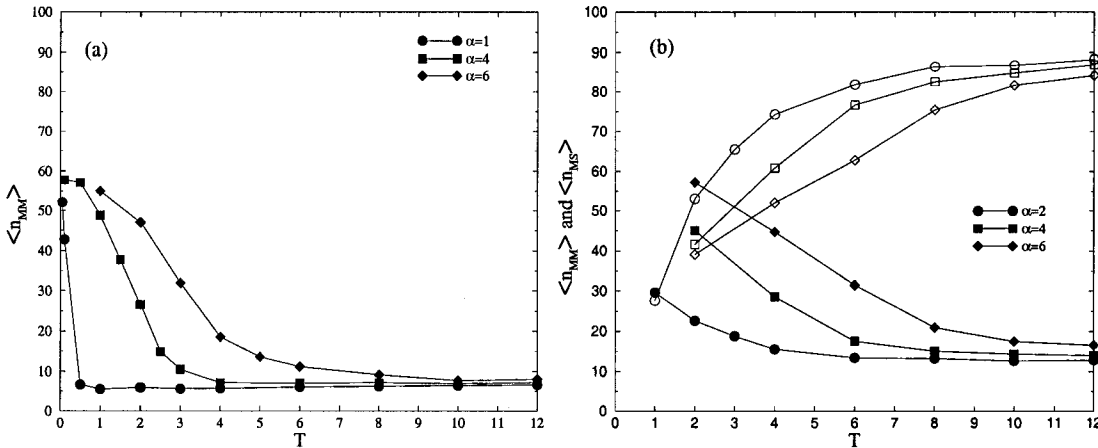


Figure 4.4: Average number of contacts versus T for a Model A type random heteropolymer of length $N = 30$ in an explicit solvent of density (a) $\rho = 0$ and $\alpha = 1, 4, 6$, and (b) $\rho = 0.7$ and $\alpha = 2, 4, 6$.

large, while the value of $\langle n_{MS} \rangle$ is small. One should be careful when defining the state of the collapsed polymer at very low temperatures ($T \leq 0.75$), since the dynamics of the system at such low temperatures can be very slow, and the chain is probably frozen inside a metastable state.

The transition from the extended coil conformation to the globular conformation is not sharp, *i.e.* there is a range of temperatures over which the transition occurs. Increasing the solvent density increases the width of the transition as well as the value of the characteristic temperature T_Θ . Increasing the value of the strength of the random monomer–monomer interactions α also increases the width of the transition as well as the value of T_Θ . Similarly, Figure 4.4 shows how changes in ρ or α affect the width of the transition and the value of T_Θ .

This transition is thermally driven and results from the definition of the free energy: $F = E - TS$, where E is the energy, T is the temperature and S is the total entropy of the system. $\langle R_{yy}^2 \rangle$ assumes the value that minimizes F . The energy E favours a decrease in $\langle R_{yy}^2 \rangle$, while the total entropy S favours an expanded coil, and therefore an increase in $\langle R_{yy}^2 \rangle$. T controls the relative strengths of the two terms. The translational part of the total entropy S favors a more compact state, and therefore helps to “drive” the transition, but the conformational contribution to the entropy is the important part.

Furthermore, high density solvents slightly compress the polymer coil at high temperature (*i.e.* in the athermal limit). Some simulations and theories predict that entropy–driven collapse transition can be observed in athermal environments (Frenkel and Louis [92]; Dijkstra and Frenkel [94]; Dijkstra, Frenkel and Hansen [94]; Luna-Bárcena et al. [96]; Escobedo and Pablo [96]; Suen, Escobedo and Pablo [97]; Polson [99]). However, this has never been observed using an additive-potential, in conjunction with an off-lattice model in a simulation. In the paper by Escobedo and Pablo [96], the hard–sphere solvent compresses the conformation of the hard–sphere polymer in order to maximize the entropy. We observed similar behavior in our system. At zero or low density, the chain assumes a particular average size $\langle R_{yy}^2 \rangle$ where the entropy, S , is maximum, *i.e.* there are many more conformations available to the chain when it is more spread out than when it is compressed. If an explicit solvent is incorporated, the chain compresses, which means that it loses conformational entropy. This appears to be a paradox but this is not the case since by compressing the polymer slightly, the free volume available for the solvent is increased, and thus the translational entropy of the solvent increases by more than enough to offset that which was lost by the chain.

Figure 4.5 illustrates this relation between $\langle R_{yy}^2 \rangle_{coil}$ and ρ quantitatively for $\alpha = 6$ and two chain lengths, $N = 30$ and $N = 60$. This figure shows that the size of the polymer coil is proportional to the solvent density with a negative proportionality constant which depends on the polymer length. Polson and Zuckermann [01] have also observed a decrease in the polymer size with increasing solvent density. It is interesting to note that the compression of the polymer coil becomes more important for a longer polymer chain. This can also be explained by the entropic effect as discussed above. In the same athermal limit, Escobedo and Pablo [96] studied a hard–sphere polymer immersed in a monomeric solvent, in a homopolymer melt and in a deformable network. A decrease in the polymer size with increasing solvent density is also observed in their work. We follow their lead and develop a scaling argument of the form $\langle R_{yy}^2 \rangle_{coil} \propto \eta^{-\gamma}$, where η is the packing fraction which is proportional to the solvent density ρ . At first glance, this power law does not seem to agree with the linear relation seen in Figure 4.5. In fact, if we fit this curve to a function of the

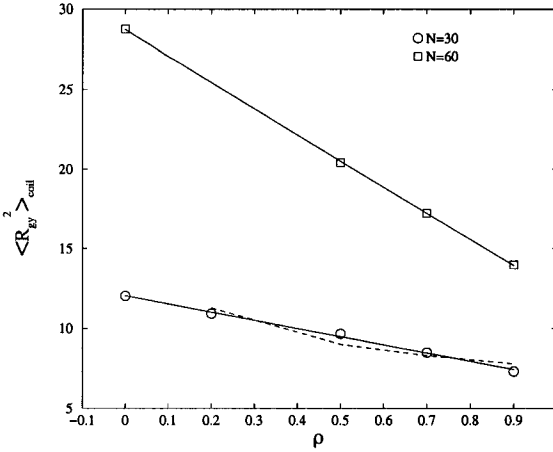


Figure 4.5: $\langle R_{yy}^2 \rangle_{coil}$ versus ρ for a Model A type random heteropolymer in an explicit Lennard-Jones solvent for $N = 30$ and $N = 60$. $\alpha = 6$ in both cases. All the $\langle R_{yy}^2 \rangle_{coil}$ were measured at $T = 16$. The error bars are all smaller than the size of the symbols, *i.e.* they are all smaller than 0.4. The dashed line is a fit to $A\rho^{-\gamma}$ where we obtained $\gamma = 0.25 \pm 0.06$

form $A\rho^{-\gamma}$, for $\rho \geq 0.2$ (dashed line in Figure 4.5), we obtain a satisfactory fit with $\gamma = 0.25 \pm 0.06$. Unfortunately, Escobedo and coworkers did not fit their results for a polymer in a monomeric solvent to such a power law. Nevertheless, our value of γ is exactly in accordance with their results for a polymer immersed in a homopolymer melt which could make one suspect that only the quality of the solvent (good or poor) is important to obtain this scaling law.

Figures 4.6 and 4.7 correspond to scaling tests which have been performed on the polymer. More specifically, Figure 4.6 shows a plot of $\langle R_{yy}^2 \rangle$ versus N on a log-log scale for a random heteropolymer with $\alpha = 6$. We examined both an isolated polymer ($\rho = 0$) and a polymer in an isolated solvent of density $\rho = 0.5$. The lines drawn through the data sets are given by $\langle R_{yy}^2 \rangle \propto N^{2\nu}$ (see Chapter 2 for a discussion about the Flory exponent). At high temperature, $T = 16$, polymer coils were observed with $\nu = 0.608 \pm 0.006$ for $\rho=0$, and $\nu = 0.59 \pm 0.02$ for $\rho=0.5$, which correspond to the value expected for a Flory coil. For low temperature, $T = 2$, globules with $\nu = 0.313 \pm 0.004$ for $\rho=0$ and $\nu = 0.35 \pm 0.01$ for $\rho=0.5$ were obtained. These values also correspond to Flory's predictions. Therefore adding an explicit solvent to the system does not change the scaling laws predicted by Flory. Thus, a temperature quench from a high temperature to a lower temperature involves a transition from an extended coil to a collapsed globule. We did not study Flory scaling more extensively in order to

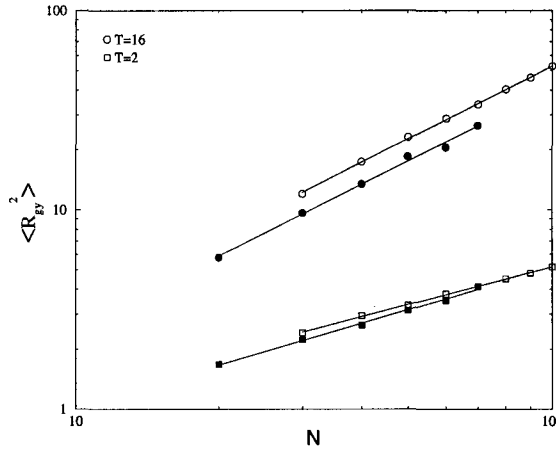


Figure 4.6: Radius of gyration squared $\langle R_{gy}^2 \rangle$ vs. number of monomers N for a Model A type random heteropolymer with $\alpha = 6$ in a solvent of density, $\rho = 0$, (no solvent and no boundary conditions) and $\rho = 0.5$. The empty symbols correspond to $\rho = 0$ and the filled symbols correspond to $\rho = 0.5$. For both densities, two temperatures were used, $T=2$ (\circ) and $T=16$ (\square). The solid lines are fits, with ν fixed as a free parameter, that predict Flory's scaling relation in three dimensions $\langle R_{gy}^2 \rangle \propto N^{2\nu}$. $T=2$ corresponds to a globule with $\nu = 0.313 \pm 0.004$ for $\rho=0$ and $\nu = 0.35 \pm 0.01$ for $\rho=0.5$. $T=16$ corresponds to a coil with $\nu = 0.608 \pm 0.006$ for $\rho=0$ and $\nu = 0.59 \pm 0.02$ for $\rho=0.5$.

determine the characteristic temperature T_Θ , as this would be computationally too demanding. Rather we chose to estimate T_Θ by examining the requirements of the present figures of $\langle R_{gy}^2 \rangle$ versus T . This method is sufficiently accurate for the project since only an approximate estimate of T_Θ is needed in order to perform systematic temperature quenches.

We next studied the parameter $\zeta = \frac{\langle R_{end}^2 \rangle}{6\langle R_{gy}^2 \rangle}$ in a similar way to Luna-Bárcena et al. [97]. Three states can be identified for the random heteropolymer in terms of ζ in three dimensions. For good solvent conditions in three dimensions, $\zeta = 1.05 - 1.07$, for the Θ -solvent condition, $\zeta = 1$, and for a collapsed chain (poor solvent), $\zeta = 1/3$. Figure 4.7 shows ζ as a function of solvent density for a Model A type random heteropolymer. Different isotherms are shown for $N = 30$ and $\alpha = 6$. These simulation results give the expected values for ζ depending on the state of the polymer. We can easily make a connection between this figure and figures like Figure 4.3 which shows $\langle R_{gy}^2 \rangle$ as a function of temperature for various solvent densities.

Finally, the characteristic temperature T_Θ was estimated by determining the points of inflection of the graphs of $\langle R_{gy}^2 \rangle$ versus T (Figure 4.3). The point of inflection was defined as the temperature at which the value of $\langle R_{gy}^2 \rangle$ is mid-way between $\langle R_{gy}^2 \rangle_{globule}$

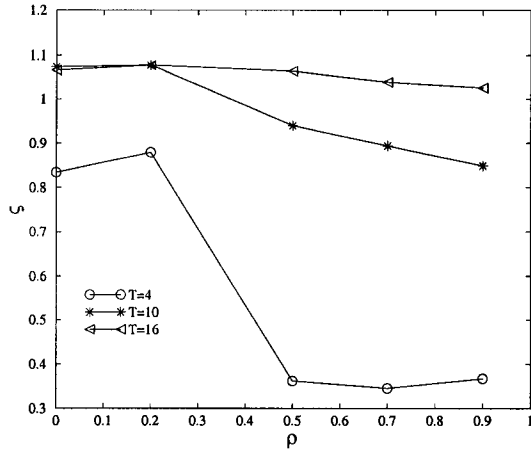


Figure 4.7: $\zeta = \frac{\langle R_{end}^2 \rangle}{6\langle R_{gy}^2 \rangle}$ as a function of solvent density for a Model A type random heteropolymer. $\zeta = 1$ denotes quasi-ideal polymer behavior (attractive and excluded volume interactions are balanced). Different isotherms are shown for $N = 30$ and $\alpha = 6$.

and $\langle R_{gy}^2 \rangle_{coil}$. The uncertainties were estimated by visual inspection of the $\langle R_{gy}^2 \rangle$ vs. T graphs, and by comparison with the related graphs for n_{MM} and n_{MS} vs. T .¹ For example, the uncertainties for $\rho = 0$ are smaller than for $\rho = 0.7$ since the $\langle R_{gy}^2 \rangle$ vs. T curves have a sharper transition for lower solvent densities. This allowed us to construct useful “phase diagrams” for random heteropolymer chains of length $N = 30$.

Figure 4.8 (a) shows a plot of T_Θ as a function of the random monomer–monomer interactions strength α for $\rho = 0$ and $\rho = 0.7$. An increase in α results in an increase in T_Θ , thus favoring the globular “phase”. The empty symbols correspond to $R_0 = 1.0\sigma$ and $k = 500$. The filled symbols correspond to the “phase diagram” from Chapter 3 (with $R_0 = 1.5\sigma$ and $k = 30$) and they were included in order to evaluate the effect of changing the bond length and the value of the spring constant on the system without an explicit solvent ($\rho = 0$). From the inset of Figure 4.8

¹To evaluate T_Θ and its error bars:

- 1- Draw a horizontal line at $\langle R_{gy}^2 \rangle_{globule} + \frac{1}{2}(\langle R_{gy}^2 \rangle_{coil} - \langle R_{gy}^2 \rangle_{globule})$ on the $\langle R_{gy}^2 \rangle$ versus T curve. The intersection of this line with the curve gives the estimate for T_Θ .
- 2- Determine the distance between the closest data point that comes before T_Θ and the closest data point that comes after T_Θ and estimate an error on T_Θ . Obviously, a sharper transition as well as a smaller interval between the data points, will reduce the error estimate.
- 3- Finally, compare the values of T_Θ and its error bars to those which would be obtained from the n_{MM} and n_{MS} versus T curves, and adjust the initial error estimates accordingly.

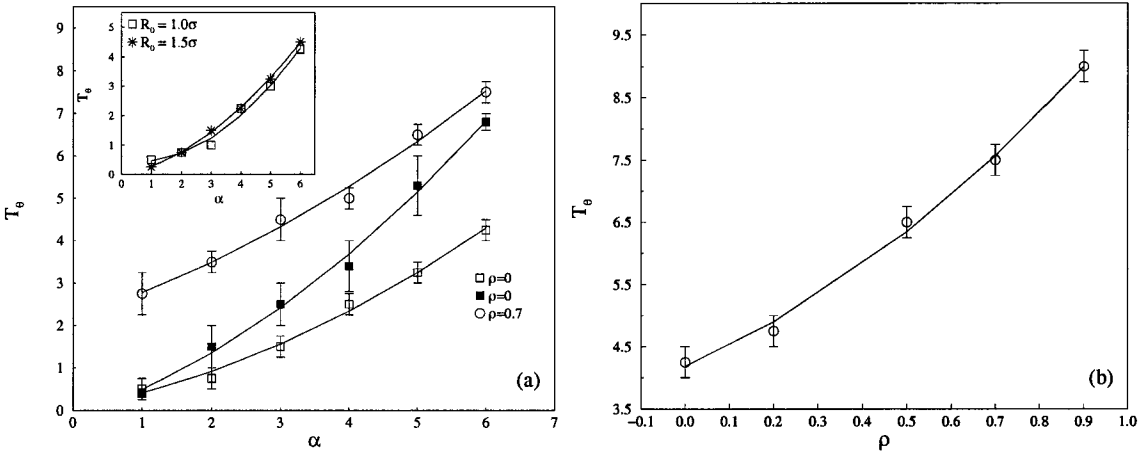


Figure 4.8: “Phase diagrams” for Model A type random heteropolymer chains of length $N = 30$ in an explicit Lennard-Jones solvent. The values of T_E were measured at the points of inflection of the $\langle R_{yy}^2 \rangle$ versus T curves (Figure 4.3) and the uncertainties were roughly estimated by visual inspection of these same curves. (a) T_E versus α for $\rho = 0$ (\square) and $\rho = 0.7$ (\circ), the empty symbols correspond to $R_0 = 1.0\sigma$ and $k = 500$ and the filled symbols correspond to $R_0 = 1.5\sigma$ and $k = 30$ (from Chapter 3). The inset shows the $\rho = 0$ and $k = 500$ curves for $R_0 = 1.0\sigma$ (\square) and $R_0 = 1.5\sigma$ (*). (b) T_E versus ρ for $\alpha = 6$.

(a), it was possible to verify that the effect related to increasing the spring constant and decreasing the bond length was completely dominated by the increase in the spring constant. Increasing the spring constant reduces the value of T_E gradually as α increases. Why would increasing the spring constant favor the coil state? Why is the effect dependent on α ? An increase in the value of the spring constant, k , will reduce the fluctuations in the positions of the monomers which will in turn render the monomer-monomer interactions less effective. This also explains why the effect was amplified for larger values of α . Softer springs (*i.e.* smaller values of k) allow for greater mobility to sample binding forces. Figure 4.8 (b) shows a plot of T_E versus ρ for $\alpha = 6$. As the solvent density is increased, the coil conformation becomes progressively more compact due to entropic effects (Figure 4.5), which in itself favors the polymer collapse.

Figure 4.9 shows several snapshots of the various conformations of a random heteropolymer with $\alpha = 6$ and length $N = 30$ in a solvent of density, $\rho = 0.7$, for several temperatures. The characteristic temperature is approximatively $T_E = 7.5$ (see Figure 4.8). The first column shows the conformations on the same scale which allows us to compare the size of the polymer. The second column shows us the equivalent con-

formations, but on an ideal scale to visualize the detail of the conformations. Finally the solvent particles were included in the third column.

The effect of the thermostat on this system was investigated by repeating some of the calculations for $\rho = 0$ and $\rho = 0.7$ using a Nosé-Hoover thermostat (see Section 2.2.2 for a discussion on the Nosé-Hoover thermostat). For $\rho = 0.7$, all the equilibrium results reproduced those obtained with the Langevin dynamics method. However, in the absence of an explicit solvent ($\rho = 0$), the results were slightly different from the Langevin equilibrium results. Based on the discussion on the Nosé-Hoover thermostat in Frenkel [96], it is likely that the discrepancy is related to ergodicity breaking. Sometimes, use of the Nosé-Hoover thermostat gives rise to ergodicity problems, and the desired Maxwell-Boltzmann velocity distribution Eq. (2.24) is not achieved. A well-known pathological case is the one dimensional harmonic oscillator. The dynamics of the oscillator are not sufficiently chaotic to sample phase space and therefore $\bar{A} \neq \langle A \rangle$. Other pathological cases include small systems or systems with high vibrational modes for which the Nosé-Hoover thermostat fails to generate a canonical distribution. A possible solution to alleviate this problem for our small heteropolymer systems is to use Nosé-Hoover chains (Martyna, Klein and Tuckerman [92]). This is a scheme in which the Nosé-Hoover thermostat is coupled to another thermostat or to a whole chain of thermostats. It allows the thermostats to fluctuate, and recovers the ergodicity of the system.

4.3 Random monomer-solvent interactions (Model B with a flexible chain)

The Hamiltonian for this case can be obtained directly from Eqs. (2.1),(2.5),(2.6),(2.7) and is given by:

$$\begin{aligned}\mathcal{H} &= \mathcal{U}_{MM} + \mathcal{U}_{MS} + \mathcal{U}_{SS} + \mathcal{K}_M + \mathcal{K}_S \\ &= \sum_{i=1, j=i+1}^{N-1} \mathcal{U}_{Spring}(r_{ij}) + \sum_{i=1}^N \sum_{j>i}^N \mathcal{U}_{LJ}(r_{ij}) + \sum_{i=1}^N \sum_{j'=1}^{N_S} \mathcal{U}_{RLJ}(r_{ij'}) \\ &\quad + \sum_{i=1}^N \sum_{j'=1}^{N_S} \mathcal{U}_{Dis}(r_{ij'}, \eta_{ij'}) + \sum_{i'=1}^{N_S} \sum_{j'>i'}^{N_S} \mathcal{U}_{LJ}(r_{i'j'}) + \mathcal{K}_M + \mathcal{K}_S\end{aligned}\quad (4.2)$$

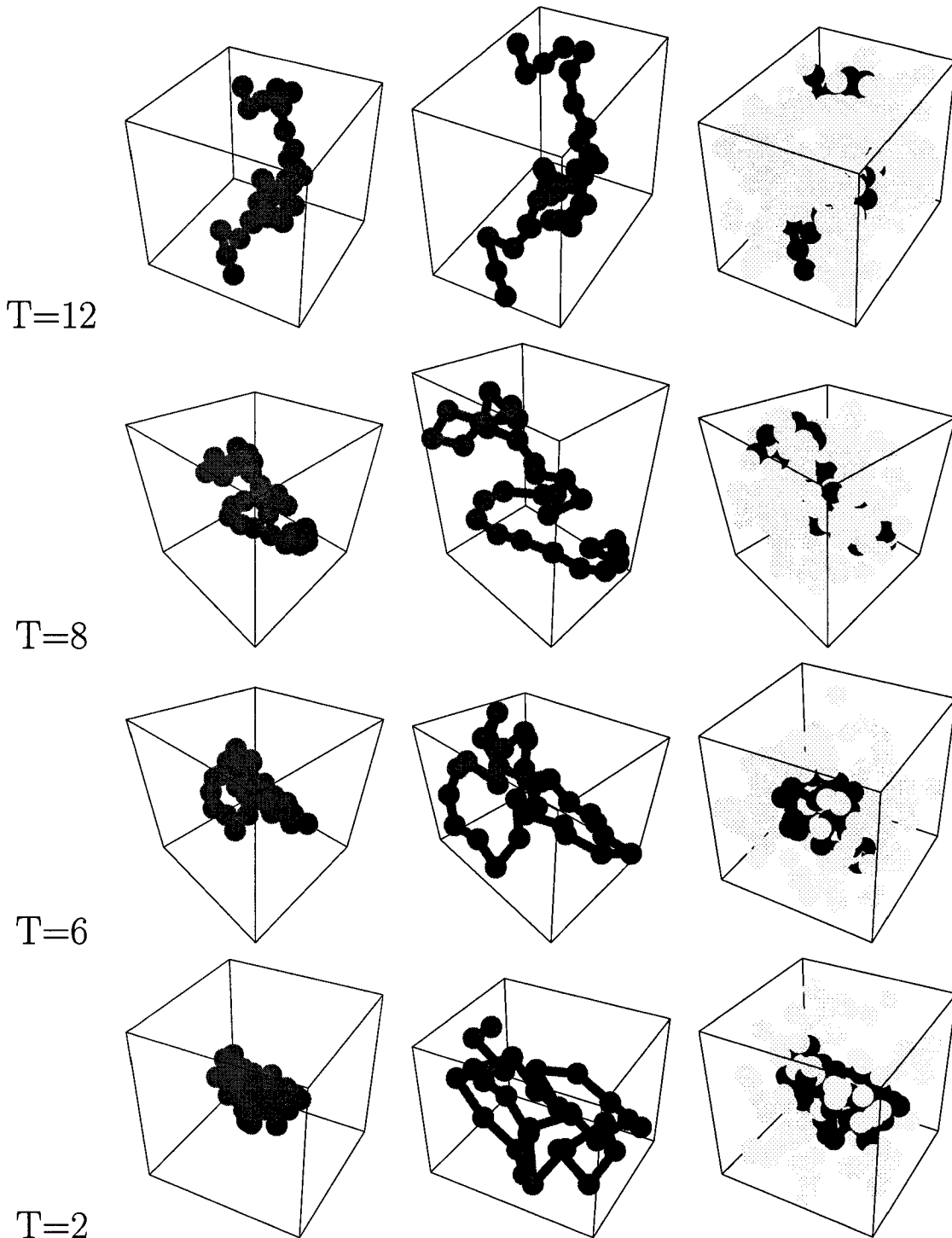


Figure 4.9: Snapshots of the conformations of a Model A type random heteropolymer in equilibrium in a solvent of density, $\rho = 0.7$, at temperatures, $T = 12$, $T = 8$, $T = 6$ and $T = 2$. The polymer has 30 monomers and the strength of the random interactions is $\alpha = 6$. The characteristic temperature is approximatively $T_\Theta = 7.5$ (see Figure 4.8). The first column shows the various conformations on the same scale which allows us to compare the size of the polymer. The second column shows us the equivalent conformations, but on an ideal scale to visualize the detail of the conformations. Finally, in the third column, we have include the solvent particles. Since it is very difficult to visualize a polymer in a solvent in three dimensions, we have only included the neighbouring solvent particles. We have also chosen various rotation angles to optimize the visualisation of the shape of the polymer.

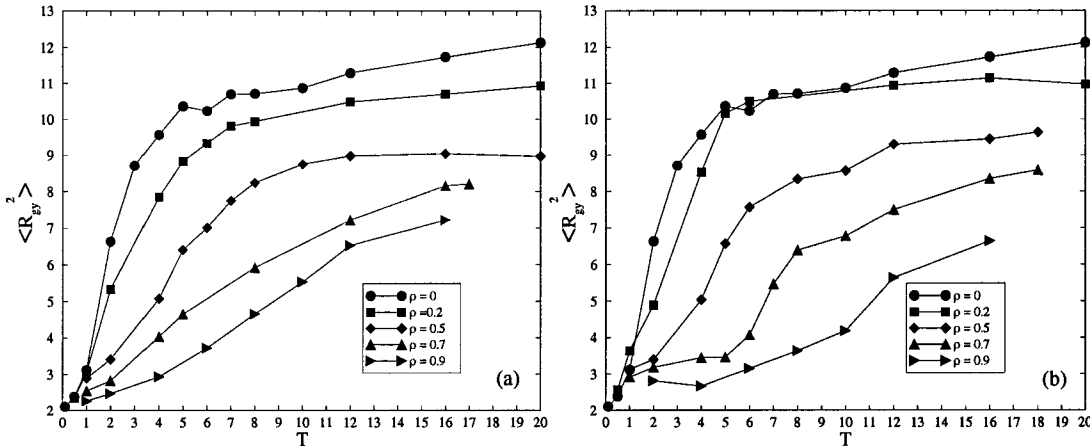


Figure 4.10: $\langle R_{yy}^2 \rangle$ versus T for a Model B flexible random heteropolymer of length $N = 30$ with random monomer–solvent interactions of strength (a) $\alpha' = 1$ and (b) $\alpha' = 6$. The number density of the system varies from $\rho = 0$ to $\rho = 0.9$ for both graphics.

The non–primed indices identify a specific monomer of the polymer chain, and the primed indices identify a specific solvent particle. The hydrophobic effect is explicit in Model B. The hydrophobic monomers tend to be located in the interior of the collapsed polymer, while the hydrophilic monomers are usually located on the outside of the globule in order to maximize contacts with the solvent particles. Note that in this case, $\rho = 0$ corresponds to a polymer in a good solvent.

Figure 4.10 shows the temperature dependence of $\langle R_{yy}^2 \rangle$ for a random heteropolymer of length $N = 30$, and Figures 4.11 and 4.12 show the corresponding temperature dependence of $\langle n_{MM} \rangle$ and $\langle n_{MS} \rangle$ respectively. The number density of the system varies from $\rho = 0$ to $\rho = 0.9$ in each of these three figures. Figure 4.10 (a), Figure 4.11 (a) and Figure 4.12 (a) correspond to a random heteropolymer with $\alpha' = 1$, while Figure 4.10 (b), Figure 4.11 (b) and Figure 4.12 (b) correspond to $\alpha' = 6$.

A decrease in $\langle R_{yy}^2 \rangle$ is again observed as the temperature, T , is lowered. A corresponding increase in $\langle n_{MM} \rangle$ is also observed as well as a decrease in $\langle n_{MS} \rangle$. For $\alpha' = 6$, some unexpected behaviour was found between $T = 4$ and $T = 6$. This is shown in Figure 4.11 (b) and Figure 4.12 (b) for $\langle n_{MM} \rangle$ and $\langle n_{MS} \rangle$ respectively. In particular, $\langle n_{MM} \rangle$ increases with increasing T in a non–monotonic manner and reaches a local maximum whereas $\langle n_{MS} \rangle$ decreases non–monotonically with increasing T and reaches a local minimum between these temperatures. The reason for this

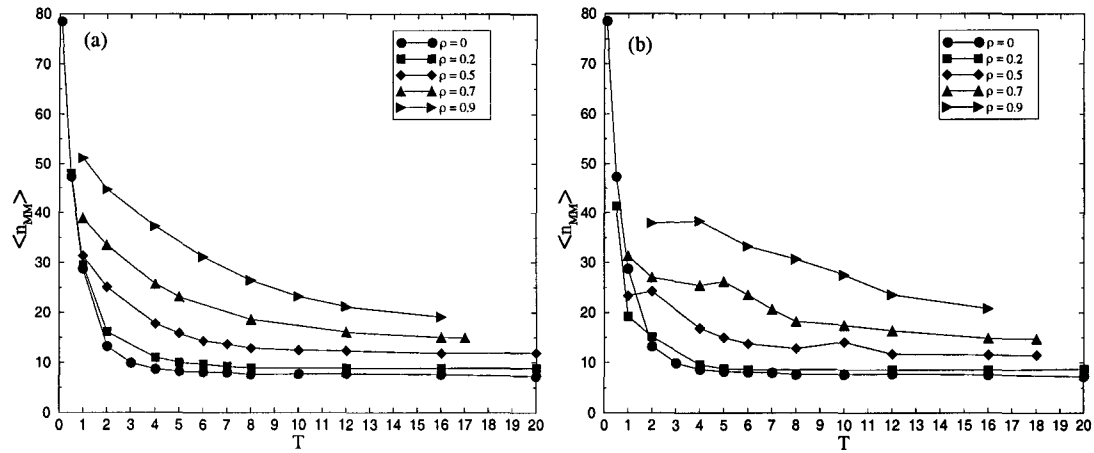


Figure 4.11: Average number of contacts between monomers versus T for a Model B flexible random heteropolymer of length $N = 30$ with random monomer–solvent interactions of strength (a) $\alpha' = 1$, and (b) $\alpha' = 6$. The number density of the system with random monomer–monomer varies from $\rho = 0$ to $\rho = 0.9$ for both graphics.

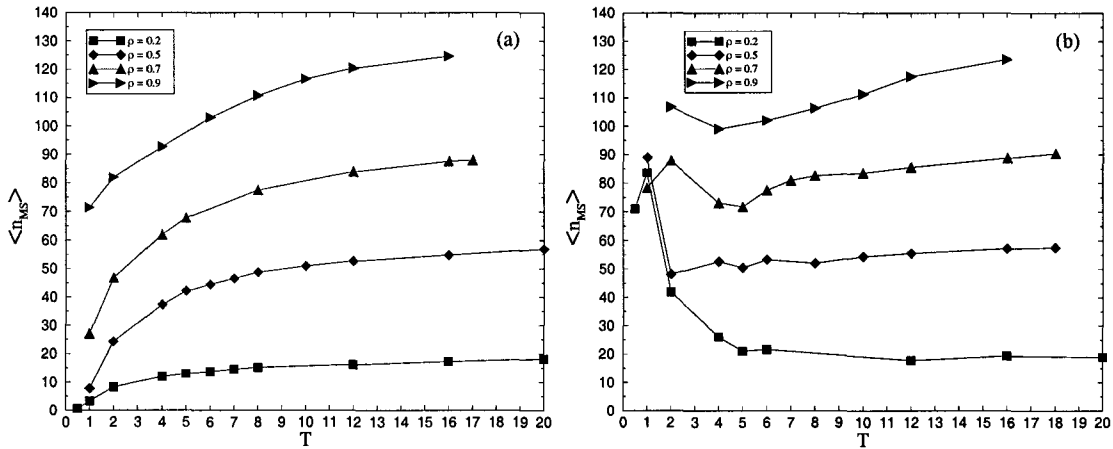


Figure 4.12: Average number of contacts between monomers and solvent particles versus T for a Model B flexible random heteropolymer of length $N = 30$ with random monomer–solvent interactions of strength (a) $\alpha' = 1$ and (b) $\alpha' = 6$. The number density of the system varies from $\rho = 0$ to $\rho = 0.9$ for both graphics.

behavior can be determined by examining the conformations of the heteropolymer at lower temperatures. Due to the nature of the random interactions, the solvent tends to repel the hydrophobic monomers more strongly while the attraction between the solvent and the hydrophilic monomers increases as α' is increased.¹ Furthermore, the related random interaction is of longer range than the short range excluded volume interaction.

Therefore, for high values of α' , the hydrophilic monomers are on the outside layer of the polymer after the initial collapse, and there is a strong attraction with the solvent which tends to “stick” to the surface of the globule (Figure 4.13). This leads to an increase in $\langle n_{MS} \rangle$ at low temperatures. This effect is more pronounced at low solvent densities. The strong interactions of the hydrophilic monomers at the surface of the globule with the solvent is also responsible for a slightly larger collapsed globule and as a result it leads to an increase in $\langle R_{yy}^2 \rangle$ and a decrease in $\langle n_{MM} \rangle$ at lower temperatures.

At higher T , $\langle R_{yy}^2 \rangle$ approaches $\langle R_{yy}^2 \rangle_{coil}$ as defined on page 59. At these temperatures, the polymer chain forms an extended coil, and the number of monomer–monomer contacts are small, while the number of monomer–solvent contacts are large. As the temperature is decreased, the value of $\langle R_{yy}^2 \rangle$ drops abruptly until it reaches a plateau at low temperatures. At this point, the polymer chain is collapsed and forms a globule of size $\langle R_{yy}^2 \rangle_{globule}$. The value of $\langle n_{MM} \rangle$ is large, while the value of $\langle n_{MS} \rangle$ is small, except in the cases where the solvent particles “stick” to the collapsed globule. The transition from the extended coil conformation occurs over a range of temperatures. Increasing the solvent density increases the width of the transition as well as the transition temperature T_Θ . Also, at higher solvent density the coil size is compressed thus reducing the values of $\langle R_{yy}^2 \rangle_{coil}$. This slight reduction in the coil size in the athermal limit (*i.e.* high T) is due to the entropic effect. Essentially, the system assumes an average size $\langle R_{yy}^2 \rangle$ which will maximize the entropy. A compressed chain will have less conformational entropy than a more spread out chain, but it will increase the translational entropy by increasing the free volume available for the solvent. Generally, the entropy of the solvent increases by more than enough to outweigh

¹The hydrophobic monomers of the heteropolymer have a random repulsive interaction with the solvent, whereas the hydrophilic monomers and the solvent particles randomly attract one another.

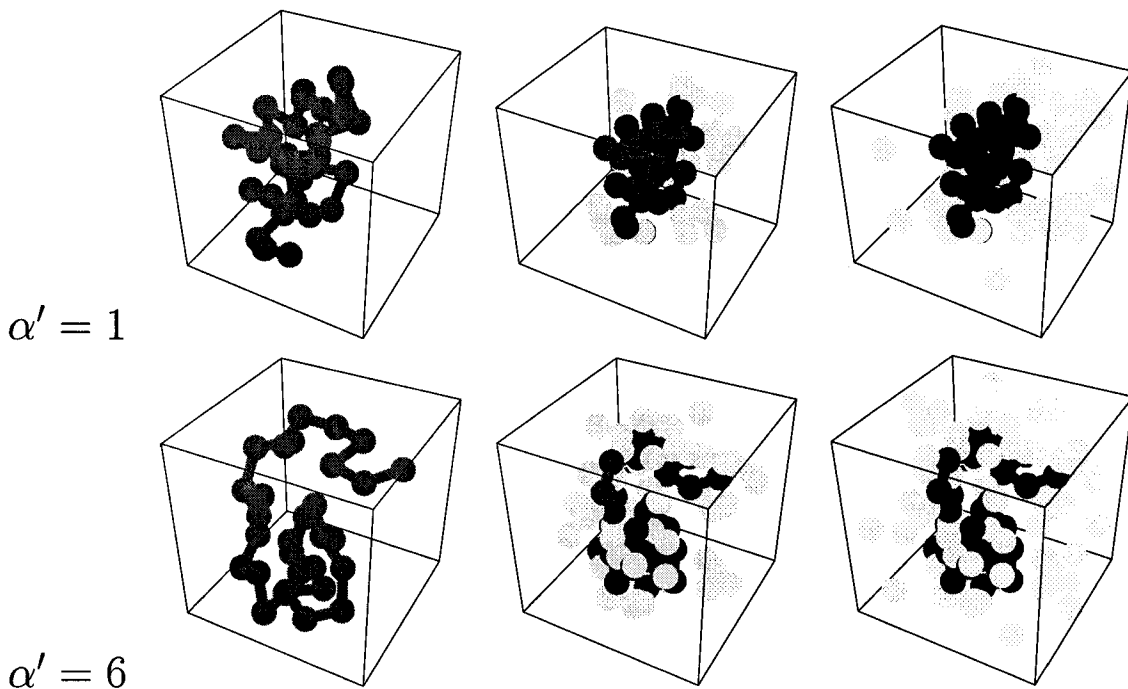


Figure 4.13: Snapshots of the conformations of a Model B flexible random heteropolymer in equilibrium in a solvent of density, $\rho = 0.2$, at temperature, $T = 1$. The polymer has 30 monomers, and the case where the strength of the random monomer–solvent interactions is $\alpha' = 6$ is compared to the one where it is $\alpha' = 1$. Each conformation in a column as been plotted on same scale in order to simplify the comparison. The first column shows globular conformations without showing the solvent particles. The second column shows us the equivalent conformations, but this time, the neighbouring solvent particles (*i.e.* solvent particles within a radius of $\sqrt{15}\sigma$ from the center of the globule and within 2σ from the edges of an imaginary box constructed from the coordinates: x_{min} , x_{max} , y_{min} , y_{max} , z_{min} and z_{max} of the polymer) were shown. Finally, in the third column, a radius, $\sqrt{27}\sigma$ of solvent particles were included around the polymer, while keeping the same conditions for the distance from the imaginary box.

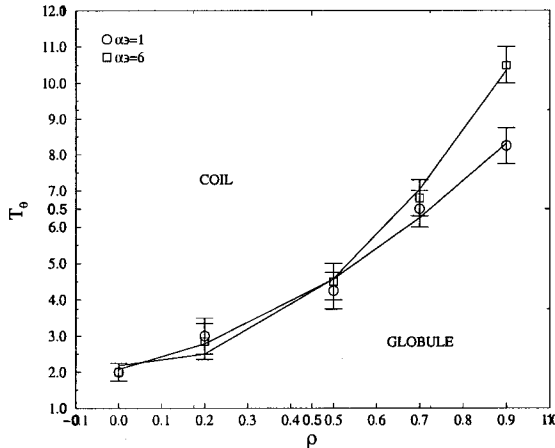


Figure 4.14: “Phase diagrams” for Model B flexible random heteropolymer chains of length $N = 30$ in an explicit Lennard–Jones solvent. T_Θ versus ρ for $\alpha' = 1$ (\circ) and $\alpha' = 6$ (\square). The values of T_Θ were measured at the points of inflection of the $\langle R_{yy}^2 \rangle$ versus T graphics (Figure 4.10) and the uncertainties were again roughly estimated by visual inspection of these same graphics.

the loss in conformational entropy. A larger solvent density will offset a greater loss in conformational entropy therefore resulting in a smaller coil size.

Finally, the characteristic temperature, T_Θ , was estimated by determining the points of inflection in the curves of $\langle R_{yy}^2 \rangle$ versus T (Figure 4.10) by using exactly the same method as the one described in the previous section. The uncertainties were again approximately estimated from the width of the transition in Figure 4.10 and comparison with Figures 4.11 and 4.12. This information was then used to construct the necessary “phase diagram” (Figure 4.14) used in Chapter 5 to perform systematic quenches across the “phase boundary”. Figure 4.14 shows the characteristic temperature T_Θ as a function of solvent density ρ for $\alpha' = 1$ and $\alpha' = 6$. The increase in T_Θ as a function of increasing density, ρ , can be observed for both $\alpha' = 1$ and $\alpha' = 6$. The effect of increasing the random monomer–solvent interactions strength, α' , is more prevalent at higher solvent densities. T_Θ is independent of α' for low densities of $\rho \leq 0.5$, but increases with increasing α' at higher densities $\rho > 0.5$. Thus, the effect of increasing α' is to stabilize the globule “phase”. The value of α' has little effect at low solvent densities, since α' is relevant only for monomer–solvent interactions, and since the driving force of the collapse is mostly the attraction between monomers.

As the solvent density is increased, the coil conformation becomes progressively more compact (Figure 4.10) which in itself makes the polymer collapse at higher

temperatures. Furthermore, the long-range repulsive part of the monomer–solvent random interaction also contributes to the collapse of the polymer to a globule. A larger solvent density will increase the effective repulsion on the polymer, which in turn will increase T_Θ . In a similar fashion, increasing the strength of the random interactions will also progressively increase the value of T_Θ at higher solvent densities.

4.4 Effect of chain stiffness (Model B with a semi-flexible chain)

We briefly examine the effect of adding stiffness to the heteropolymer chain by introducing angular restrictions in the form of a bending angle (Figure 2.3). This simulates the effect of the side chains of the amino-acids constituting a protein. Longer persistence lengths are expected to result from this added stiffness. The position of three adjacent monomers needs to be considered in order to determine the value of the bending angle. Free rotation will be allowed, and our attention will be focused on the bending effect which is modeled by an harmonic oscillator of spring constant $k_\theta = 500$ and an equilibrium angle $\Theta_0 = 109.47 \text{ deg}$. k_θ was chosen to be high enough to restrict angular fluctuations to within a few degrees for all the temperatures studied, and low enough so as to not require an extremely short time step. Θ_0 was chosen somewhat arbitrarily, but close to values for hydrocarbon chains. This may not be directly relevant to proteins.

The Hamiltonian for this case can be obtained directly from Eqs. (2.1),(2.5),(2.6),(2.7) and is given by:

$$\begin{aligned} \mathcal{H} &= \mathcal{U}_{MM} + \mathcal{U}_{MS} + \mathcal{U}_{SS} + \mathcal{K}_M + \mathcal{K}_S \\ &= \sum_{i=1, j=i+1}^{N-1} \mathcal{U}_{Spring}(r_{ij}) + \sum_{i=1}^N \sum_{j>i}^N \mathcal{U}_{LJ}(r_{ij}) + \sum_{i=1}^{N-2} \mathcal{U}_{Bend}(\theta_i) \\ &\quad + \sum_{i=1}^N \sum_{j'=1}^{N_S} \mathcal{U}_{RLJ}(r_{ij'}) + \sum_{i=1}^N \sum_{j'=1}^{N_S} \mathcal{U}_{Dis}(r_{ij'}, \eta_{ij'}) + \sum_{i'=1}^{N_S} \sum_{j'>i'}^{N_S} \mathcal{U}_{LJ}(r_{i'j'}) + \mathcal{K}_M + \mathcal{K}_S \end{aligned} \quad (4.3)$$

Non-primed indices were again used to identify a specific monomer of the polymer chain, and primed indices were used to identify a specific solvent particle. This is exactly the same system as in Section 4.3 with the added bending restriction on the

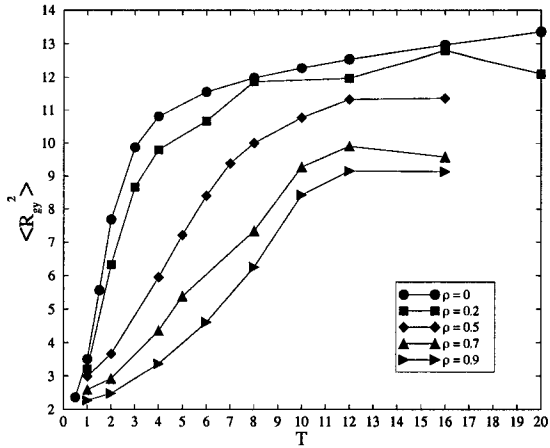


Figure 4.15: $\langle R_{yy}^2 \rangle$ versus T for a Model B semi-flexible random heteropolymer of length $N = 30$ with random monomer-solvent interactions of strength, $\alpha' = 1$, in an explicit solvent of density $\rho = 0, 0.2, 0.5, 0.7, 0.9$.

polymeric chain. The results of this section can therefore be compared directly to those of Section 4.3.

The angular restrictions have the effect of swelling the coil conformation and therefore $\langle R_{yy}^2 \rangle$ (Figure 4.15) approaches a higher plateau value $\langle R_{yy}^2 \rangle_{coil}$ at higher temperatures. For the same reason, $\langle n_{MM} \rangle$ (Figure 4.16) approaches a lower plateau, and $\langle n_{MS} \rangle$ (Figure 4.17) approaches a higher plateau at higher temperatures. As the temperature is reduced, $\langle R_{yy}^2 \rangle$ collapses to a globule conformation which does not seem to be affected by the angular restrictions.

Using the same method as the one described in the two previous sections, the characteristic temperature, T_Θ , was evaluated from Figure 4.15. Figure 4.18 shows a plot of T_Θ versus ρ for $\alpha' = 1$, with and without bending restriction. The curve that corresponds to the case without bending restriction is simply the same as the one shown in the previous section (Figure 4.14). At higher density ($\rho > 0.5$), T_Θ is smaller because of the angular restrictions which stabilize the coil “phase”.

4.5 Summary

In this chapter, we have studied the equilibrium properties of various systems consisting of a random heteropolymer in an explicit solvent. For all systems, the size of the polymer (*i.e.* $\langle R_{yy}^2 \rangle$) decreases as the temperature is lowered. Consequently, $\langle n_{MM} \rangle$

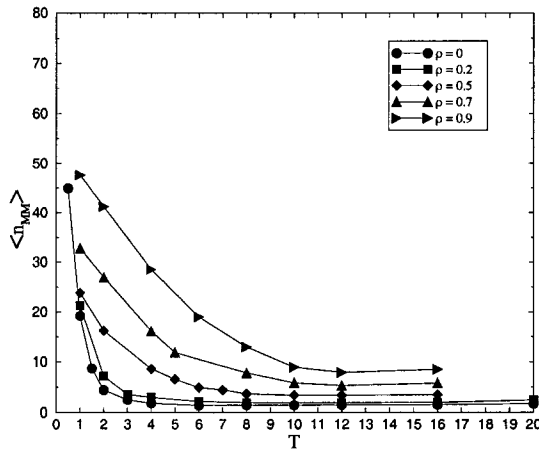


Figure 4.16: Average number of contacts between monomers versus T for a Model B semi-flexible random heteropolymer of length $N = 30$ with $\alpha' = 1$, in an explicit solvent of density $\rho = 0, 0.2, 0.5, 0.7, 0.9$.

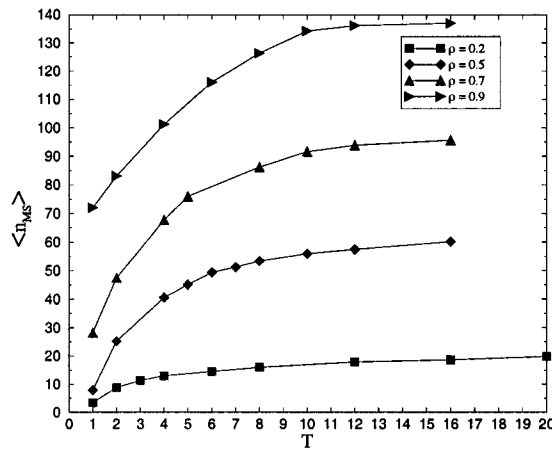


Figure 4.17: Average number of contacts between monomers and solvent particles versus T for a Model B semi-flexible random heteropolymer of length, $N = 30$ with $\alpha' = 1$, in an explicit solvent of density $\rho = 0, 0.2, 0.5, 0.7, 0.9$.

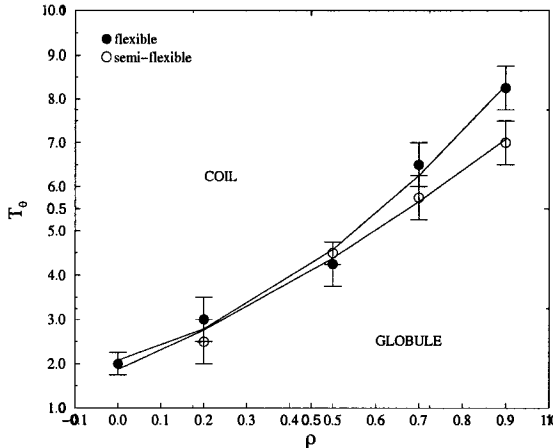


Figure 4.18: “Phase diagrams” for Model B random heteropolymer chains of length $N = 30$. The values of T_Θ were measured at the points of inflection of the $\langle R_{gy}^2 \rangle$ versus T graphics (Figure 4.15) and the uncertainties were roughly estimated by visual inspection of these same graphics. T_Θ versus ρ for $\alpha' = 1$, with (empty circles) and without (filled circles) angular restrictions.

increases while $\langle n_{MS} \rangle$ decreases as the temperature is lowered.

The size of the extended coil, which is quantified by $\langle R_{gy}^2 \rangle_{coil}$, decreases as the density of the solvent is increased, in both the case where the random interaction is between the monomers of the heteropolymer (Model A) and the case where the random interaction is between the monomers and the solvent atoms (Model B). At low solvent densities, the entropy of the system is dominated by the conformational entropy of the polymer and thus the system favors an extended coil conformation in order to maximize the conformations available to the chain and the total entropy of the system. At higher solvent densities, the translational entropy related to the solvent particles becomes more important and the system favors a slightly compressed coil conformation for the polymer in order to increase the free volume available for the solvent. Thus the translational entropy of the solvent increases by more than enough to offset that which was lost by the chain. Furthermore, the size of the polymer coil is inversely proportional to the solvent density with a proportionality constant which depends on the polymer length. It is interesting to note that the compression of the polymer coil becomes more important for a longer polymer chain. This can also be explained by the entropic effect. The linear relation between $\langle R_{gy}^2 \rangle_{coil}$ and ρ , seen in Figure 4.5, is quite different from the relation obtained by Escobedo and Pablo [96], in the same athermal limit.

$\langle R_{gy}^2 \rangle_{coil}$ also decreases as a function of the strength of the random interactions between monomers while it does not seem to significantly depend on the monomer–solvent random interaction. Furthermore, the angular restrictions have the effect of swelling the coil conformation thereby increasing the value of $\langle R_{gy}^2 \rangle_{coil}$. As for the size of the collapsed globule, $\langle R_{gy}^2 \rangle_{globule}$, it was difficult to determine if it varies with ρ , α , or angular restrictions. We can only affirm that if $\langle R_{gy}^2 \rangle_{globule}$ does indeed depend on ρ , α , or angular restrictions, it is a very weak dependence.

The transition from the extended coil conformation to the globular conformation is thermally driven and results from the system selecting conformations which will minimize the free energy, $F = E - TS$, of the system. T controls the strengths of the two terms contributing to the free energy. A globular conformation (a decrease in $\langle R_{gy}^2 \rangle$) is favored by the energy term, E , while an expanded coil (an increase in $\langle R_{gy}^2 \rangle$) is favoured by the total entropy term. The total entropy can be divided into translational entropy and conformational entropy. The translational part favours a globular state, but the conformational contribution is the dominant part, and it favours an expanded coil conformation.

Increasing the solvent density increases the value of the characteristic temperature, T_Θ . As the solvent density is increased, the coil conformation becomes progressively more compact which in itself makes the polymer collapse at higher temperatures. Furthermore, the long-range repulsive part of the monomer–solvent random interaction also contributes to the collapse of the polymer to a globule. A larger solvent density increases the effective repulsion on the polymer, which in turn increases T_Θ . Increasing the value of the strength of the random monomer–monomer interactions, increases the value of T_Θ , thus favoring the globular “phase”. Increasing the value of the strength of the random monomer–solvent interactions increases the value of T_Θ progressively, at higher solvent densities. Thus, the effect of increasing α' is to stabilize the globule “phase”. The value of α' has little effect at low solvent densities, since α' is relevant only for monomer–solvent interactions, and since the driving force of the collapse is mostly the attraction between monomers. Furthermore, the addition of a bending restriction to the chain reduces the value of T_Θ , at higher densities, since the angular restrictions stabilize the coil “phase”.

The appropriate “phase diagrams” are now available to perform systematic quenches across the “phase boundary” separating the coil conformation and the globular conformation. These will be presented in the next chapter.

Model A is closer in spirit to the effective pair potential approach, since the heterogeneity is incorporated into the monomer–monomer interactions, while for Model B, these are incorporated into the monomer–solvent interactions. By choosing to study Model A and Model B, we were basically making our system gradually more realistic. We went from the study of a random heteropolymer with an implicit solvent to the study of a random heteropolymer immersed in an explicit solvent in two steps.

COLLAPSE KINETICS OF A RANDOM HETEROPOLYMER IN SOLVENT

In this chapter, we examine the collapse kinetics of a random heteropolymer in an explicit solvent on the basis of the equilibrium properties examined in the previous chapter. This is in contrast to the collapse kinetics examined in Chapter 3 where the effect of a solvent is included implicitly in the random heteropolymer model via the monomer–monomer interactions. The inclusion of an explicit solvent is clearly more realistic and the collapse kinetics of polymers immersed in an explicit solvent are expected to be qualitatively different from the case of isolated polymers, where the solvent is implicit. For the sake of completeness, we again give a brief introduction to polymer collapse in general and in the presence of an explicit solvent before examining the particular case of the collapse kinetics of random heteropolymers.

The polymer collapse problem has been quite popular since the 1980's and many analytical and computational methods have been used to further the knowledge in this field. Considerably more is known about the collapse dynamics of homopolymers because of their relative simplicity compared to the more complex heteropolymers. Because of the high computational demands associated with the study of models which include an explicit solvent, the solvent is most often incorporated implicitly into the effective monomer–monomer interactions.

The work of de Gennes [85] is the first theoretical study of homopolymer collapse. This work used a mean-field scheme for dynamics near the Θ –solvent conditions. De Gennes observed a two–stage collapse where the polymer initially collapsed into a “sausage” shape by forming connected blobs of locally collapsed monomers. A slower collapse follows when the effect of diffusion (or hydrodynamic friction) causes a uniform thickening of the “sausage” as the ends contract until the polymer becomes almost spherical. The effects of topological constraints, on later stages of the col-

lapse, were later examined by Grosberg, Nechaev and Shakhnovich [88]. Dawson and his colleagues proposed another analytical method, the Gaussian Self-Consistent theory employing the Langevin equation, which was used to describe both the collapse dynamics of homopolymers (Timoshenko, Kuznetsov and Dawson [95]; Kuznetsov, Timoshenko and Dawson [96b]) and heteropolymers (Timoshenko, Kuznetsov and Dawson [98]). Their results show that the collapse of a heteropolymer is a complicated process which strongly depends on the sequence of the chain.

Various computer simulation methods were also used to study polymer collapse. Ostrovsky and Bar-Yam [95]; [94] studied homopolymers using Monte Carlo simulations in two and three dimensions. Their model used irreversible monomer aggregation. They observed the formation of a pearl necklace and the gradual diffusion of large pearls from the chain ends. Dawson and his colleagues used Langevin (Kiernan, Green and Dawson [95]) and Monte Carlo (Yu et al. [95]) simulations to study both the collapse of homopolymers and random copolymers. In these cases, monomer aggregation was reversible. They observed that upon collapse, long chains form local clusters (or pearls) at random positions along the chain at short times, which coalesce at longer times. This is the same mechanism which was observed in Chapter 3.

Polson and Zuckermann (Polson and Zuckermann [00]) used molecular dynamics simulations to study the equilibrium properties and collapse dynamics of homopolymers and random copolymers in two dimensions. They went further than their predecessors by incorporating an explicit solvent. In the case of homopolymers, they found that the collapse rates increase monotonically with increasing hydrophobicity, and decreases with increasing solvent density. They also found that the degree of hydrophobicity had similar effect on the collapse times of homopolymers and random copolymers, except at very low degrees for hydrophobicity. Furthermore, Polson and Zuckermann [01] have recently repeated this work for three dimensional systems and among other interesting results, they showed that the relationship of the collapse rates to the well depth (*i.e.* to the degree of hydrophobicity) is not strongly affected by the dimensionality of the system. Very recently, Chang and Yethiraj [01] have published a computer simulation study of the effect of the solvent on the collapse dynamics of neutral homopolymers. First, they used Brownian dynamics simulations

to examine the case where the solvent was incorporated implicitly via a pairwise additive attraction between the monomers. Next, they used molecular dynamics simulations to study the case where the solvent is incorporated explicitly. The objective of their work was to compare these two systems by using an integral equation theory to map the homopolymer–solvent system unto the two–body monomer–monomer potential model for an isolated homopolymer. In the work of Grayce [97], it is shown that a many–body potential would be better to perform such a mapping. In both Brownian dynamics and the molecular dynamics cases, the homopolymer collapsed in two stages. The first stage is rapid and consists in the formation of local blobs that eventually grow and coalesce to form a “sausage” shape. The second stage is slow and consists in the thickening and shortening of the sausage until it becomes a spherical globule. When the homopolymer is immersed in an explicit solvent, the size of the polymer varies smoothly in time during the second stage while it varies through discrete jumps in the case of the isolated homopolymer because it is getting trapped in low energy local minima.

The studies described so far do not include hydrodynamic effects. However, the complicated hydrodynamic interactions related to the addition of an explicit solvent, as included in the Rouse–Zimm theory of equilibrium polymer dynamics (Doi and Edwards [86]) result in dynamic properties which scale with polymer size in a way which differs significantly from the case where the effects of hydrodynamics are omitted. For example, the diffusion constant, D , and the relaxation time, τ_R , of a free Rouse molecule scale with the number of beads, N , as follows: $D \propto N^{-1}$ and $\tau_R \propto N^2$. On the other hand, a Rouse–Zimm molecule has the following scaling laws which are in agreement with experimental results: $D \propto N^{-1/2}$ and $\tau_R \propto N^{3/2}$. Various research groups have verified these predictions numerically with constant energy simulations of single polymer in an explicit solvent (Dünweg and Kremer [91]; Pierleoni and Ryckaert [91]; Shannon and Choy [97]). As a result, the hydrodynamic effect was included in work like Dawson’s Self–Consistent analytical theory (Timoshenko, Kuznetsov and Dawson [95]; [96]; [98]; Kuznetsov, Timoshenko and Dawson [96a]; [96b]; Dawson, Timoshenko and Kuznetsov [97]), de Gennes’ (Buguin, Brochard-Wyart and de Gennes [96]) and Halperin’s (Halperin and Goldbart [00])

phenomenological models, and Pitard's (Pitard [99]) and Ganazzoli's (Ganazzoli, Ferla and Allegra [95]) Langevin models.

Though the simulations of polymer collapse in an explicit solvent have a high computational cost, it is worthwhile to study this problem since the collapse behavior could differ qualitatively from that seen in simulations of isolated chain systems (Chapter 3), or even from theories which include all of the effects of hydrodynamic interactions. In contrast to most of the earlier work on collapse kinetics, we study heteropolymer collapse and our systems of interest are the same three systems described in Chapter 4. All simulations will use a Langevin thermostat. The polymer length is $N = 30$. The number of solvent particles N_S was chosen so that $N_S + N = 512$ for low densities and $N_S + N = 1000$ for densities higher than $\rho = 0.3$.

Both a change in temperature T or a change in the strength of the random interaction¹ can drive the transition from the coil "phase" to the collapsed globule "phase", but mostly temperature quenches will be implemented by using the characteristic temperatures T_Θ found in Chapter 4. The quenches are performed by first bringing the polymer to thermal equilibrium at $T_I > T_\Theta$ and then quenching to $T_F < T_\Theta$. The initial state of the system was obtained by the equilibrium simulations of Chapter 4. To study the relaxation dynamics after a temperature quench for a given initial equilibrium conformation, 5×10^4 time steps per monomer (*i.e.* a time interval of $250\tau_0$) were used and the relaxational process was monitored by following the decay of a few selected quantities. The results were then averaged over 20 independent quench runs for the same initial conditions (*i.e.* for a given $\{\eta_{ij}\}$) to reduce fluctuations in the data since the only difference between each quench run is the thermal noise. Finally, up to 10 impurity averages for different realizations of $\{\eta_{ij}\}$ for a given α were performed for a given set of the remaining system parameters.

In all of the calculations reported here the value of the time step is $\Delta t = 0.005\tau_0$, and the coupling friction between the particles and a heat bath is $\Gamma = 0.5\tau_0$. The value of Γ was chosen to be large enough so that the thermostat relaxation is fast compared to the polymer collapse. Furthermore, the unstretched bond length was taken to be $R_0 = \sigma$, and the value of the coupling constant, k , for the harmonic

¹The strength of the random interaction, α , is also a measure of the polymer heterogeneity and of the overall hydrophobicity.

interaction of Eq. (2.8) used in the simulations was chosen as $k\sigma^2/\epsilon = 500$. As in the previous chapters, all quantities described below will be in Lennard–Jones reduced units. Distances will be expressed in terms of σ , temperatures in terms of k_B/ϵ and time in terms of $\sqrt{m\sigma^2/\epsilon}$ where m is the mass of each monomer and each solvent particle.

In order to make our system gradually more realistic, we proceeded systematically from the study of a random heteropolymer with an implicit solvent to the study of a random heteropolymer immersed in an explicit solvent in two steps. In Section 5.1, the random interactions are taken to be between the monomers (Model A). In Section 5.2, the random interactions occur between the monomers and the solvent particles (Model B with a flexible chain). In Section 5.3, the random interactions are again taken between the monomers and the solvent particles but this time a bending restriction is added to the polymeric chain which becomes semi-flexible (Model B with a flexible chain). Finally, Section 5.4 summarises the results of the quenches performed in this chapter.

5.1 Random monomer-monomer interactions (Model A)

In this section, we consider the time-dependence of R_{yy} and n_{MM} during a quench, averaged over a few different random sequences. The temperature or the strength of the monomer–monomer random interaction is abruptly changed from T_I to T_F or α_I to α_F respectively, and the system then undergoes a conformational change from an extended coil to a globule state. As in the case of the equilibrium properties, we are interested in the differences in the collapse behavior upon variation of the strength of the monomer–monomer random interaction, α , and the value of the solvent density, ρ .

5.1.1 Temperature–driven random heteropolymer collapse

In this subsection, we examine the effects of solvent density and of polymer heterogeneity (α) on polymer collapse driven by a sudden change in temperature. We first investigate the effects of solvent density on the rate of polymer collapse.

Effects of solvent density on the polymer collapse rate

Here we compare the polymer collapse times for the cases of $\alpha = 4$ and $\alpha = 6$. These values of α were chosen from Figure 4.8 such as to have constant values of T_I and constant values of T_F over the entire range of densities considered. T_I has to be such that we can select a time step which allows for reasonable computational time and maintains the stability of the MD simulations. Also, T_F has to be sufficiently high to avoid trapping the polymer chain in a local minimum of the energy landscape. Polymer collapse is induced by performing temperature quenches from $T_I = 16$ to $T_F = 1$ for $\alpha = 4$ and $T_I = 16$ to $T_F = 2$ for $\alpha = 6$. Figure 4.8 shows that the polymer chain is in an extended coil conformation for these values of T_I and in a collapsed globule conformation for these values of T_F .

Figures 5.1 and 5.2 give averaged values of (a) $R_{yy}(t)$, (b) $n_{MM}(t)$ and (c) $T^*(t)$ ¹, for random heteropolymers with random monomer–monomer interactions of strength $\alpha = 4$ and $\alpha = 6$ for various solvent densities. As observed in Figure 4.5, the initial equilibrium coil size is dependent on the solvent density. In general, the value of $R_{yy}(t_I)$ decreases with increasing values of ρ and it follows that the value of $n_{MM}(t_I)$ increases with increasing values of ρ , where t_I is the time at which we started to acquire data ($t_I = 5$). $R_{yy}(t_I)$ does not however follow the trend for the specific case where $\alpha = 4$ and $\rho = 0.3$. Furthermore, for quenches to the same final temperature T_F , which is under T_Θ for the entire range of ρ , the final collapsed conformation size $R_{yy}(t_F)$ tends to decrease slightly with increasing values of ρ while $n_{MM}(t_F)$ increases with increasing values of ρ . This is more obvious for $n_{MM}(t)$ than $R_{yy}(t)$. $R_{yy}(t_F)$ does not follow the trend for the specific case where $\alpha = 6$ and $\rho = 0.9$, as well as the case where $\alpha = 4$ and $\rho = 0.3$. The discrepancies in the trends of $R_{yy}(t)$ at both $t = 0$ and $t = t_F$ are most likely to be due to insufficient sampling of both initial conformations and sequences. Note that t_F is the final time of the quench and for the work presented in this chapter, $t_F = 250$. In fact, all that is important is that t_F is long enough so that the chain has equilibrated to its final globule size.

It is not straightforward to determine whether the decay is more or less rapid for increasing solvent densities by just looking at Figures 5.1 (a) and (b) as well as

¹ $T^*(t)$ is the instantaneous kinetic temperature of the system as defined in Section 2.2.3

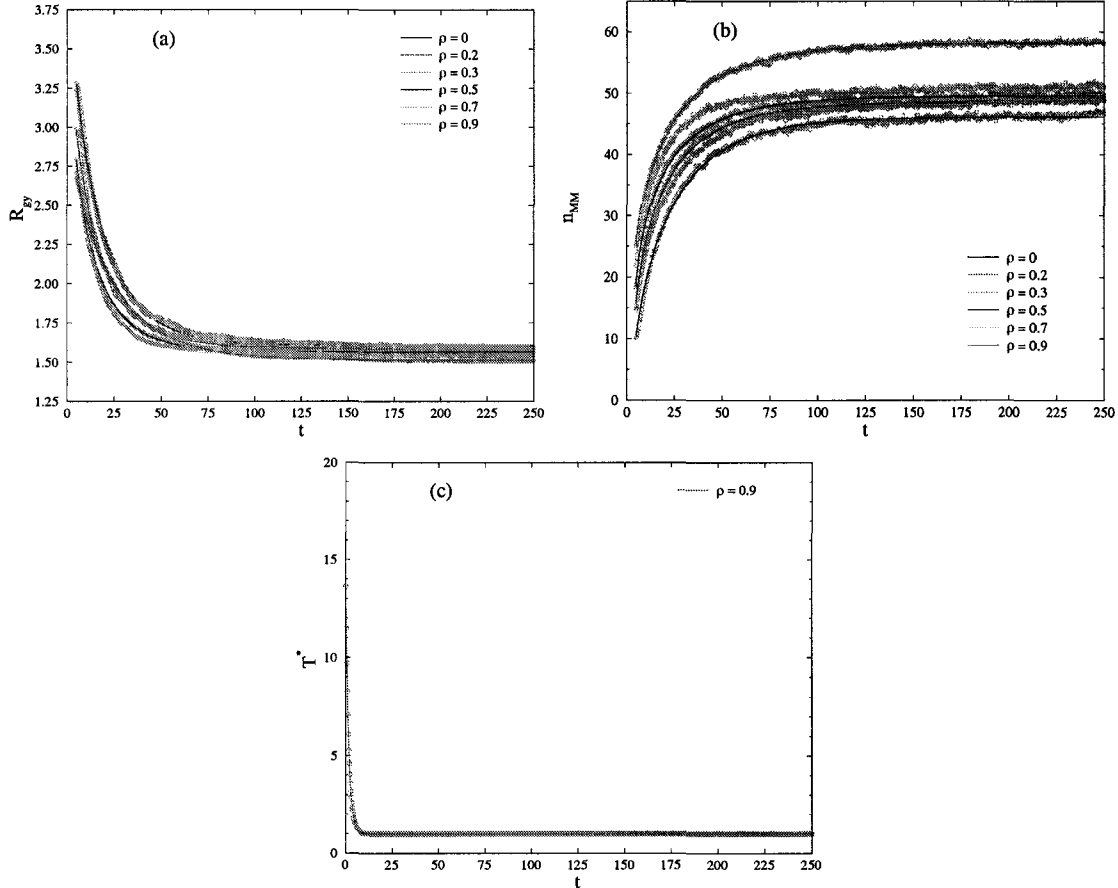


Figure 5.1: Relaxation curves for a Model A type random heteropolymer of length, $N = 30$ and random monomer–monomer interactions strength, $\alpha = 4$ for solvent densities $\rho = 0, 0.2, 0.3, 0.5, 0.7, 0.9$: (a) R_{gy} versus t , (b) n_{MM} versus t and (c) T^* versus t (only $\rho = 0.9$). All the temperature quenches were performed from $T_I = 16$ to $T_F = 1$. Each curve corresponds to an average over 20 independent quench runs for the same initial condition. Finally, up to 10 impurity averages for different realizations of $\{\eta_{ij}\}$ for a given α were performed for a given set of the remaining system parameters.

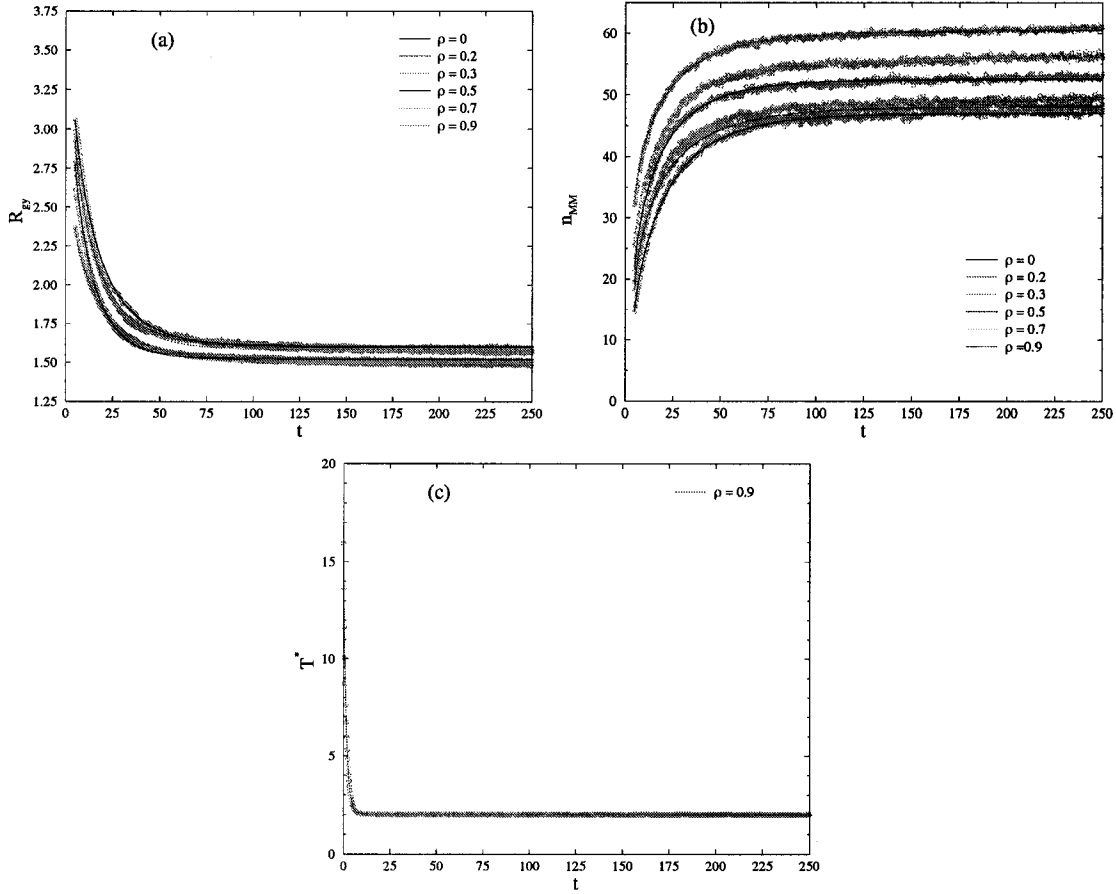


Figure 5.2: Relaxation curves for a Model A type random heteropolymer of length, $N = 30$ and random monomer–monomer interactions strength, $\alpha = 6$ for solvent densities $\rho = 0, 0.2, 0.3, 0.5, 0.7, 0.9$: (a) R_{gy} versus t , (b) n_{MM} versus t and (c) T^* versus t (only $\rho = 0.9$). All the temperature quenches were performed from $T_I = 16$ to $T_F = 2$. Each curve corresponds to an average over 20 independent quench runs for the same initial condition. Finally, up to 10 impurity averages for different realizations of $\{\eta_{ij}\}$ for a given α were performed for a given set of the remaining system parameters.

Figures 5.2 (a) and (b) since the curves do not start nor end at the same values. It was therefore necessary to use a quantitative method in order to compare the rate of collapse for various solvent densities. To do so, the curves were fitted to a stretched exponential function:

$$y(t) = a_0 e^{-((t-t_I)/\tau)^\beta} - a_1, \quad (5.1)$$

to determine the collapse times t_{50} and t_{90} as evaluated from the decay of both $R_{gy}(t)$ (Figures 5.3 (a)) and $n_{MM}(t)$ ((Figures 5.3 (b)). t_{50} and t_{90} are the 50% and the 90% decay times defined in Section 2.2.3 and in Appendix A.2. Note that in Chapter 3, we have fitted the total energy of the system to a stretched exponential. This was a satisfying choice of a physical quantity to monitor during the polymer collapse since it was well defined. On the other hand, with the added explicit solvent, the energy to monitor was not well defined and it was more appropriate to study the effect of the explicit solvent by monitoring the radius of gyration and the contacts between monomers.

The collapse of random heteropolymers with $\alpha = 1$ and various solvent densities were studied in a similar manner by performing temperature quenches from $T_I = 16$ to $T_F = 1$ for $\rho > 0.5$. The collapse times for this scenario is also included in Figure 5.3. Note that it was not possible to perform the quenches at densities lower than $\rho = 0.5$ in this case due to the fact that $T_F = 1$ is below T_Θ for lower densities. One could argue that we could have used $T_F = 0.1$ for the entire range of densities but quenches to such a low temperature as $T_F = 0.1$ could lead to unreliable results. The dynamics of the system at such low temperatures are likely to be very sluggish, and the chain is usually in a glassy state (*i.e.* it is trapped in a local minima of the free energy landscape). The rate of escape from a local minimum is probably extremely slow which brings about ergodicity breaking.

Figure 5.3 shows a plot of t_{50} and t_{90} as determined by the decay of both (a) R_{gy} and (b) n_{MM} . Appendix A.2 describes the calculations of the error bars which were smaller than the size of the symbols. Note that the main source of the scatter in the data is due to using small samples of both initial conformations and sequences. From these figures, the collapse times are generally shorter for higher values of α , *i.e.* increased heterogeneity leads to faster collapse. However, note that the values of

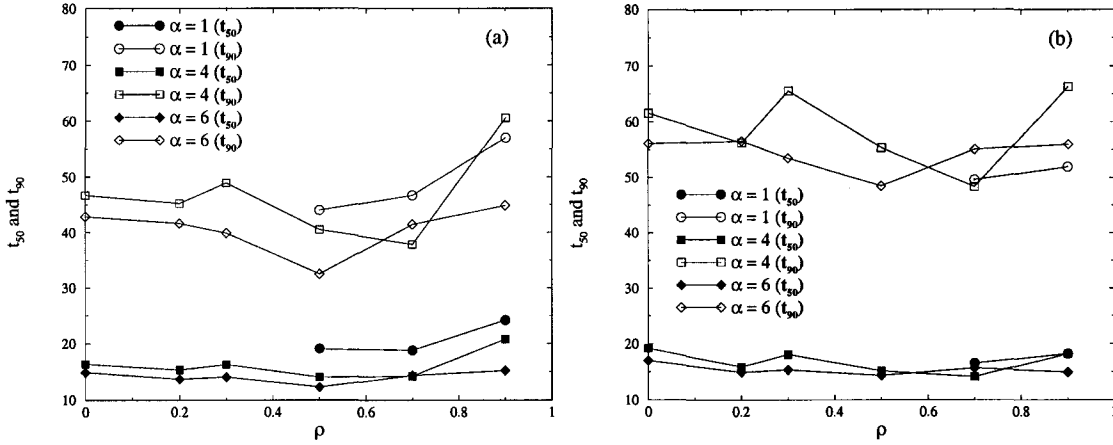


Figure 5.3: t_{50} and t_{90} as a function of ρ for a Model A type random heteropolymer with monomer-monomer random interaction strength $\alpha = 1$, $\alpha = 4$ and $\alpha = 6$. $T_I = 16$ for all values of α . $T_F = 1$ for $\alpha = 1$ and $\alpha = 4$, and $T_F = 2$ for $\alpha = 6$. t_{50} and t_{90} were evaluated from: (a) the R_{yy} versus t plots of Figures 5.1 (a) and 5.2 (a); (b) the n_{MM} versus t plots of Figures 5.1 (b) and 5.2 (b). The case where $\alpha = 1$ was treated in a similar manner as for $\alpha = 4$ and $\alpha = 6$.

$\alpha = 1$ and $\alpha = 4$ cannot directly be compared with those of $\alpha = 6$ since we employed a different value of T_F for $\alpha = 6$. Furthermore, the curves are almost flat, meaning that varying the density of the solvent had very little effect on the rate of collapse at least for $\alpha = 4$ and $\alpha = 6$. Conclusions concerning the $\alpha = 1$ curve should be treated with caution due to the small range of densities. This is definitely a different result from that obtained by Polson and Zuckermann [01] where the collapse rate decreases monotonically with increasing solvent density.

It should be remembered that the random heteropolymers considered in this section are similar to the ones considered in Chapter 3 but with added solvent particles which only interact via a short range repulsive interaction with the monomers of the random heteropolymer. The density-independence of the collapse rate could suggest that the collapse rate is determined by a competition of the monomer-monomer repulsion and attraction with the monomer-solvent interactions, especially for the high values of α considered here. The interactions between the solvent particles could also have an indirect effect though this should be relatively minor in comparison to the monomer-monomer and monomer-solvent interactions. Another possibility is that the independence of the collapse time on the solvent density is an artifact of the Langevin thermostat. Using a high friction coefficient could indeed overdamp the

	ρ	0	0.2	0.3	0.5	0.7	0.9
$\alpha = 4$	β	0.93	0.96	0.96	0.96	0.97	0.91
	τ	1.33	1.03	1.06	1.12	1.24	1.31
$\alpha = 6$	β	0.87	0.99	0.98	0.98	0.98	0.96
	τ	1.34	1.07	1.08	1.15	1.25	1.38

Table 5.1: β and τ for the thermal relaxation of a Model A random heteropolymer with $\alpha = 4$ from $T_I = 16$ to $T_F = 1$ and $\alpha = 6$ from $T_I = 16$ to $T_F = 2$.

system and reduce the influence of the interactions with the solvent. Further studies would be required to clearly determine if this is a thermostat-independent effect and a real property of the "real" interactions of the system (i.e. the conservative forces between particles). However, we expect that at higher solvent densities, the collapse rate will decrease since the solvent will then act as an obstacle to the collapse of the polymer chain. From Figure 5.3 we could thus argue that such an increase in the collapse times occurs for $\rho = 0.9$ but the scatter of the data prevents us from making a firm statement about this. As in the case of equilibrium average R_{gy} and n_{MM} , we find that the collapse time of the two quantities follow a similar trend over the entire range of ρ for both systems. In some cases the values are in fact very close over most of the range of ρ .

We plotted $T^*(t)$ (Figures 5.1 (c) and 5.2 (c)) in order to examine the relaxation of the Langevin thermostat. Note that for clarity, these figures only show the result for $\rho = 0.9$. $T^*(t)$ was fitted to a stretched exponential (Eq. (5.1) with $t_I = 0$) and values of the stretched exponent β and the time scale τ were obtained for various values of ρ . These values of β and τ can be found in Table 5.1. β is essentially independent of ρ over the range of $\rho = 0.2$ to $\rho = 0.7$ and is very close to the value for a pure exponential. In the special case where there is no solvent, the relaxation of the thermostat is slightly slower since there are no explicit solvent atoms to diffuse away the extra energy. On the other hand, the time scale appears to increase with increasing solvent density except for the case without explicit solvent. In this latter case, the time scale is comparable to the time scale obtained for $\rho = 0.9$, i.e. $\tau(\rho = 0) \approx \tau(\rho = 0.9)$. By doing further studies, we observed that β and τ are independent of the values of

T_I and T_F . This applies to T_F above and below T_Θ .

Effects of polymer heterogeneity (α) on the polymer collapse rate

Next, we investigate the effect of polymer heterogeneity on the polymer collapse rate for $\rho = 0$, $\rho = 0.7$ and $\rho = 0.9$. From Figure 4.8, T_I and T_F were chosen such as to have constant values of T_I and constant values of T_F over the entire range of α considered for a given solvent density. Furthermore T_I was chosen to be greater than T_Θ to allow for an initial extended coil conformation, and T_F was chosen to be lower than T_Θ to allow for a final collapsed globule conformation. Polymer collapse is induced by performing temperature quenches from $T_I = 16$ to $T_F = 0.1$ for $\rho = 0$ and $T_I = 16$ to $T_F = 1$ for $\rho = 0.7$ and $\rho = 0.9$.

Figures 5.4, 5.5 and 5.6 show averaged values for (a) $R_{yy}(t)$, (b) $n_{MM}(t)$ and (c) $T^*(t)$ for random heteropolymers with several random monomer–monomer interaction strengths α without an explicit solvent ($\rho = 0$) (Figure 5.4) and immersed in an explicit solvent of density $\rho = 0.7$ (Figure 5.5) and $\rho = 0.9$ (Figure 5.6). As observed in Figures 4.3 and 4.4, the initial equilibrium coil size is dependent on the strength of the monomer–monomer random interactions α . At constant density, the size of the coil decreases with increasing values of α . In other words, $R_{yy}(t_I)$ decreases with increasing α , while $n_{MM}(t_I)$ increases with increasing α . We observe, however, a few exceptions to the trend of $R_{yy}(t_I)$ for $\rho = 0$ and $\rho = 0.9$. Again, we argue that this is related to insufficient sampling of both initial conformations and sequences. Note that the coil size depends much less on α than it does on ρ making it easier to determine that the rate of collapse increases with α . Furthermore, for quenches to the same final temperature T_F , which is below T_Θ for the entire range of α , the final collapsed conformation size $R_{yy}(t_F)$ tends to decrease with increasing values of α while $n_{MM}(t_F)$ increases with increasing values of α . Again, a quantitative method was used in order compare the rate of collapse for various values of α . To do so, the curves were fitted to a stretched exponential function (Eq. (5.1)) to determine the collapse times t_{50} and t_{90} as evaluated from the decay of both $R_{yy}(t)$ (Figure 5.7 (a) and Figure 5.8 (a)) and $n_{MM}(t)$ (Figure 5.7 (b) and Figure 5.8 (b)). Appendix A.2 provides the calculations of the error bars which were smaller than the symbol size. The main source of the scatter in the data is related to the small sampling of both

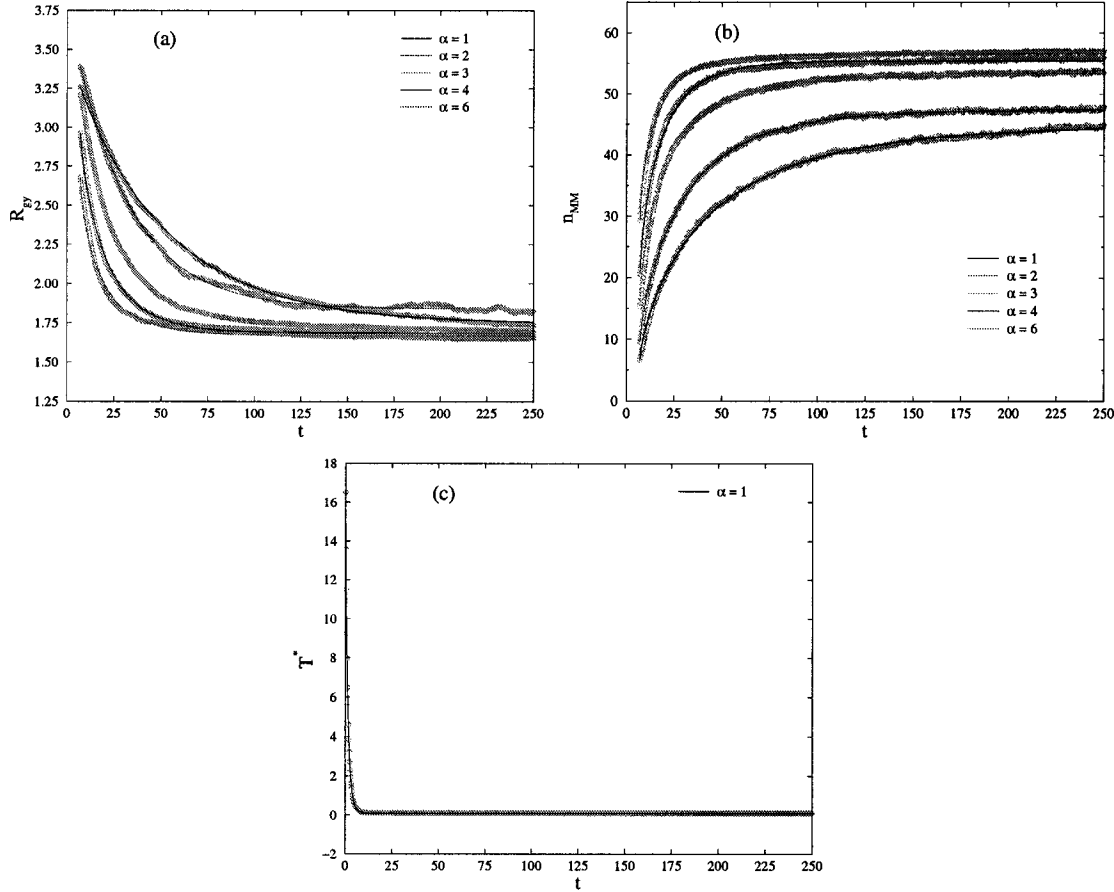


Figure 5.4: Relaxation curves for a Model A type random heteropolymer. The length of the chain was $N = 30$, the solvent density was $\rho = 0$ and the random monomer-monomer interactions strength was $\alpha = 1, 2, 3, 4, 6$: (a) R_{gy} versus t , (b) n_{MM} versus t and (c) T^* versus t (only for $\alpha = 1$ for clarity). All the temperature quenches were performed from $T_I = 16$ to $T_F = 0.1$ for all values of α . Each curve corresponds to an average over 20 independent quench runs for the same initial condition. Finally, 10 impurity averages for different realizations of $\{\eta_{ij}\}$ for a given α were performed for a given set of the remaining system parameters.

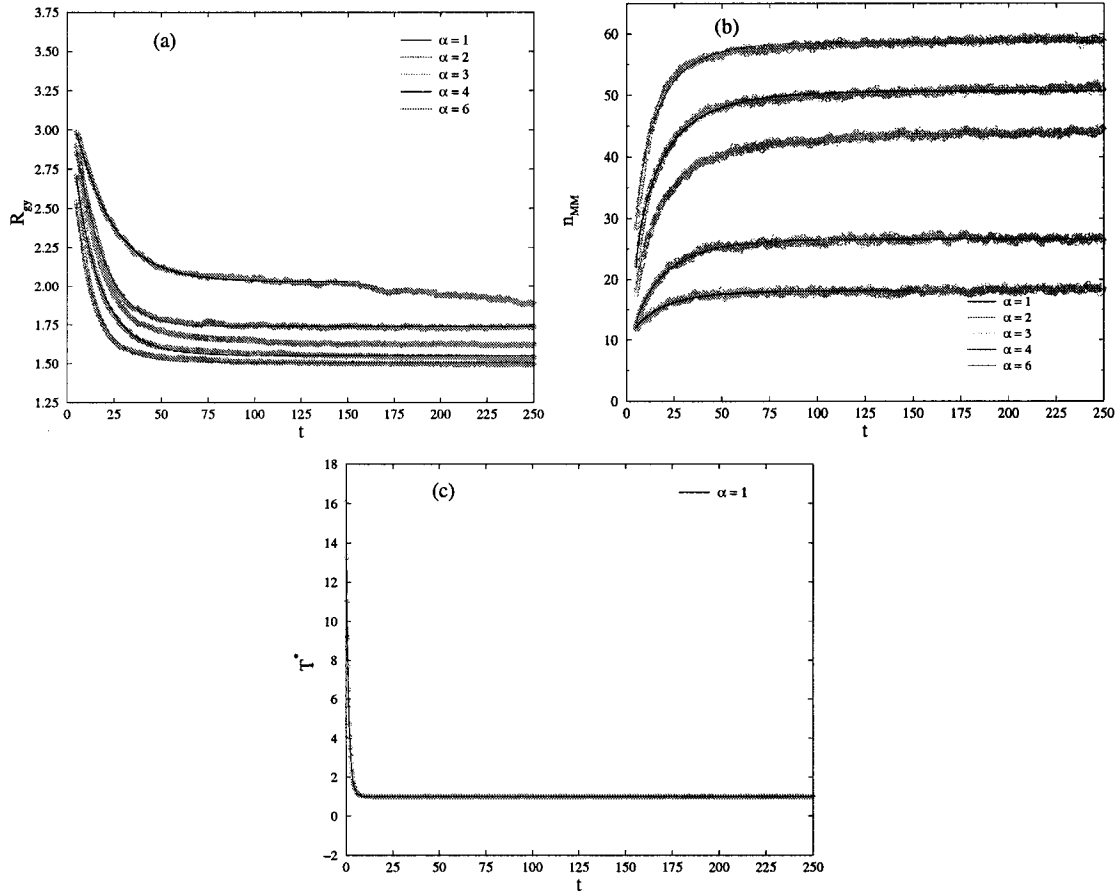


Figure 5.5: Relaxation curves for a Model A type random heteropolymer. The length of the chain was $N = 30$, the solvent density was $\rho = 0.7$ and the random monomer–monomer interactions strength was $\alpha = 1, 2, 3, 4, 6$: (a) R_{gy} versus t , (b) n_{MM} versus t and (c) T^* versus t (only for $\alpha = 1$ for clarity). All the temperature quenches were performed from $T_I = 16$ to $T_F = 1$. Each curve corresponds to an average over 20 independent quench runs for the same initial condition. Finally, 10 impurity averages for different realizations of $\{\eta_{ij}\}$ for a given α were performed for a given set of the remaining system parameters.

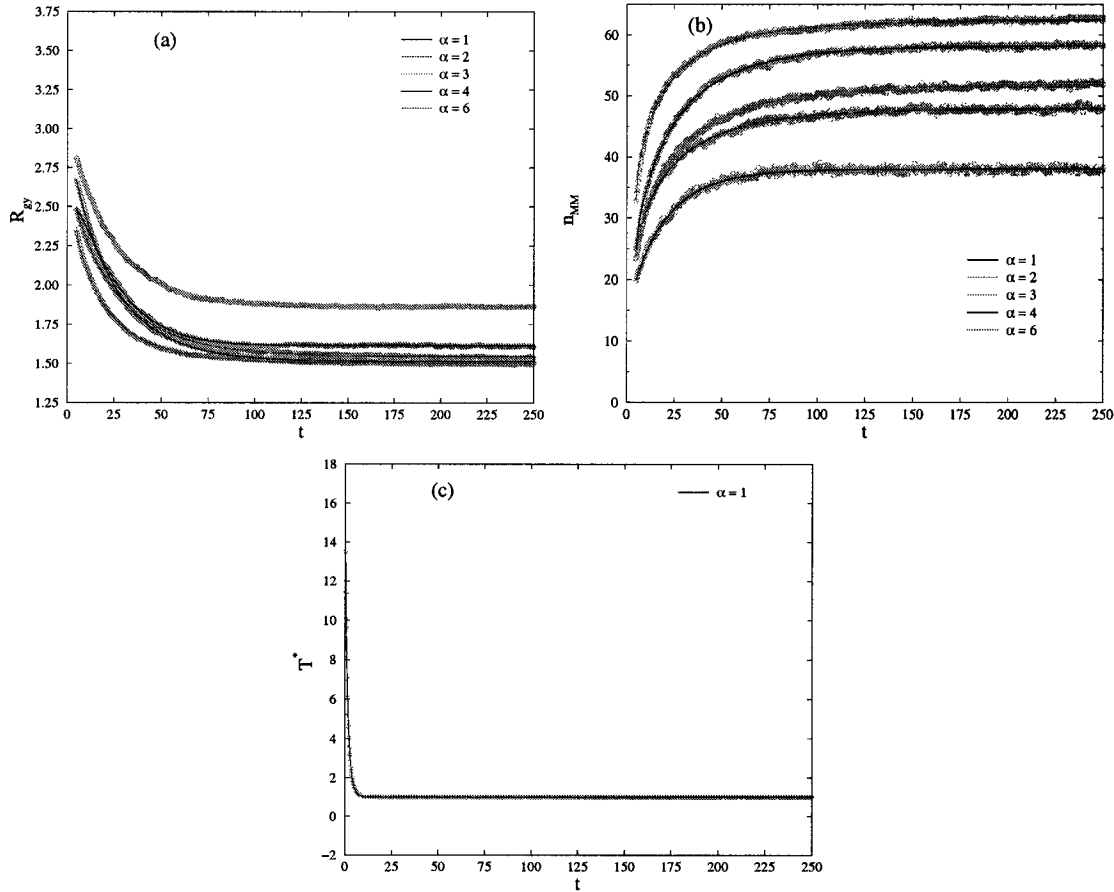


Figure 5.6: Relaxation curves for a Model A type random heteropolymer. The length of the chain was $N = 30$, the solvent density was $\rho = 0.9$ and the random monomer-monomer interactions strength was $\alpha = 1, 2, 3, 4, 6$: (a) R_{gy} versus t , (b) n_{MM} versus t and (c) T^* versus t (only for $\alpha = 1$ for clarity). All the temperature quenches were performed from $T_I = 16$ to $T_F = 1$. Each curve corresponds to an average over 20 independent quench runs for the same initial condition. Finally, 10 impurity averages for different realizations of $\{\eta_{ij}\}$ for a given α were performed for a given set of the remaining system parameters.

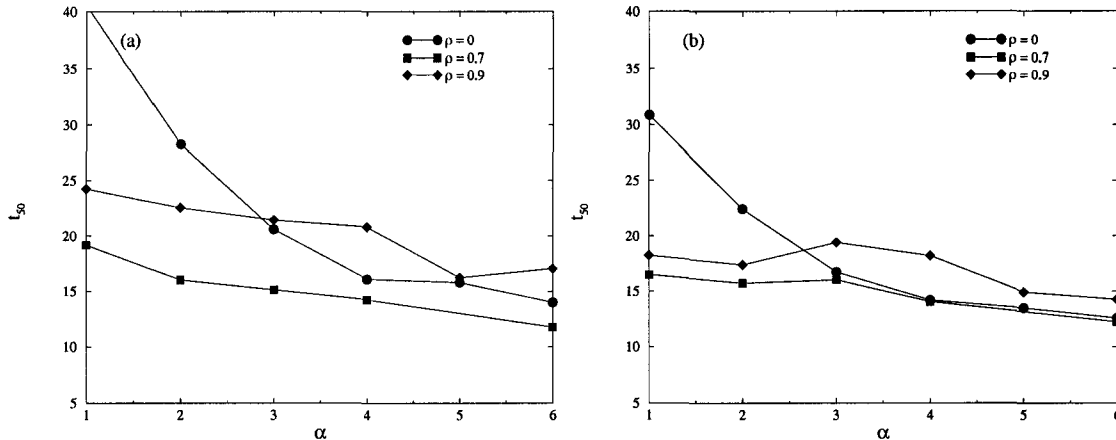


Figure 5.7: t_{50} as a function of the strength of the random monomer–monomer interactions, α for $\rho = 0$, $\rho = 0.7$ and $\rho = 0.9$. $T_I = 16$ for all values of ρ . $T_F = 0.1$ for $\rho = 0$, and $T_F = 1$ for $\rho = 0.7$ and $\rho = 0.9$. t_{50} was evaluated from: (a) the R_{gy} versus t plots of Figures 5.4 (a), 5.5 (a) and 5.6 (a); and (b) the n_{MM} versus t plots of Figures 5.4 (b), 5.5 (b) and 5.6 (b).

initial conformations and sequences.

From these figures (Figures 5.7 and 5.8), we can see that the collapse times generally become shorter for increasing values of α (*i.e.* with simultaneously increasing the heterogeneity and the overall hydrophobicity of the polymer). This effect is clearer for $\rho = 0$ than $\rho = 0.7$ and $\rho = 0.9$ but we should not compare the $\rho = 0$ case to the others since the quenches were not performed for the same T_F . We should interpret the results for $\rho = 0$ carefully since, as can be seen in Figure 4.8, it was necessary to perform the temperature quenches to very low temperatures such as $T_F = 0.1$ in order for T_F to be below T_Θ for the entire range of α . At $T_F = 0.1$, the monomers which feel an attraction quickly attract and stick together since the potential well depth is much bigger than $k_B T_F$. This implies that the chain gets locked into conformations which retain a high radius of gyration even though it is far from the free energy minimum. This is the difficulty of a rough energy landscape, which is problematic when $k_B T$ is much smaller than the well depths of local free energy minima. The increase in the collapse rate as α gets larger could be amplified by the fact that, at such low temperatures, the chain is more likely to get trapped in local free energy minima as the chain tries to collapse. However, we can compare $\rho = 0.7$ to $\rho = 0.9$ and we find that the collapse is invariably slower for $\rho = 0.9$. Also the difference between their respective collapse rates remains almost constant and relatively small for the entire

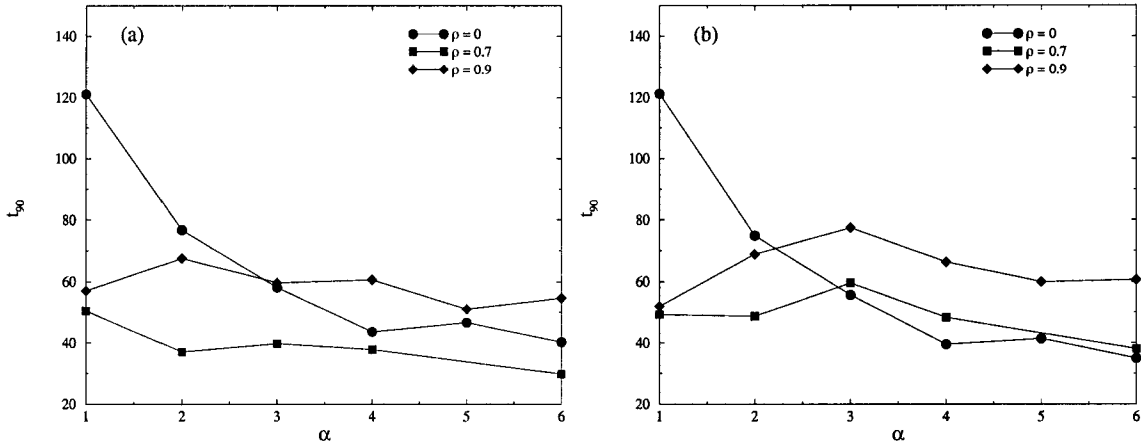


Figure 5.8: t_{90} as a function of the strength of the random monomer–monomer interactions, α for $\rho = 0$, $\rho = 0.7$ and $\rho = 0.9$. t_{90} was evaluated from: (a) the R_{gy} versus t plots of Figures 5.4 (a), 5.5 (a) and 5.6 (a); and (b) the n_{MM} versus t plots of Figures 5.4 (b), 5.5 (b) and 5.6 (b).

	α	1	2	3	4	6
$\rho = 0$	β	0.97	0.99	0.97	0.92	0.81
	τ	1.34	1.40	1.42	1.34	1.35
$\rho = 0.7$	β	0.97	0.97	0.96	0.97	0.97
	τ	1.24	1.25	1.24	1.25	1.25
$\rho = 0.9$	β	0.92	0.91	0.91	0.91	0.91
	τ	1.32	1.32	1.31	1.31	1.31

Table 5.2: β and τ for the thermal relaxation of a Model A random heteropolymer with $\rho = 0$, $\rho = 0.7$ and $\rho = 0.9$.

range of α . Furthermore, we find that the collapse times for R_{gy} and n_{MM} follow similar trends over the entire range of α for $\rho = 0$, $\rho = 0.7$ and $\rho = 0.9$. In some cases the values are in fact very close over most of the range of α .

We plotted $T^*(t)$ for $\rho = 0$ (Figure 5.4 (c)) and for $\rho = 0.7$ (Figure 5.5 (c)). Note that for clarity, we decided to show only the $\alpha = 1$ case. $T^*(t)$ was then fitted to a stretched exponential (Eq. (5.1) with $t_I = 0$). The values of β and τ for $\rho = 0$ and $\rho = 0.7$ can be found in Table 5.2 for various values of α . β and τ are also essentially independent of α . For all cases, $\beta \approx 1$ and therefore the relaxation is basically exponential. By doing further studies, we have observed that β and τ are

independent of the values of T_I and T_F . This is true for both T_F above and below T_Θ .

5.1.2 α -driven random heteropolymer collapse

Another way to induce collapse is to abruptly increase the value of α . In this subsection, we will compare α -driven polymer collapse to the previous T -driven polymer collapse. In particular, we examine the effects of solvent density on polymer collapse driven by an abrupt change in α from $\alpha_I = 1$ to $\alpha_F = 6$ at constant temperature T . The temperature used was $T = 1.5$ for $\rho = 0$ and $\rho = 0.2$, while $T = 4$ for $\rho = 0.5$ and $\rho = 0.7$. These parameters were selected from Figure 4.8 to assure that the initial conformation is always an extended coil and that the final conformation is always a collapsed globule.

Figure 5.9 shows averaged values for (a) $R_{yy}(t)$, (b) $n_{MM}(t)$, (c) $T^*(t)$ and $E(t) \equiv (\mathcal{U}_{MM}(t) + \mathcal{U}_{MS}(t) + \mathcal{K}_M(t))/N$ for Model A type random heteropolymers at various solvent densities. Unfortunately, it was not possible to use a common temperature for the entire range of solvent densities (see Figure 4.8). Thus, it makes sense that the collapse rates for $\rho = 0$ and $\rho = 0.2$ should be faster than for $\rho = 0.5$ and $\rho = 0.7$ based simply on the fact that the quench was deeper for the lower temperature cases. Nevertheless, from Figures 5.9 (a) and (b), lowering the density increases the collapse rate at a given temperature. The curves of t_{50} and t_{90} versus ρ of Figure 5.10 also confirm this trend.

The previous results of Figure 5.3 showed that the collapse times were roughly independent of solvent density. However, those results were only obtained for $\alpha = 4$ and $\alpha = 6$ for the entire range of densities. $\alpha = 1$ is considerably lower than these values of α and therefore the monomer-monomer attractions and monomer-monomer repulsions are both no longer quite so strong. As a result, lowering density increases the collapse rate.

The temperature showed an initial sudden increase, especially at very low densities (Figure 5.9 (c)), which can be explained by the fact that for an abrupt increase in α , some monomer pairs that were not overlapping will suddenly be overlapping. There will be enormous (and completely artificial) repulsive forces now present which will push these monomers apart and the average velocity (temporarily) up, until the

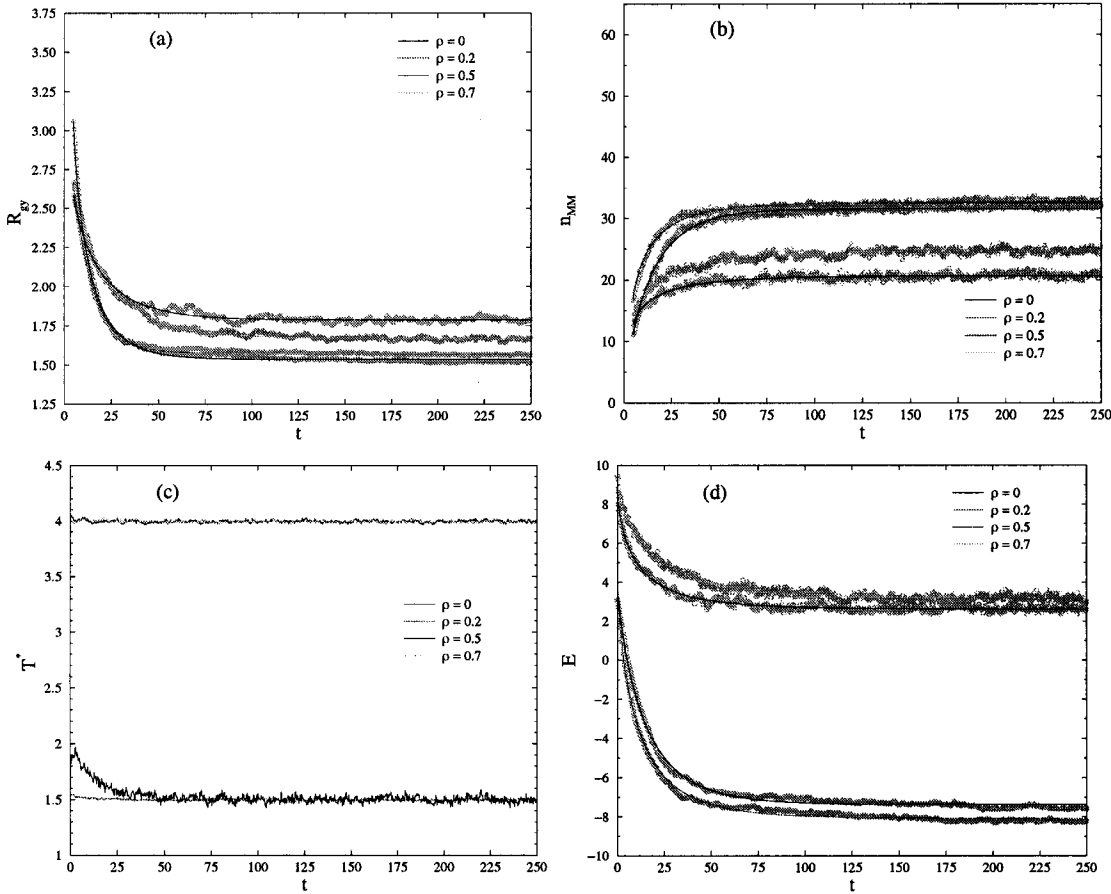


Figure 5.9: Relaxation curves corresponding to a constant temperature collapse for a Model A type random heteropolymer. The length of the chain was $N = 30$, the temperature of the system was $T = 1.5$ for solvent densities $\rho = 0$ and $\rho = 0.2$, $T = 4$ for $\rho = 0.5$ and $\rho = 0.7$: (a) R_{gy} versus t , (b) n_{MM} versus t , (c) T^* versus t and (d) E versus t . All the quenches were performed from a random monomer-monomer interactions strength, $\alpha_I = 1$ to $\alpha_F = 6$. Each curve corresponds to an average over 20 independent quench runs for the same initial condition. Finally, 5 impurity averages for different realizations of $\{\eta_{ij}\}$ for a given α were performed for a given set of the remaining system parameters.

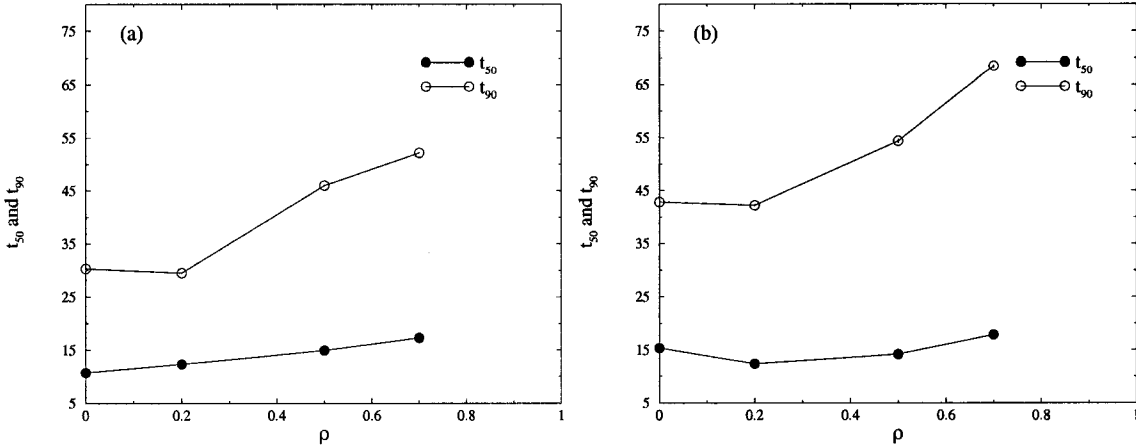


Figure 5.10: t_{50} and t_{90} as a function of ρ for an α driven collapse at constant temperature of a Model A type random heteropolymer. The quenches were performed from $\alpha_I = 1$ to $\alpha_F = 6$ at a temperature of $T = 1.5$ for $\rho = 0$ and $\rho = 0.2$, and $T = 4$ for $\rho = 0.5$ and $\rho = 0.7$. t_{50} and t_{90} were evaluated from: (a) the R_{yy} versus t plots of Figure 5.9 (a); (b) the n_{MM} versus t plots of Figure 5.9 (b).

ρ	0	0.2	0.5	0.7
β	0.83	0.70	0.63	0.73
τ	14.93	11.02	10.61	19.15

Table 5.3: β and τ for the relaxation of the energy of a Type A random heteropolymer from $\alpha_I = 1$ to $\alpha_F = 6$.

thermostat corrects the situation. The presence of solvent atoms tends to moderate this effect. Unfortunately, due to the fact that the width of the transition increases with density (Figures 4.3 and 4.4), it was impossible to collapse the polymer from an extended coil to a globule at constant temperature by suddenly changing the strength of the random interaction from $\alpha_I = 1$ to $\alpha_F = 6$ for $\rho > 0.7$.

Figure 5.9 (d) shows the relaxation of the polymer energy $E = (\mathcal{U}_{MM} + \mathcal{U}_{MS} + \mathcal{K}_M)/N$. The stretched exponential (Eq. (5.1) with $t_I = 0$) fits of these curves gave β and τ for various values of ρ . These values of β and τ can be found in Table 5.3. The values of β are comparable to those obtained in Chapter 3 while the values of τ are an order of magnitude larger than those obtained in Chapter 3.

5.2 Random monomer–solvent interactions (Model B with a flexible chain)

In this section, we describe a similar study of relaxational dynamics that was performed in Section 5.1 but this time the random interaction are taken to be between the monomers and the solvent particles (Model B with a flexible chain). This is a more appropriate model for the hydrophobicity and hydrophilicity of the monomers since it is entirely determined by the monomer–solvent interactions which give the dominant contribution to polymer collapse in “real” systems. We are particularly interested in the effect of solvent density on the random heteropolymer collapse during a temperature quench from T_I to T_F . We required the initial conformation to be an extended coil; therefore, from Figure 4.14, we have chosen a value of $T_I = 16$ which is greater than T_Θ for the entire range of solvent densities. Furthermore, to ensure a collapse to a compact globule for the entire range of solvent densities, we used $T_F = 1$ which is below T_Θ (Figure 4.14). The quantities that were monitored during the polymer collapse were averaged over 20 independent quench runs for the same initial conditions and over 10 (5 for $\rho = 0$) different realizations of $\{\eta_{ij}\}$ for a given α' and a given set of the remaining system parameters.

Figure 5.11 shows averaged values of (a) $R_{yy}(t)$, (b) $n_{MM}(t)$, (c) $T^*(t)$ and (d) $E(t) \equiv (\mathcal{U}_{MM}(t) + \mathcal{U}_{MS}(t) + \mathcal{K}_M(t))/N$ for random heteropolymers with random monomer–solvent interaction strength with $\alpha' = 1$ and several solvent densities. In this section, we used $t_I = 5$ and $t_F = 250$. As observed in Section 4.3, the initial equilibrium coil size decreases with increasing solvent density. The value of $R_{yy}(t_I)$ decreases with increasing values of ρ (Figure 4.10) and it follows that the value of $n_{MM}(t_I)$ increases with increasing values of ρ (Figure 4.11). Furthermore, for quenches to the same final temperature $T_F = 1$, which is below T_Θ for the entire range of ρ , the final collapsed conformation size $R_{yy}(t_F)$ decreases with increasing values of ρ while $n_{MM}(t_F)$ increases with increasing values of ρ .

The collapse times t_{50} and t_{90} were evaluated by fitting a stretched exponential function (Eq. (5.1)) to $R_{yy}(t)$ and $n_{MM}(t)$. Figure 5.12 shows a plot of t_{50} determined by the decay of both (a) R_{yy} and (b) n_{MM} , and Figure 5.13 shows a plot of t_{90} determined by the decay of both (a) R_{yy} and (b) n_{MM} . Appendix A.2 gives the

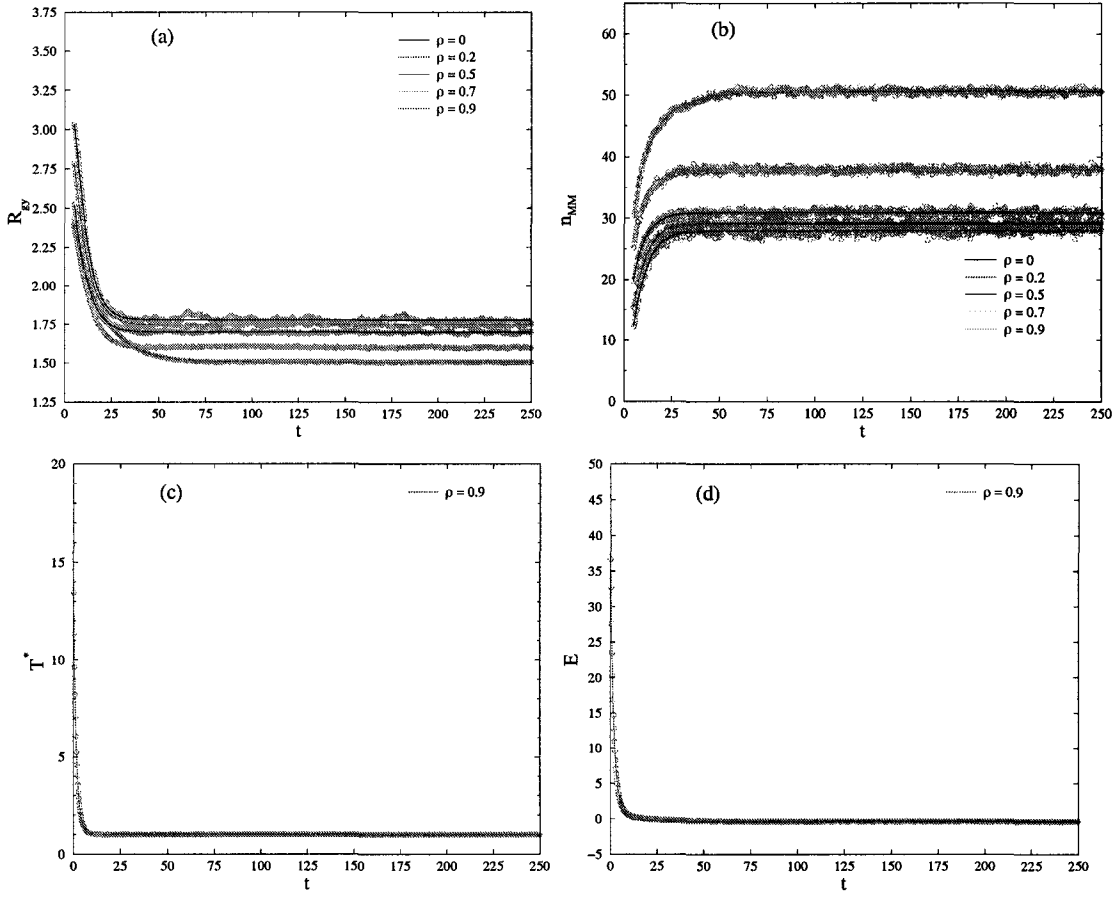


Figure 5.11: Relaxation curves for a Model B type flexible random heteropolymer. The length of the chain was $N = 30$, the random monomer-solvent interactions strength was $\alpha' = 1$ and the solvent densities were $\rho = 0, 0.2, 0.5, 0.7, 0.9$: (a) R_{gy} versus t , (b) n_{MM} versus t , (c) T^* versus t (only for $\rho = 0.9$ for clarity) and (d) E versus t (only for $\rho = 0.9$ for clarity). All the temperature quenches were performed from $T_I = 16$ to $T_F = 1$. Each curve corresponds to an average over 20 independent quench runs for the same initial condition. Finally, 10 (5 for $\rho = 0$) impurity averages for different realizations of $\{\eta_{ij}\}$ for a given α' were performed for a given set of the remaining system parameters.

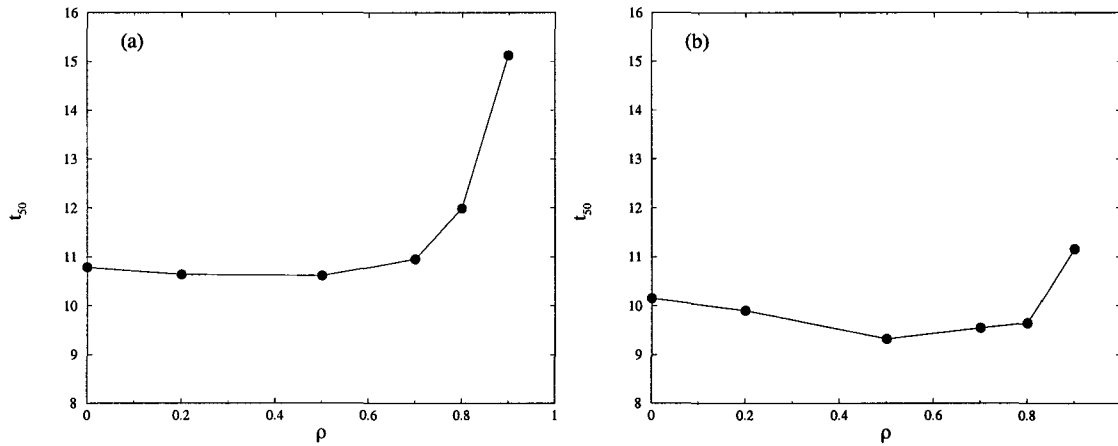


Figure 5.12: t_{50} as a function of ρ for a Model B type flexible random heteropolymer with random monomer-solvent interactions with $\alpha' = 1$. t_{50} was evaluated from: (a) the R_{yy} versus t plots of Figure 5.11 (a); and (b) the n_{MM} versus t plots of Figure 5.11 (b).

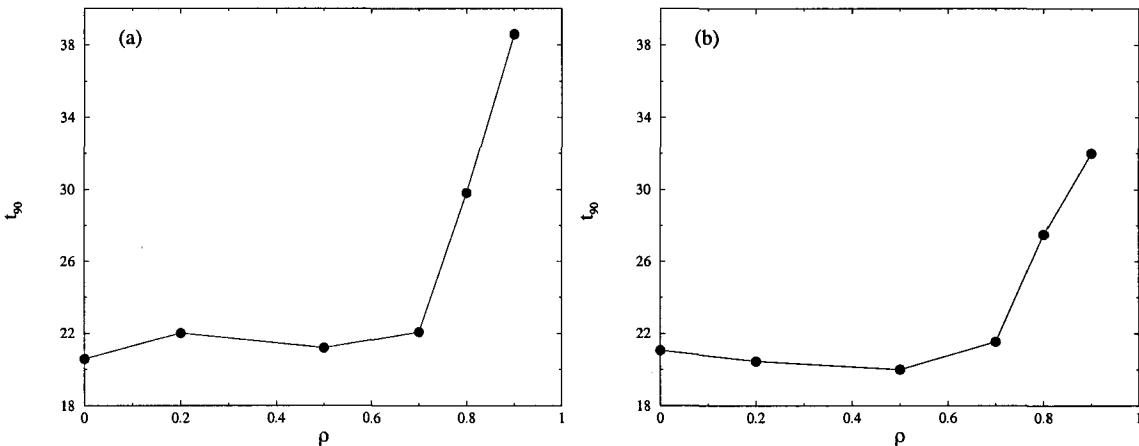


Figure 5.13: t_{90} as a function of ρ for a Model B type flexible random heteropolymer with random monomer-solvent interactions with $\alpha' = 1$. t_{90} was evaluated from: (a) the R_{yy} versus t plots of Figure 5.11 (a); and (b) the n_{MM} versus t plots of Figure 5.11 (b).

	ρ	0	0.2	0.5	0.7	0.9
$T^*(t)$	β	0.98	0.99	0.98	0.96	0.92
	τ	1.39	1.07	1.15	1.23	1.32
$E(t)$	β	0.81	0.97	0.95	0.97	0.81
	τ	1.44	1.39	1.35	1.47	1.44

Table 5.4: β and τ for the thermal relaxation and the relaxation of the energy of a type B flexible random heteropolymer with $\alpha' = 1$.

calculations of the error bars which were smaller than the size of the symbols.

At low densities, the rate of collapse increases slightly but is almost independent of the solvent density, particularly for t_{50} and t_{90} evaluated from $R_{yy}(t)$. At higher densities, the trend is reversed and the rate of collapse decreases with solvent density. In this case, the collapse is driven by the attractive part of the Lennard–Jones interaction between the monomers as well as the random interaction between the monomers and the solvent particles. Note that the random interaction can be both attractive and repulsive. For $\alpha' = 1$, the solvent particles seem to only act as obstacles to the collapse of the polymer. At low and medium densities, the collapse seems to be almost solely driven by the attractive part of the Lennard–Jones interaction between the monomers. Therefore, at low densities, the collapse times are basically constant with at most a small contribution from the random monomer–solvent interaction favoring a slightly shorter collapse time. At higher densities the “obstacle” nature of the solvent particles due to the repulsive interaction part of the monomer–solvent interaction takes over and reduces the rate of collapse. This was also observed by Polson and Zuckermann [01]. Note that these rates of collapse are in general much faster than those of Section 5.1.

We plot $T^*(t)$ for $\alpha' = 1$ in Figure 5.11. Only the case of $\rho = 0.9$ is shown for clarity. $T^*(t)$ was then fitted in Figure 5.11 (c) to a stretched exponential (Eq. (5.1) with $t_I = 0$) and a stretched exponent β and a time scale τ were obtained for various values of ρ . These values of β and τ can be found in Table 5.4. As demonstrated in Section 5.1, β is essentially independent of ρ and is again very close to a pure exponential. On the other hand, the relaxation time increases with increasing solvent

density. In the latter case, the time scale is comparable to the time scale obtained for $\rho = 0.9$, *i.e.* $\tau(\rho = 0) \approx \tau(\rho = 0.9)$.

Furthermore, we plotted $E(t)$ versus t for $\alpha' = 1$ (Figure 5.14 (d)). Again, since the curves are quite similar, we show only the curve for $\rho = 0.9$. These curves were fitted to a stretched exponential (Eq. (5.1) with $t_I = 0$). Both a stretched exponent β and a time scale τ were obtained and are shown in Table 5.4 for various value of ρ .

5.3 Effect of chain stiffness (Model B with a semi-flexible chain)

Both regular polymers and biopolymers such as proteins and DNA exhibit substantial bending stiffness which makes compact conformations unfavorable. For this reason, it is valuable to incorporate such a bending restriction into our model. Furthermore, we expect some important effects due to the fact that the added stiffness of the chain leads to more limited collapse pathways. Finally, in this section, we study the effect of bending stiffness on the relaxational dynamics of the system described in Section 5.2 (Model B with a semi-flexible chain). Semi-flexible random heteropolymers have a longer Kuhn length and introduce a new value of T_Θ to the collapse of such a system since the addition of bending stiffness favors extended conformations.

The temperature quenches were performed with $T_I = 16$ and $T_F = 1$. The measured quantities were averaged over 20 independent quench runs for the same initial conditions and over 10 different realizations of $\{\eta_{ij}\}$ for a given α' and a given set of the remaining system parameters. Figure 5.14 shows averaged values for (a) $R_{yy}(t)$, (b) $n_{MM}(t)$, (c) $T^*(t)$ and (d) $E(t) \equiv (\mathcal{U}_{MM}(t) + \mathcal{U}_{MS}(t) + \mathcal{K}_M(t))/N$ for random heteropolymers with random monomer solvent interaction strength $\alpha' = 1$ and several solvent densities. As observed in Section 4.4, the initial equilibrium coil size decreases with increasing solvent density. The value of $R_{yy}(t_I)$ decreases with increasing values of ρ (Figure 4.15) and it follows that the value of $n_{MM}(t_I)$ increases with increasing values of ρ (Figure 4.15). Furthermore, for quenches to the same final temperature $T_F = 1$, which is below T_Θ for the entire range of ρ , the final collapsed conformation size $R_{yy}(t_F)$ tends to slightly decrease with increasing values of ρ while $n_{MM}(t_F)$ increases with increasing values of ρ .

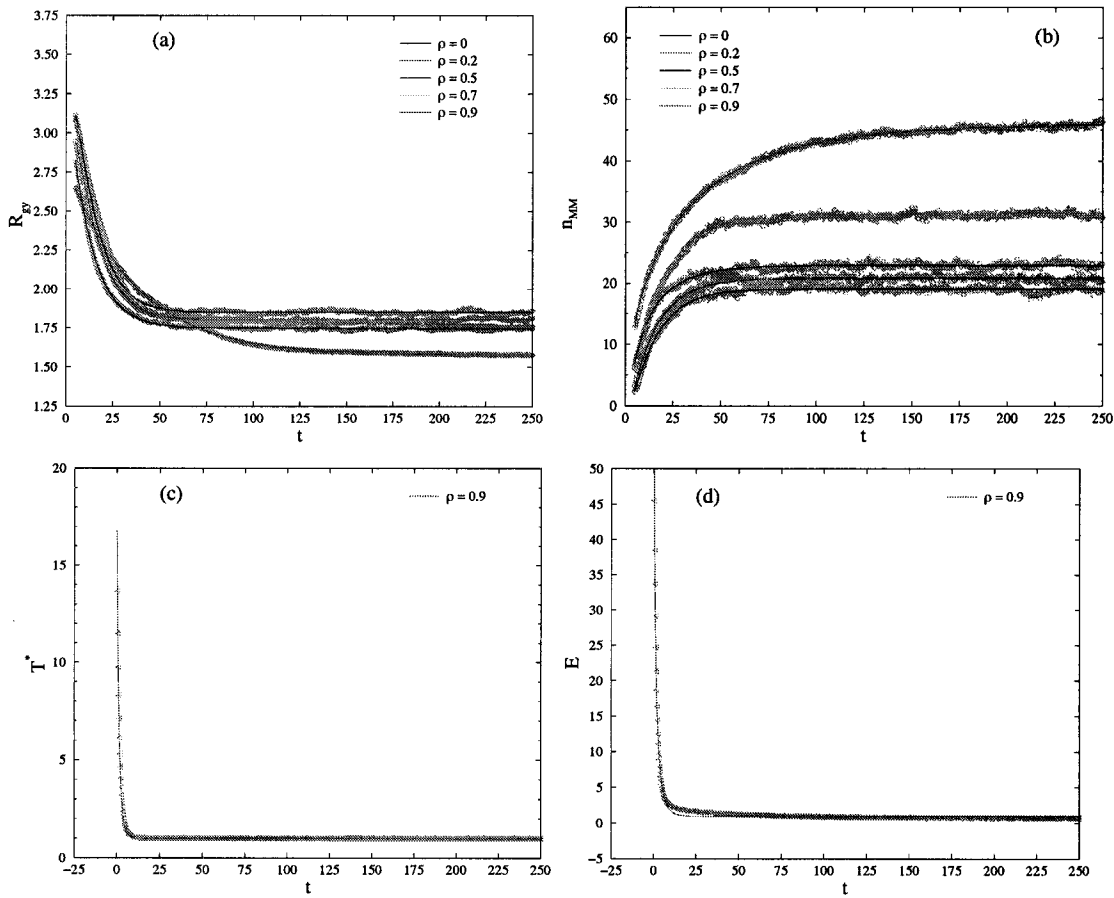


Figure 5.14: Relaxation curves for a Model B type semi-flexible random heteropolymer. The length of the chain was $N = 30$, the random monomer–solvent interactions strength was $\alpha' = 1$ and the solvent densities were $\rho = 0, 0.2, 0.5, 0.7, 0.9$: (a) R_{gy} versus t , (b) n_{MM} versus t , (c) T^* versus t (only for $\rho = 0.9$ for clarity) and (d) E versus t (only for $\rho = 0.9$ for clarity). All the temperature quenches were performed from $T_I = 16$ to $T_F = 1$ all values of ρ . Each curve corresponds to an average over 20 independent quench runs for the same initial condition. Finally, 10 impurity averages for different realizations of $\{\eta_{ij}\}$ for a given α' were performed for a given set of the remaining system parameters.

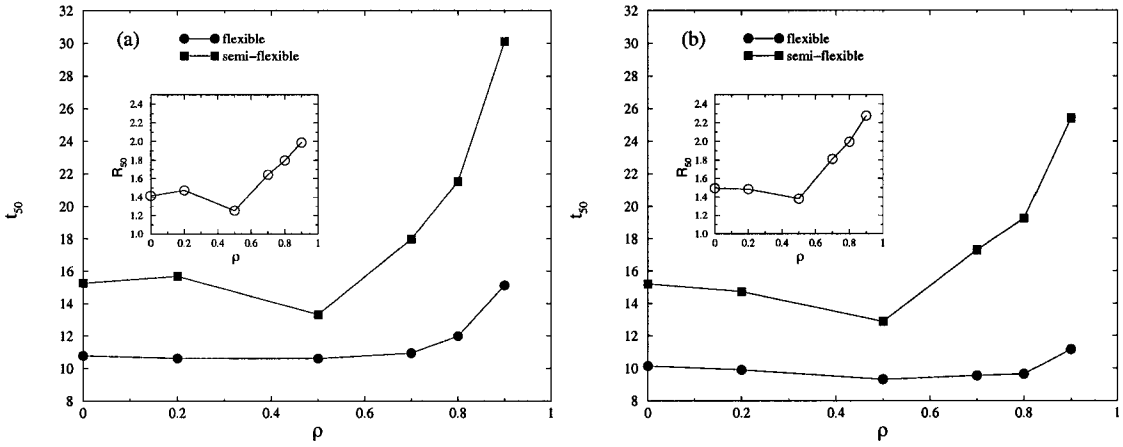


Figure 5.15: t_{50} as a function of ρ for random monomer–solvent strength $\alpha' = 1$. t_{50} was evaluated from: (a) the R_{gy} versus t plots and (b) the n_{MM} versus t plots. (○) corresponds to a flexible chain and (□) corresponds to a semi–flexible chain. The insets show R_{50} vs. ρ (the ratio of t_{50} for the semi–flexible chain relative to the fully flexible chain).

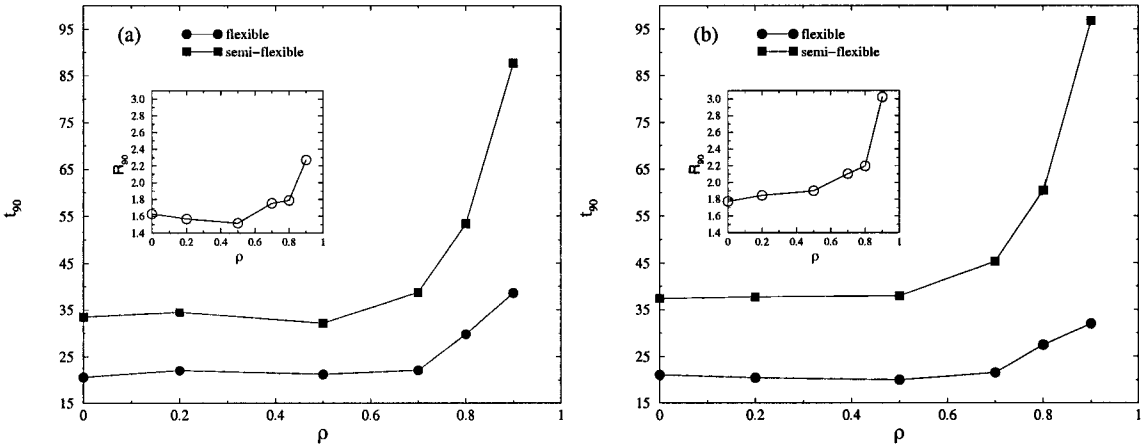


Figure 5.16: t_{90} as a function of ρ for random monomer–solvent strength $\alpha' = 1$. t_{50} was evaluated from: (a) the R_{gy} versus t plots and (b) the n_{MM} versus t plots. (○) corresponds to a flexible chain and (□) corresponds to a semi–flexible chain. The insets show R_{90} vs. ρ (the ratio of t_{90} for the semi–flexible chain relative to the fully flexible chain).

The collapse times t_{50} and t_{90} were evaluated by fitting $R_{gg}(t)$ and $n_{MM}(t)$ to a stretched exponential function (Eq. (5.1)). Figure 5.15 shows a plot of t_{50} determined by the decay of both (a) R_{gg} and (b) n_{MM} , and Figure 5.16 shows a plot of t_{90} determined by the decay of both (a) R_{gg} and (b) n_{MM} . Appendix A.2 discusses the method used for the calculations of the error bars which were smaller than the size of the symbols. From Figures 5.15 and 5.16 it can be seen that the behavior of the curves for the semi-flexible chain is quite similar to that observed for the flexible chain except for a marked increase in the collapse time. This difference in the rate of collapse is constant over a broad range of values of ρ , especially for t_{90} . However, between $\rho = 0.7$ and $\rho = 0.9$, the difference in the rate of collapse becomes larger. We quantified this difference using the quantity R_{50} which represents the ratio of the collapse time t_{50} for the semi-flexible chain relative to the fully flexible chain, and the quantity R_{90} which is the same ratio for the t_{90} collapse time (see inset of Figures 5.15 and 5.16). Neither R_{50} nor R_{90} vary significantly for low values of ρ . Some anomalies in t_{50} that were not present for the flexible chain were observed for the semi-flexible chain at $\rho = 0.5$. It is not clear if this is only due to statistical fluctuations in the data or if it is a real effect where the solvent enhances the collapse at medium densities. Nevertheless, the ratios increase significantly at higher densities. For example, the ratios at $\rho = 0.9$ are roughly between 1.5 and 1.65 times that of the ratios at $\rho = 0.5$. Finally, our results for semi-flexible chains are qualitatively similar to those of Polson and Zuckermann [01], *i.e.* the collapse times are longer for stiffer chains, and the effect of the stiffness is most pronounced at higher ρ . The increase in R_{50} and R_{90} with ρ at higher solvent densities is related to the fact that an increase in the solvent density has a considerably stronger effect on the slowing down of the collapse dynamics of a conformationally restricted polymer chain.

We plotted $T^*(t)$ versus t for $\alpha' = 1$ (Figure 5.14 (c)). Note that for clarity, we only show the $\rho = 0.9$ case. The $T^*(t)$ curves were then fitted to a stretched exponential (Eq. (5.1) with $t_I = 0$) and a stretched exponent β and a time scale τ were obtained for various values of ρ . These values of β and τ are given in Table 5.5. As demonstrated in Sections 5.1 and 5.2, β is essentially independent of ρ and is again very close to a pure exponential. On the other hand, the time scale increases with

	α	0	0.2	0.5	0.7	0.9
$T^*(t)$	β	1.01	0.96	0.96	0.95	0.92
	τ	1.73	1.05	1.13	1.23	1.32
$E(t)$	β	0.82	0.80	0.83	0.75	0.70
	τ	1.58	1.29	1.19	1.12	1.20

Table 5.5: β and τ for the relaxation of the thermostat and the energy of a type B semi-flexible random heteropolymer with $\alpha' = 1$.

increasing solvent density except for the case without solvent which has a significantly larger time scale.

We also plotted E versus t for $\alpha' = 1$ (Figure 5.14 (d)). Again, since the curves are extremely similar, we only show the $\rho = 0.9$ curve. The curves of E versus t were then fitted to a stretched exponential (Eq. (5.1) with $t_I = 0$) and the stretched exponents β and τ were obtained for various values of the solvent density (see Table 5.5).

5.4 Summary

Many attempts have been made to simulate polymer collapse using a variety of methods (MC, LD, MD). The related results have some limitations due to the absence of hydrodynamics and the use of effective monomer–monomer pair potentials to regulate hydrophobicity. These effective pair potentials are supposed to mimic the combined effects of monomer–solvent, solvent–solvent and monomer–monomer interactions, but are known to be insufficient for equilibrium properties of polymers (Grayce [97]). Thus, they are also expected to be insufficient for the study of collapse dynamics. A many–body effective interaction scheme would be required in order to describe solvent effects in a satisfactory manner. The next step is to immerse the polymer in an explicit solvent and/or include all hydrodynamic effects. Here, we focussed on investigating the effects of direct monomer–solvent and solvent–solvent interactions by immersing our polymer in an explicit solvent, though the solvent–solvent interactions were found to be less important.

In this Chapter, we have investigated the collapse transition properties of three types of random heteropolymers immersed in a Lennard–Jones explicit solvent. The

first model (Model A) consisted of a polymer with random interactions between the monomers which could be both attractive and repulsive, and a solvent which had a short range repulsive interaction between the monomers. The second model (Model B with a flexible chain) was a polymer with a Lennard–Jones interaction between its monomers, and a solvent that interacted via a random interaction with the monomers which could be both attractive and repulsive. The third model (Model B with a semi-flexible chain) is the same as the second one except for an added stiffness to the polymer chain. Model A is closer in spirit to the effective pair potential approach, since the heterogeneity is incorporated into the monomer–monomer interactions, while for Model B, these are incorporated into the monomer–solvent interactions. By choosing to study Model A and Model B, we were basically bridging the difference between implicit and explicit solvent in two steps. In all cases, we chose to study the collapse kinetics by making an abrupt change in T or α .

For our first model (Model A), an increase in the heterogeneity (and simultaneously an increase in the overall hydrophobicity) of the heteropolymer leads to shorter collapse times, but varying the density of the solvent had almost no effect on the rate of collapse for high values of α and the range of ρ that was considered. Polson and Zuckermann [01] obtained a similar monotonic increase in the collapse rate with increasing hydrophobicity. However, the density–independence of the collapse rate is different from that obtained for homopolymers in three dimensions by Polson and Zuckermann [01]. In their work, the collapse rate decreases monotonically with increasing solvent density. If this is not an artifact of the thermostat, the density–independence would suggest that the collapse rate depends on a competition of the monomer–monomer repulsion and attraction with the monomer–solvent interactions, and indirectly with the solvent–solvent interactions which plays a relatively minor role. This is in fact possible since the monomer–monomer attractions and repulsions, for these high values of α , are very strong. Nevertheless, at very high solvent densities, we expect the “obstacle” nature of the solvent atoms to interfere with the collapse of the polymer chain and the collapse time to increase. Furthermore, the decrease in the collapse rate most probably occurs at different solvent densities for different values of α . Unfortunately, studying the effect of higher densities of solvent involves a significant increase

in computational time and for this reason this is not part of this dissertation even though it would be quite interesting to pursue it further. Also, it is not clear that the collapse rate decreases at densities for which the liquid phase is thermodynamically stable with respect to the solid phase. Comparing the difference between the collapse rates of a system with $\rho = 0.7$ and one with $\rho = 0.9$ shows that the difference remains almost constant and relatively small for the entire range of α . Finally, the collapse times for the constant temperature quenches which are driven by a sudden increase in the value of α , decrease as the density is decreased. This is not the same behavior that was observed for the temperature induced collapse where the collapse rate was essentially independent of the solvent density. However, these results were obtained for considerably lower values of α for the α -quenches than for the T -quenches and therefore the monomer–monomer attractions and monomer–monomer repulsions are both no longer quite so strong. As a result, lowering density increases the collapse rate. We used Model A to study the effect of changing the polymer heterogeneity and the overall hydrophobicity simultaneously. A future project would be to examine these effects separately.

For our second model (Model B), the rate of collapse at low densities increases slightly but is almost independent of the solvent density. At higher densities, the trend is reversed and the rate of collapse starts to decrease. In this case, the collapse is driven by the attractive part of the Lennard–Jones interaction between the monomers as well as the random interaction between the monomers and the solvent particles which can be both attractive and repulsive. For the strength of the random monomer–solvent interaction used in the simulations, the solvent particles seem to only act as obstacles to the collapse of the polymer. At low and medium densities, the collapse appears to be almost solely driven by the attractive part of the Lennard–Jones interaction between the monomers. The repulsive interaction of the solvent particles on the hydrophobic monomers could also help the collapse but for our values of α' this contribution is quite weak. Therefore, at low densities, the collapse times are basically constant while at higher densities the “obstacle” nature of the solvent particles takes over and reduces the rate of collapse. Polson and Zuckermann also observed a slower decay from an extended coil to a globule with increasing ρ ,

at higher densities, for both a two-dimensional homopolymer and copolymer (Polson and Zuckermann [00]) and a three-dimensional homopolymer (Polson and Zuckermann [01]). Finally, we observed an increase in the collapse times for stiffer chains, and that the effect of the stiffness is most pronounced at higher ρ . Such an effect related to an increase in the stiffness of the random heteropolymer chain was also observed by Polson and Zuckermann in their three dimensional molecular dynamics simulations of the collapse dynamics of a homopolymer chain immersed in a Lennard-Jones solvent (Polson and Zuckermann [01]). They have explained that the stiffness effect seems to be most pronounced at higher ρ since an increase in the solvent density has a considerably stronger effect on the slowing down of the collapse dynamics of a conformationally restricted polymer chain.

Furthermore, Polson and Zuckermann showed that for their model, HP sequencing has practically no effect on the rate of collapse of HP copolymers (Polson and Zuckermann [00]). Nevertheless, they proposed that it should be possible to design HP sequences that will collapse more rapidly. The sequence dependence of the collapse rate of heteropolymers has generally accepted and an entire field of research is concerned with designing fast folding proteins (Pande, Grosberg and Tanaka [00]; Khokhlov and Khalatur [99] [98]; Timoshenko, Kuznetsov and Dawson [98] [96]; Mélin et al. [99]; Skorobogatyy, Guo and Zuckermann [97a] for example).

In this chapter, we have not included any snapshots of conformations following the heteropolymer collapse since the polymer is so short that it is very difficult to determine collapse mechanism such as the formation of blobs. In Chapter 3, we have shown that we require a polymer of about 100 monomers in order to determine a clear collapse mechanism. Indeed, a very important future project is to carefully study finite size effect with an explicit solvent.

6

DISCUSSION AND CONCLUSION

In this dissertation, we investigated the equilibrium properties and the collapse dynamics of various types of random heteropolymers in three dimensions. The equilibrium and relaxational data were obtained by performing extensive off-lattice molecular dynamics simulations. We proceeded systematically by determining an equilibrium “phase diagram” which allowed us to find a characteristic temperature T_Θ which separates extended states from collapsed states of the random heteropolymer. Such “phase diagrams” allowed us to find appropriate initial and final temperatures for the quenches from an extended coil to a collapsed globule. In our model, the random heteropolymer is composed of N monomers connected by harmonic springs.

First, we considered a single fully flexible isolated random heteropolymer without an explicit solvent. The solvent is incorporated implicitly in the monomer–monomer interactions. The monomers mutually interact via a repulsive Lennard-Jones potential and the random interactions between the monomers were included by means of a Van der Waal’s interaction whose coupling constants are chosen from a Gaussian distribution of width α . The equilibrium “phase diagram” shows that T_Θ increases with increasing values of α . Furthermore, relaxation to equilibrium for temperature quenches inside the extended “phase” show a pure exponential decay of the total energy whereas relaxation process to the collapsed “phase” exhibits a stretched exponential behavior of the total energy. We found that the relaxation after a quench from above the theta point to below could be characterized by a two-stage process. The first time regime is characterized by a faster stretched exponential relaxation process with exponent $\beta \approx 0.7$. This value does not depend on the values of α and is quite generic. In the first time regime, the chains locally collapse into separate blobs but the entire chain is still quite extended. In the second time regime the local blobs

coalesce to form the final compact structure, but with different stretched exponential form and a lower value of the exponent β . For very short chains such as those examined in Iori, Marinari and Parisi [91], the second time regime is absent as no local collapse takes place. Finally, for a quench from below the theta point to further below, the relaxation is a one stage process which is also well fitted with a stretched exponential form.

Furthermore, we have shown that for sufficiently long chains, a qualitative inspection of snapshots of the heteropolymer conformations upon collapse suggest that the chains collapse by forming local blobs which later aggregate to form a collapsed globule. This two-step collapse scheme leads to the two time regimes. We propose that our relaxation data can be interpreted in terms of the molten globule concept since we found an initial relaxation to an intermediate conformation in the first time regime after a temperature quench from above to below the theta point. We feel that this conformation is analogous to the “compact but extended” structure discussed by Daggett and Levitt [92] for proteins. This relaxation regime is then followed by a slower relaxation to a collapsed conformation. Finally, we note that the relaxation process studied here is quite different from that of the homopolymer collapse which proceeds via a single exponential.

The next step was to immerse the polymer in an explicit solvent. We studied the effects of direct monomer–solvent (and solvent–solvent which are less important) interactions by immersing our polymer in an explicit solvent. We went from the study of a random heteropolymer with an implicit solvent to the study of a random heteropolymer immersed in an explicit solvent in two steps. First, we immersed a polymer with random interactions between the monomers (similar to the one studied with an implicit solvent) in a solvent which had a short range repulsive interaction between the monomers (Model A). Then, we considered a polymer with a Lennard–Jones interaction between its monomers immersed in a solvent that interacted via a random interaction with the monomers.

We started by examining the equilibrium properties of several systems consisting of a random heteropolymer in an explicit solvent before considering the collapse dynamics. For all models studied, the size of the polymer decreases as the temperature

is lowered. Also, the size of the extended coil decreases as the density of the solvent is increased, in cases where the random interaction is imposed between the monomers (Model A) and the case where the random interaction occurs between the monomers and the solvent atoms (Model B). At low solvent densities, the entropy of the system is dominated by the conformational entropy of the polymer and thus the system favors a spread out coil conformation in order to maximize the conformations available to the chain, and maximize the total entropy of the system. At higher solvent densities, the translational entropy related to the solvent particles becomes more important and the system will favor a slightly compressed coil conformation for the polymer, in order to increase the free volume available for the solvent. Thus the translational entropy of the solvent increases by more than enough to offset that which was lost by the chain. Furthermore, the size of the polymer coil is inversely proportional to the solvent density with a proportionality constant which depends on the polymer length. It is interesting to see how the compression (*i.e.*, the reduction of the equilibrium size due to the presence of the solvent) of the polymer coil becomes more important for a longer polymer chain. This can also be explained by the entropic effect. The size of the extended coil also decreases as a function of the strength of the monomer–monomer random interactions while it does not seem to significantly depend on the monomer–solvent atom random interaction. Furthermore, the angular restrictions have the effect of swelling the coil conformation.

The transition from the extended coil conformation to the globular conformation is thermally driven and results from the system selecting conformations which will minimize the free energy, $F = E - TS$, of the system. The temperature T , controls the strengths of the two terms contributing to the free energy. A globular conformation is favored by the internal energy term while an expanded coil is favoured by entropy. The total entropy can be divided into translational entropy and conformational entropy. The translational entropy part favours a globular state, but the conformational contribution which favours the expanded coil conformation is the dominant part.

Increasing the solvent density increases the value of the characteristic temperature, T_Θ . As the solvent density is increased, the coil conformation becomes progressively more compact which in itself makes the polymer collapse at higher temperatures. Fur-

thermore, the long-range repulsive part of the monomer–solvent random interaction also contributes to the collapse of the polymer to a globule. A larger solvent density will increase the effective repulsion on the polymer, which in turn will increase T_Θ . Increasing the value of the strength of the random monomer–monomer interactions, α , increases the value of T_Θ , thus favoring the globular “phase”. Increasing the value of the strength of the random monomer–solvent interactions increases the value of T_Θ progressively, at higher solvent densities. Thus, the effect of increasing α' is to stabilize the globule “phase”. The value of α' has little effect at low solvent densities, since α' is relevant only for monomer–solvent interactions, and since the driving force of the collapse is mostly the attraction between monomers. Furthermore, the addition of a bending restriction to the chain reduces the value of T_Θ , at higher densities, since the angular restrictions stabilize the coil “phase”.

The appropriate “phase diagrams” are now available to perform systematic quenches across the “phase boundary” separating the coil conformation and the globular conformation. The collapse transition properties of the three types of random heteropolymers immersed in a Lennard–Jones explicit solvent mentioned earlier were investigated by making an abrupt change in T or α .

For Model A, an increase in the heterogeneity, which in turn increases the overall hydrophobicity of the heteropolymer, leads to shorter collapse times. This result is in agreement with the work of Polson and Zuckermann [01]. On the other hand, contrary to their work which finds that the collapse rate decreases monotonically with increasing solvent density, varying the density of the solvent had almost no effect on the rate of collapse of our random heteropolymer for high values of α . Nevertheless, at very high solvent densities, we expect that the “obstacle” nature of the solvent atom will interfere with the collapse of the polymer chain and the collapse time will increase. Our data have shown indications of this effect. Furthermore, the decrease in the collapse rate will most probably occur at different solvent densities for different values of α . Unfortunately, studying the effect of higher densities of solvent involves a significant increase in computational time and for this reason it is not part of this thesis. Another problem related to studying higher solvent densities is the possibility that the system will end up in a region of the phase diagram where the liquid phase is

thermodynamically stable with respect to the solid phase. Comparing the difference between the collapse rates of a system with $\rho = 0.7$ and one with $\rho = 0.9$ shows that the difference remains almost constant and relatively small for the entire range of α . Finally, the collapse times for the constant temperature collapse, which is driven by a sudden increase in the value of α , decreases as the density is decreased. This is not the same behavior that was observed for the temperature induced collapse where the collapse rate was essentially independent of the solvent density. However, these results were obtained for considerably lower values of α for the α -quenches than for the T -quenches and therefore the monomer-monomer attractions and monomer-monomer repulsions are not as strong.

For Model B with a fully flexible chain, the rate of collapse increases slightly but is almost constant at low densities. At higher densities, the trend is reversed and the rate of collapse decreases as a function of density. In this case, the collapse is driven by the attractive part of the Lennard-Jones interaction between the monomers as well as the random interaction between the monomers and the solvent particles which can be both attractive and repulsive. For the strengths of the random monomer-solvent interaction used here, the solvent particles seem to only act as obstacles to the collapse of the polymer. At lower densities, the collapse appears to be almost completely driven by the attractive part of the Lennard-Jones interaction between the monomers. The repulsive interaction of the solvent particles on the hydrophobic monomers could also assist the collapse but for the value of α' used this contribution is very weak. Therefore, at low densities, the collapse times are basically constant while at higher densities the “obstacle” nature of the solvent particles take over and reduces the rate of collapse. These results are in agreement with the study by Polson and Zuckermann in 2-D (Polson and Zuckermann [00]) and 3-D (Polson and Zuckermann [01]) on homopolymers and copolymers.

Finally, when a bending restriction was added to the fully flexible chain of Model B, a marked increase in the collapsed time was observed. Furthermore, the effect of the bending restriction were most pronounced at higher ρ . These results are also in agreement with the work of Polson and Zuckermann [01] who proposed that the stiffness effect is most pronounced at higher ρ since an increase in the solvent density

has a considerably stronger effect on the slowing down of the collapse dynamics of a conformationally restricted polymer chain.

In our study of both equilibrium properties and collapse dynamics of polymers, we used a discrete monomeric solvent where the solvent particles are of the same size as the monomers constituting the polymer. On the other extreme, many studies of polymer collapse use a continuous solvent. In fact, in reality, the ratio of the size of the solvent particles to the size of the monomers are most often somewhere between these two extremes. For this reason, it would be useful to study the effect of varying the solvent/monomer particle size ratio. Such a study would significantly increase the computational demands since the number of degrees of freedom would be increased.

Another interesting contribution would be to include all the hydrodynamic modes to Model B by using standard constant energy MD. Furthermore, there are no studies of the hydrodynamic effects on collapse in the absence of an explicit solvent even though some interesting techniques are already being used to include hydrodynamics in the study of equilibrium polymer dynamics with an intrinsic solvent. Oseen tensor methods, as well as coarse-grained solvent methods (see, Malevanets and Yeomans [00]) are currently used.

The heavy computational demands related to the study of an explicit solvent on the conformation of a polymer has encouraged researchers to develop techniques to reduce the computational cost. An example is the technique of dissipative particle dynamics (DPD) which consists in coarse graining the description of the fluid. Kong et al. [97] state that even though DPD is not atomically detailed, both excluded volume and hydrodynamic interactions are present. Other methods include the density functional theory (Takahashi and Munakata [97]) and the polymer–solvent integral equations theory for the correlation functions of the polymer and the solvent (Gan and Eu [98]). Nevertheless, it is important to simulate polymer collapse in an explicit solvent since interesting effects have been found for this case, notably the solvent induced entropic polymer collapse transition observed in hard–core models.¹ As anticipated, the collapse behavior for models including an explicit solvent usually differs

¹Dijkstra, Frenkel and Hansen [94]; Dijkstra and Frenkel [94]; Frenkel and Louis [92]; Polson [99]; Khalatur, Zherenkova and Khokhlov [98]; van der Schoot [98]; Luna-Bárcena et al. [96]; Suen, Escobedo and Pablo [97]

qualitatively from that observed in simulation studies of isolated chain systems, or even from theories which include the effect of hydrodynamic interactions (Chang and Yethiraj [01]).

Finally, even the best algorithms using semi-classical pseudo-potentials for interactions between amino acids can only be used to study the dynamics of protein folding in the regime $1ns$ - $1\mu s$ for an all atom model of a protein in a solvent, while a relative time scale for a real system is $10\mu s$ - $1s$. Duan and Kollman have succeeded in performing a molecular dynamic simulation with full atomic representation of both the peptide (36-residue villin headpiece subdomain) and solvent (~ 3000 water molecules) at 300 K for $1-\mu s$ (Duan and Kollman [98]). Those limitations have led researchers to use minimal models or simply short peptides as a first step study of protein folding. Many universal properties that are not dependent on the details of the model can be found in this way.

Real protein sequences statistically look very much like random sequences which is consistent with the idea that an evolutionary search could explore only a tiny part of the sequence space and thus could not pull sequences too far away from random (Ptitsyn [95] and Monod [71]). Therefore, random heteropolymers are able to give a lot of information about the kinetics of protein folding but the non-randomness of sequences still remains crucially important for protein design (Pande et al. [96]). For this reason, it would be useful to study heteropolymers with well defined sequences mimicking proteins. We have performed a few molecular dynamics simulations with such a model by using an Hamiltonian similar to the one used in the paper by Li et al. [96] combined with the Miyazawa-Jernigan contact matrix for amino acids (Miyazawa and Jernigan [85]; Li, Tang and Wingreen [97]). We studied mainly short protein sequences from the protein data bank (Berman et al. [00]). These results are beyond the scope of this dissertation and are therefore not reported here even though it would definitively be worth pursuing our research in this area in order to compare random sequence to real sequences.

There are many other questions of interest concerning the kinetics of random heteropolymers. Among these, it would clearly be useful to examine the kinetics of “unfolding”, as protein denaturation is of great interest (Daggett and Levitt [92]). A

minimal model to study how the presence of chaperon proteins whose role is to help proteins to fold could also bring a lot of insight to the protein folding problem. A study of the absorption of a random heteropolymer on a surface as well as a study of the collapse dynamics of polyampholytes could also contribute to the increasing knowledge of the dynamics of heteropolymer collapse.

APPENDICES

A.1 Langevin equation

This section “derives” the Langevin equation by following the development of Reif [65] and generalizing it to three dimensions and N particles¹. A sufficiently small macroscopic particle immersed in a liquid exhibits a random type motion. This phenomenon is called the “Brownian motion” and reveals very clearly the statistical fluctuations which occur in a system in thermal equilibrium. Such fluctuations constitute a background of “noise” which imposes limitations on the possible accuracy of delicate physical measurements.

A particle i is immersed in a liquid at temperature T , it would be a very complicated task to describe in detail the interaction of this particle at position \mathbf{r}_i with all the other degrees of freedom of the system (*i.e.*, those describing the internal motions of the atoms in the macroscopic particle, as well as those describing the motion of the molecules in the surrounding liquid). But these other degrees of freedom can be regarded as constituting a heat reservoir at temperature T and their interaction with \mathbf{r}_i can be lumped into some net force $\mathbf{W}_i(t)$ effective in determining the time dependence of \mathbf{r}_i . Newton’s equation of motion can then be written as

$$m \frac{d\mathbf{v}_i}{dt} = m \frac{d^2\mathbf{r}_i}{dt^2} = \mathbf{F}_i + \mathbf{W}_i(t). \quad (\text{A.1})$$

Here very little is known about the force $\mathbf{W}_i(t)$ which describes the interaction of \mathbf{r}_i with many other degrees of freedom of the system. Basically, $\mathbf{W}_i(t)$ must depend on the position of very many atoms which are in constant motion. Thus, $\mathbf{W}_i(t)$ is some rapidly fluctuating function of the time t and varies in a very irregular fashion. Indeed, one cannot specify the precise functional dependence of $\mathbf{W}_i(t)$ on t . In order to make progress, one must formulate the problem in statistical terms. One must therefore envisage an ensemble of very many similarly prepared systems, each of

¹A very good treatment of Brownian dynamics can also be found in chapter 13 of Pathria [72].

them consisting of a particle i and its surrounding medium. For each of these, the force $\mathbf{W}_i(t)$ is some random function of t . One can then attempt to make statistical statements about this ensemble.

The rate at which $\mathbf{W}_i(t)$ varies can be characterized by some correlation time τ^* which measures roughly the mean time between two successive maxima (or minima) of the fluctuating function $\mathbf{W}_i(t)$. τ^* is quite small on the macroscopic scale. It is roughly of the order of the ratio of mean intermolecular separation and a mean molecular velocity ($\sim 10^{-13}$ s.). Furthermore, if one contemplates a situation where the particle is imagined clamped so as to be stationary, there is no preferred direction in space; the $\mathbf{W}_i(t)$ is as often positive as negative so that the ensemble average $\langle \mathbf{W}_i(t) \rangle$ vanishes.

Since $\mathbf{W}_i(t)$ is a rapidly fluctuating function of time, it follows by Eq. (A.1) that \mathbf{v}_i also fluctuates in time. But superimposed upon these fluctuations, the time dependence of \mathbf{v}_i may also exhibit a more slowly varying trend. One can focus the attention on the ensemble average $\bar{\mathbf{v}}_i$ of the velocity, which is a much more slowly varying function than \mathbf{v}_i itself, and write

$$\mathbf{v}_i = \bar{\mathbf{v}}_i + \mathbf{v}'_i, \quad (\text{A.2})$$

where \mathbf{v}'_i denotes the part of \mathbf{v}_i which fluctuates rapidly (although less rapidly than $\mathbf{W}_i(t)$ since the mass m is appreciable) and whose mean value vanishes. The slowly varying part $\bar{\mathbf{v}}_i$ is of crucial importance since it is of primary significance in determining the behavior of the particle over long periods of time. To investigate its time dependence, let us integrate Eq. (A.1) over some time interval δt which is small on a macroscopic scale, but large in the sense that $\delta t \gg \tau^*$. Then one gets

$$m [\mathbf{v}_i(t + \delta t) - \mathbf{v}_i(t)] = \mathbf{F}_i \delta t + \int_t^{t+\delta t} \mathbf{W}_i(t') dt', \quad (\text{A.3})$$

where we have assumed that \mathbf{F}_i is varying slowly enough that it changes by a negligible amount during a time δt . The last integral in Eq. (A.3) ought to be very small since $\mathbf{W}_i(t)$ changes signs many times in the time δt . Hence, one might expect that any slow varying part of \mathbf{v}_i should be due only to \mathbf{F}_i (*i.e.* $m \frac{d\bar{\mathbf{v}}_i}{dt} = \mathbf{F}_i$) but this order of approximation is too crude to describe the physical situation. Indeed, the interaction with the environment expressed by $\mathbf{W}_i(t)$ must be such that it always tends to restore

the particle to the equilibrium situation. If $\mathbf{F}_i = 0$, the interaction expressed by \mathbf{W}_i must then be such that, if $\bar{\mathbf{v}}_i \neq 0$ at some initial time, it causes $\bar{\mathbf{v}}_i$ to approach its ultimate equilibrium value $\bar{\mathbf{v}}_i = 0$. But $m\frac{d\bar{\mathbf{v}}_i}{dt} = \mathbf{F}_i$ fails to predict this kind of trend of $\bar{\mathbf{v}}_i$ towards its equilibrium value. The reason is that we did not consider the fact that \mathbf{W}_i must be affected by the motion of the particle in such a way that \mathbf{W}_i itself also contains a slowly varying part $\bar{\mathbf{W}}_i$ tending to restore the particle to equilibrium. Hence, as we did for the velocities,

$$\mathbf{W}_i = \bar{\mathbf{W}}_i + \mathbf{W}'_i, \quad (\text{A.4})$$

where \mathbf{W}'_i is the rapidly fluctuating part of \mathbf{W}_i whose average value vanishes. The slowly varying part $\bar{\mathbf{W}}_i$ must be some function of $\bar{\mathbf{v}}_i$ such that $\bar{\mathbf{W}}_i(\bar{\mathbf{v}}_i) = 0$ in equilibrium when $\bar{\mathbf{v}}_i = 0$. If $\bar{\mathbf{v}}_i$ is not too large, $\bar{\mathbf{W}}_i(\bar{\mathbf{v}}_i)$ can be expanded in a power series in $\bar{\mathbf{v}}_i$ whose first non-vanishing term must then be linear in $\bar{\mathbf{v}}_i$. Thus $\bar{\mathbf{W}}_i$ must have the general form

$$\bar{\mathbf{W}}_i = -\alpha\bar{\mathbf{v}}_i \quad (\text{A.5})$$

where α is some positive constant called the friction constant. The minus signs indicates explicitly that the force $\bar{\mathbf{W}}_i$ tends to reduce $\bar{\mathbf{v}}_i$ to zero as time increases.

In the general case, the slowly varying part of Eq. (A.1) becomes then

$$m\frac{d\bar{\mathbf{v}}_i}{dt} = \mathbf{F}_i + \bar{\mathbf{W}}_i = \mathbf{F}_i - \alpha\bar{\mathbf{v}}_i. \quad (\text{A.6})$$

If one includes the rapidly fluctuating parts \mathbf{v}'_i and \mathbf{W}'_i of equations (A.2) and (A.4), Eq. (A.1) can be written

$$m\frac{d\mathbf{v}_i}{dt} = m\frac{d^2\mathbf{r}_i}{dt^2} = \mathbf{F}_i - \alpha\mathbf{v}_i + \mathbf{W}'_i(t) \quad (\text{A.7})$$

where we have put $\alpha\bar{\mathbf{v}}_i \approx \alpha\mathbf{v}_i$ with negligible error since the rapidly fluctuating contribution \mathbf{v}'_i can be neglected compared to the predominant fluctuating term \mathbf{W}'_i . Eq. (A.7) is called the Langevin equation. Note that in the rest of the dissertation, we have dropped the prime from \mathbf{W}'_i and set $\Gamma \equiv \alpha/m$ (see Eq. (2.25)). It differs from the original equation (A.1) by explicitly decomposing the force \mathbf{W}'_i into a slowly varying part $-\alpha\mathbf{v}_i$ and into a fluctuating part \mathbf{W}'_i which is purely random, *i.e.*, such that its mean value always vanishes irrespective of the velocity or the position of the

particle. The Langevin equation (A.7) describes the behavior of the particle at all later times if its initial conditions are specified.

Since the Langevin equation contains the frictional force $-\alpha \mathbf{v}_i$, it implies the existence of processes whereby the energy associated with the coordinate \mathbf{r}_i of the particle is dissipated in the course of time to the other degrees of freedom (the heat reservoir). The total energy is not conserved and the motion is not reversible. What does reversible motion mean? If the sign of the time t were reversed, the equations of motion would be essentially unchanged and all particles would (classically) retrace their paths in time.

We will now show how we can calculate the diffusion constant D . Let us assume that Langevin's equation is a valid phenomenological description of Brownian motion. In the absence of external forces Eq. (A.7) becomes

$$m \frac{d\mathbf{v}_i}{dt} = -\alpha \mathbf{v}_i + \mathbf{W}'_i(t) \quad (\text{A.8})$$

In thermal equilibrium, the mean displacement of the particle vanishes ($\bar{\mathbf{r}}_i = 0$) since there are no preferred direction in space. To calculate the magnitude of the fluctuations, we now use Eq. (A.8) to find the mean-square displacement $\langle \mathbf{v}_i^2 \rangle = \bar{\mathbf{r}}_i^2$ of the particle in a time interval t . We shall indicate ensemble averages by bars and angular brackets interchangeably. Let us replace $\mathbf{v}_i = \dot{\mathbf{r}}_i$ and $d\mathbf{v}_i/dt = d\dot{\mathbf{r}}_i/dt$ in Eq. (A.8) and multiply both sides by \mathbf{r}_i .

$$m \mathbf{r}_i \frac{d\dot{\mathbf{r}}_i}{dt} = m \left[\frac{d(\mathbf{r}_i \dot{\mathbf{r}}_i)}{dt} - \dot{\mathbf{r}}_i^2 \right] = -\alpha \mathbf{r}_i \dot{\mathbf{r}}_i + \mathbf{r}_i \mathbf{W}'_i(t) \quad (\text{A.9})$$

One can now take the ensemble average of both sides of Eq. (A.9). As we have previously pointed it out, the mean value of the fluctuating force \mathbf{W}'_i always vanishes, irrespective of \mathbf{v}_i or \mathbf{r}_i . Hence, $\langle \mathbf{r}_i \mathbf{W}'_i \rangle = \langle \mathbf{r}_i \rangle \langle \mathbf{W}'_i \rangle = 0$. Furthermore, the equipartition theorem gives $\frac{1}{2}m\langle \dot{\mathbf{r}}_i^2 \rangle = \frac{3}{2}k_B T$ thus Eq. (A.9) becomes

$$m \left\langle \frac{d(\mathbf{r}_i \dot{\mathbf{r}}_i)}{dt} \right\rangle = m \frac{d\langle \mathbf{r}_i \dot{\mathbf{r}}_i \rangle}{dt} = 3k_B T - \alpha \langle \mathbf{r}_i \dot{\mathbf{r}}_i \rangle \quad (\text{A.10})$$

The relation (A.9) is a simple differential equation which can be solved for $\langle \mathbf{r}_i \dot{\mathbf{r}}_i \rangle$ and we obtain

$$\langle \mathbf{r}_i \dot{\mathbf{r}}_i \rangle = c e^{-\Gamma t} + \frac{3k_B T}{\alpha} \quad (\text{A.11})$$

where c is an integration constant and $\Gamma \equiv \alpha/m$. Γ^{-1} denotes a characteristic time constant of the system. Assuming that each particle in the ensemble starts out at $t = 0$ at position $\mathbf{r}_i = 0$, the constant c must be such that $0 = c + 3k_B T/\alpha$. Hence (A.11) becomes

$$\langle \mathbf{r}_i \dot{\mathbf{r}}_i \rangle = \frac{1}{2} \frac{d\langle \mathbf{r}_i^2 \rangle}{dt} = \frac{3k_B T}{\alpha} (1 - e^{-\Gamma t}) \quad (\text{A.12})$$

Integrating once more, we obtain the final result

$$\langle \mathbf{r}_i^2 \rangle = \frac{6k_B T}{\alpha} [t - \Gamma^{-1} (1 - e^{-\Gamma t})] \quad (\text{A.13})$$

Note two interesting limiting cases. If $t < \Gamma^{-1}$, then

$$e^{-\Gamma t} = 1 - \Gamma t + \frac{1}{2}\Gamma^2 t^2 - \dots \quad (\text{A.14})$$

Thus

for $t \ll \Gamma^{-1}$,

$$\langle \mathbf{r}_i^2 \rangle = \frac{3k_B T}{m} t^2. \quad (\text{A.15})$$

The particle then behaves for a short initial time interval as though it were a free particle moving with constant velocity $\mathbf{v}_i = \sqrt{3k_B T/m}$.

On the other hand, if $t \gg \Gamma^{-1}$, $e^{-\Gamma t} \rightarrow 0$. thus Eq. (A.13) becomes simply for $t \gg \Gamma^{-1}$

$$\langle \mathbf{r}_i^2 \rangle = \frac{6k_B T}{\alpha} t. \quad (\text{A.16})$$

The particle then behaves like a diffusing particle executing a random walk so that $\langle \mathbf{r}_i^2 \rangle \propto t$. But since the diffusion equation leads to $\langle \mathbf{r}_i^2 \rangle = 6Dt$, we can determine the diffusion coefficient,

$$D = \frac{k_B T}{\alpha} = \frac{k_B T}{m\Gamma}. \quad (\text{A.17})$$

We will now do a more detailed investigation of the approximations which lead to the irreversible Langevin equation (A.7). The question is to understand in detail what conditions must be satisfied for this description to be approximatively valid, and how the modified equation of motion (A.7) are derivable from microscopic equations. In order to gain better understanding of the frictional force, we will return to Eq. (A.1) and attempt to analyse it in greater detail. Let us consider a time interval δt which macroscopically is very small, but which is large on a microscopic scale so that $\delta t \gg$

τ^* , as we have done before. τ^* is the correlation time which is of the order of the mean period of the fluctuations of the force $\mathbf{W}_i(t)$. τ^* also measures the relaxation time required for the degrees of freedom responsible for the force \mathbf{W}_i to come to internal equilibrium when disturbed by a sudden small change of \mathbf{r}_i . We again assume that the external force \mathbf{F}_i is slowly varying and we want to find the slowly varying part of the velocity \mathbf{v}_i . A quantity is slowly varying if it changes by negligible amounts in the time interval δt .

Let us assume an ensemble of similarly prepared systems which satisfy Eq. (A.1). We take the ensemble average on both side of the integrated form of this equation (Eq. (A.3)).

$$m\langle \mathbf{v}_i(t + \delta t) - \mathbf{v}_i(t) \rangle = \mathbf{F}_i(t)\delta t + \int_t^{t+\delta t} \langle \mathbf{W}_i(t') \rangle dt', \quad (\text{A.18})$$

If we neglect any effect of the particle's motion on the force \mathbf{W}_i exerted on it by the environment, the mean value $\langle \mathbf{W}_i \rangle$ would be the same as the static equilibrium (stationary with respect to its environment) mean value $\langle \mathbf{W}_i \rangle_0 = 0$. As we pointed out earlier, an order of approximation that would put $\langle \mathbf{W}_i \rangle = \langle \mathbf{W}_i \rangle_0$ is inadequate since it doesn't yield a slowly varying velocity which tends to restore the particle to thermal equilibrium. We have to estimate how $\langle \mathbf{W}_i \rangle$ is affected as the velocity \mathbf{v}_i of the particle changes.

We will make an approximate analysis by assuming a small system described by \mathbf{r}_i and a heat bath which contains all the other degrees of freedom. The temperature $T \equiv (k_B\beta)^{-1}$ of the heat bath is essentially constant, irrespective of any small changes in its energy. For a given value of \mathbf{v}_i , the possible states of the particle i can be labeled S ; in such a state, the force \mathbf{W}_i assumes some value \mathbf{W}_i^S .

At some time t , the velocity of the particle is $\mathbf{v}_i(t)$. As a first approximation, we can assume that at time t , the system is in an equilibrium situation and $\langle \mathbf{W}_i \rangle = 0$ where the probability of being in state S is $P_S^{(0)}$. In the next approximation, we must investigate how $\langle \mathbf{W}_i \rangle$ is affected by the motion of the particle. Consider then the situation at a slightly later time $t' = t + \delta t'$ when the particle has a velocity $\mathbf{v}_i(t + \delta t')$. The motion of the particle affects its environment and if $\delta t'$ is sufficiently short, the mean force $\langle \mathbf{W}_i(t') \rangle$ depends on the situation at earlier time t . As the particle velocity changes, the internal equilibrium of environment is disturbed but after a time of the

order of τ^* , the equilibrium conditions consistent with the new value of $\mathbf{v}_i(t + \delta t')$ will be re-established. This means that the heat bath will again be found with equal likelihood in its Ω accessible states. Let us suppose that in a time interval $\delta t' > \tau^*$ the velocity of the particle changes by $\Delta\mathbf{v}_i(\delta t')$ and that the energy of the heat bath changes from E' to $E' + \Delta E'(\delta t')$. Since in a situation of equilibrium the probability of occurrence of a given state S is proportional to the corresponding number of states accessible to the heat bath, we can write

$$\frac{P_S(t + \delta t')}{P_S^{(0)}} = \frac{\Omega(E' + \Delta E'(\delta t'))}{\Omega(E')} = e^{\beta\Delta E'} \quad (\text{A.19})$$

where $\beta \equiv (\partial \ln \Omega / \partial E')$ is the temperature parameter of the heat bath. Physically, this means that the likelihood of particle i being found in a given state at a later time is increased if more energy becomes available to the heat reservoir. Thus

$$P_S(t + \delta t') = P_S^{(0)} e^{\beta\Delta E'} \approx P_S^{(0)} (1 + \beta\Delta E') \quad (\text{A.20})$$

At a slightly later time $t' = t + \delta t'$ the mean value of \mathbf{W}_i is then given by

$$\langle \mathbf{W}_i \rangle = \frac{1}{3} \sum_S P_S(t + \delta t') \mathbf{W}_i^S = \frac{1}{3} \sum_S P_S^{(0)} (1 + \beta\Delta E') \mathbf{W}_i^S = \frac{1}{3} \langle (1 + \beta\Delta E') \mathbf{W}_i \rangle_0 \quad (\text{A.21})$$

where the last mean value is to be computed with the equilibrium probability $P_S^{(0)}$. Since $\langle \mathbf{W}_i \rangle_0 = 0$, we get

$$\langle \mathbf{W}_i \rangle = \frac{\beta}{3} \langle \mathbf{W}_i \Delta E' \rangle_0 \quad (\text{A.22})$$

which, in general, does not vanish. Note the factor of 3 which is related to the splitting of the degrees of freedom in isotropic 3-dimensional space.

We can now use these approximations in Eq. (A.18), where $\delta t \gg \tau^*$. The integral in that expression extends over a time integral sufficiently long that $\delta t' = t' - t \gg \tau^*$ over practically the entire range of integration, making it possible to use the approximation (A.22).

The energy increase of the heat bath in the time $t' - t$ is simply the negative of the work done by the force \mathbf{W}_i on the particle. Thus

$$\Delta E' = - \int_t^{t'} \mathbf{v}_i(t'') \mathbf{W}_i(t'') dt'' \approx -\mathbf{v}_i(t) \int_t^{t'} \mathbf{W}_i(t'') dt'' \quad (\text{A.23})$$

where we have made the approximation, consistent with Eq. (A.18), that $\mathbf{v}_i(t)$ does not vary appreciably over times of the order of δt . Hence, we can use Eq. (A.22) to write the integrand of Eq. (A.18) in the following manner

$$\langle \mathbf{W}_i(t') \rangle = -\frac{\beta}{3} \left\langle \mathbf{W}_i(t') \mathbf{v}_i(t) \int_t^{t'} \mathbf{W}_i(t'') dt'' \right\rangle_0 = -\frac{\beta}{3} \bar{\mathbf{v}}_i(t) \int_t^{t'} dt'' \langle \mathbf{W}_i(t') \mathbf{W}_i(t'') \rangle_0 \quad (\text{A.24})$$

We have first averaged separately over $\mathbf{v}_i(t)$, since it varies much more slowly than $\mathbf{W}_i(t)$. Let us write Eq. (A.24) in terms of $s \equiv t'' - t'$. Equation (A.18) then becomes

$$m \langle \mathbf{v}_i(t + \delta t) - \mathbf{v}_i(t) \rangle = \mathbf{F}_i(t) \delta t - \frac{\beta}{3} \bar{\mathbf{v}}_i(t) \int_t^{t+\delta t} dt' \int_{t-t'}^0 ds \langle \mathbf{W}_i(t') \mathbf{W}_i(t' + s) \rangle_0 \quad (\text{A.25})$$

The last term on the right is slowly varying and leads to dissipation.

The ensemble average which occurs in Eq. (A.25) is the correlation function of $\mathbf{W}_i(t)$.

$$C(s) \equiv \langle \mathbf{W}_i(t') \mathbf{W}_i(t' + s) \rangle_0 \quad (\text{A.26})$$

The ensemble average is here taken at equilibrium where the distribution of systems in the ensemble is independent of the absolute value of the time. This average is independent of the time t' and depends only on the time difference s .

Let us now study correlation functions more closely by letting \mathbf{W}_i be any random function of t . we shall drop the prime in t' and the subscript from the averaging brackets for convenience,

$$C(0) = \langle \mathbf{W}_i(t) \mathbf{W}_i(t) \rangle = \langle \mathbf{W}_i^2(t) \rangle > 0 \quad (\text{A.27})$$

Thus $C(0)$ is equal to the mean-square value of \mathbf{W}_i , or to its dispersion if $\langle \mathbf{W}_i \rangle = 0$. In equilibrium, $\langle \mathbf{W}_i^2(t) \rangle$ is independent of the time t .

If s becomes sufficiently large, then $\langle \mathbf{W}_i(t) \rangle$ and $\langle \mathbf{W}_i(t + s) \rangle$ must become uncorrelated. Thus for $s \rightarrow \infty$, $C(s) \rightarrow \langle \mathbf{W}_i(t) \rangle \langle \mathbf{W}_i(t + s) \rangle$ and $C(s) \rightarrow 0$ if $\langle \mathbf{W}_i \rangle = 0$. We can also show that $|C(0)| \leq C(0)$ and that $C(s) = C(-s)$ (*i.e.*, $C(s)$ is a symmetric function). Values assumed by the force $\mathbf{W}_i(t)$ become uncorrelated over times of the order of τ^* . The correlation function contains a lot of information about the statistical properties of the random force.

We now return to the evaluation of the integral in Eq. (A.25). The integrand is just the correlation function $C(s)$ of the force \mathbf{W}_i and differs from zero only in the

small region where $|s| \leq \tau^* \ll \delta t$, the integrand is proportional to $\tau^* \delta t$ rather than to the area δt^2 of the complete domain of integration. Thus the integral is proportional to the first power of δt . Since $C(s)$ is independent of t' , the integration over t' can be done first and we get

$$\int_t^{t+\delta t} dt' \int_{t-t'}^0 ds C(s) = \int_{-\delta t}^0 ds \int_{t-s}^{t+\delta t} dt' C(s) = \int_{-\delta t}^0 ds C(s)(\delta t + s) \quad (\text{A.28})$$

Since $\delta t \gg \tau^*$, while $C(s) \rightarrow 0$ when $|s| \gg \tau^*$, we can neglect s compared to δt in the entire range where the integrand is appreciable. Furthermore, the lower limit in the last integral can be replaced by $-\infty$ with negligible error. Hence, we obtain

$$\int_t^{t+\delta t} dt' \int_{t-t'}^0 ds C(s) \approx \delta t \int_{-\infty}^0 ds C(s) = \frac{1}{2} \delta t \int_{-\infty}^{\infty} ds C(s) \quad (\text{A.29})$$

where we have used the symmetry property in the last step. We can now rewrite Eq. (A.25) as follow

$$m\langle \mathbf{v}_i(t + \delta t) - \mathbf{v}_i(t) \rangle = \mathbf{F}_i(t)\delta t - \alpha \bar{\mathbf{v}}_i(t)\delta t \quad (\text{A.30})$$

where the constant α is given by

$$\alpha \equiv \frac{1}{6k_B T} \int_{-\infty}^{\infty} \langle \mathbf{W}_i(t) \mathbf{W}_i(t+s) \rangle ds \quad (\text{A.31})$$

Eq. (A.31) is the fluctuation–dissipation theorem which gives us an explicit expression for the friction constant α in terms of the correlation function of the fluctuating force \mathbf{W}_i at equilibrium. This brings us back to Eq. (A.6) from which we can obtain Langevin’s equation of motion Eq. (A.7) but this time we have some microscopical insight into how the frictional force $-\alpha \bar{\mathbf{v}}_i$ arises from the fluctuating force. This random process may be taken to have a delta function correlation function for each molecule. Thus we can write

$$\langle \mathbf{W}_i(t) \mathbf{W}_j(t') \rangle = 6k_B T m \Gamma \delta_{ij} \delta(t - t') \quad (\text{A.32})$$

which satisfies Eq. (A.31).

The above discussion satisfies the use of Eq. (2.25) in Chapter 2.

A.2 Error propagation for t_{50} and t_{90}

In this appendix, we discuss the stretched exponential is of the form (see Eq. (5.1))

$$y(t) = a_0 e^{-(t-t_I)/\tau} - a_1 \quad (\text{A.33})$$

where $y(\infty) = -a_1$ and $y(t_I) = a_0 - a_1$. t_I is the time at which we started acquiring data.

A very important point with regard to numerical data fitting is that the results for t_{50} and t_{90} obtained from the curve are very sensitive to the initial point of the fitted curve. This initial point should be as close as possible to that of the raw data, therefore, we have fixed a_1 to the value that would cause the initial point on the fitted curve to exactly match the initial point of the raw data. There is no problem in doing this since the only reason we do the fit is to find the 50 % and 90 % decay times. When a fit is performed, there is always some deviation between raw data and the fit at any given point, including the $t = t_I$ point here. In fact, for functions of the sort considered, i.e. rapidly varying functions near $t = t_I$, the deviation can be expected to be especially large here. So the solution is to fix the fit at $t = t_I$ to the raw data. On the other hand, if we were interested in the τ and β parameter values, then this should not be done.

We define the 50 % and 90 % decay has follow:

$$y_{50} \equiv y(t_I) + \frac{1}{2}(y(\infty) - y(t_I)) = \frac{1}{2}a_0 - a_1 \quad (\text{A.34})$$

$$y_{90} \equiv y(t_I) + \frac{9}{10}(y(\infty) - y(t_I)) = \frac{1}{10}a_0 - a_1 \quad (\text{A.35})$$

and from Eqs. (A.33), (A.34) and (A.35), we obtain t_{50} and t_{90} .

$$t_{50} = \tau(\ln 2)^{1/\beta} + t_I \quad (\text{A.36})$$

$$t_{90} = \tau(\ln 10)^{1/\beta} + t_I \quad (\text{A.37})$$

Now, let us calculate the error propagation:

$$\Delta t_{50} = \frac{\partial t_{50}}{\partial \tau} \Delta \tau + \frac{\partial t_{50}}{\partial \beta} \Delta \beta \quad (\text{A.38})$$

$$\frac{\partial t_{50}}{\partial \tau} = (\ln 2)^{1/\beta} = \frac{t_{50} - t_I}{\tau} \quad (\text{A.39})$$

$$\begin{aligned}\ln(t_{50} - t_I) &= \ln \tau + \frac{1}{\beta} \ln(\ln 2) \\ \frac{1}{t_{50} - t_I} \frac{\partial(t_{50} - t_I)}{\partial \beta} &= -\frac{1}{\beta^2} \ln(\ln 2) \\ \frac{\partial t_{50}}{\partial \beta} &= -\frac{t_{50} - t_I}{\beta^2} \ln(\ln 2)\end{aligned}\tag{A.40}$$

Therefore we obtain:

$$\Delta t_{50} = (t_{50} - t_I) \left\{ \frac{\Delta \tau}{\tau} - \frac{\Delta \beta}{\beta^2} \ln(\ln 2) \right\} \tag{A.41}$$

and similarly,

$$\Delta t_{90} = (t_{90} - t_I) \left\{ \frac{\Delta \tau}{\tau} - \frac{\Delta \beta}{\beta^2} \ln(\ln 10) \right\}. \tag{A.42}$$

Eqs. (A.41) and (A.42) are used in Chapter 5 to estimate the systematic errors in the data fitting procedure.

REFERENCES

- ALLEN, M. P. AND TILDESLEY, D. J. [87]. *Computer simulation of liquids*. Oxford University Press, Oxford, 1987.
- ANDERSEN, H. C. [80]. Molecular dynamics simulations at constant pressure and/or temperature. *J. Chem. Phys.*, **72**(4), 2384 (1980).
- BALDWIN, R. L. [94]. Pathways and mechanisms of protein folding. In Doniach, S., editor, *Statistical mechanics, protein structure and protein substrate interactions*, NATO ASI Series, pages 3–4. Plenum Press, Heidelberg and London.
- BAUMGÄRTNER, A. [87]. Simulations in polymer physics. In Binder, K., editor, *Topics in current physics: Applications of the Monte Carlo method in statistical physics*, pages 145–180. Springer Verlag, Heidelberg and London.
- BERMAN, H. M., WESTBROOK, J., FENG, Z., GILLILAND, G., BHAT, T. N., WEISSIG, H., SHINDYALOV, I. N., AND BOURNE, P. E. [00]. Protein data bank. *Nucleic Acids Research*, **28**, 235 (2000).
- BEVINGTON, P. R. AND ROBINSON, D. K. [92]. *Data reduction and error analysis for the physical sciences*. McGraw-Hill, Inc., New York, second edition, 1992.
- BRYNGELSON, J. AND WOLYNES, P. [87]. Spin glasses and the statistical mechanics of protein folding. *Proc. Natl. Acad. Sci. USA*, **84**, 7524 (1987).
- BRYNGELSON, J. AND WOLYNES, P. [89]. Intermediate and barrier crossing in a random energy model (with applications to protein folding). *J. Phys. Chem.*, **93**, 6902 (1989).
- BUGUIN, A., BROCHARD-WYART, F., AND DE GENNES, P. G. [96]. Collapse of a flexible coil in a poor solvent. *C. R. Acad. Sci. Paris*, **322**, 741 (1996).
- CHANG, R. AND YETHIRAJ, A. [01]. Solvent effects on the collapse dynamics of polymers. *J. Chem. Phys.*, **114**(17), 7688 (2001).

- CHU, B., YING, Q. C., AND GROSBERG, A. Y. [95]. 2-stage kinetics of single chain collapse - polystyrene in cyclohexane. *Macromolecules*, **28**, 180 (1995).
- CICCOTTI, G., FRENKEL, D., AND McDONALD, I. R. [87]. In Ciccotti, G., Frenkel, D., and McDonald, I. R., editors, *Simulation of liquids and solids: Molecular dynamics and Monte Carlo methods in statistical mechanics*. Elsevier Science Pub. Co., New York.
- COTTIN, X. AND MONSON, P. A. [96]. Solid-fluid phase equilibrium for single component and binary lennard-jones system: A cell theory approach. *J. Chem. Phys.*, **105**(22), 10022 (1996).
- CREIGHTON, T. [92]. *Protein folding*. Freeman and Company, New York, 1992.
- CROOKS, G. E., OSTROVSKI, B., AND BAR-YAM, Y. [99]. The mesostrurture of polymer collapse and fractal smoothing. *Phys. Rev. E*, **60**, 4559 (1999).
- DAGGETT, V. AND LEVITT, M. [92]. A model of the molten globule state from molecular dynamics simulations. *Proc. Nat. Acad. Sci. USA*, **89**, 5142 (1992).
- DAWSON, K. A., TIMOSHENKO, E. G., AND KUZNETSOV, Y. A. [97]. Kinetics of conformational transitions of a single polymer chain. *Physica A*, **236**(1-2), 58 (1997).
- DE GENNES, P. [79]. *Scaling concepts in polymer physics*. Cornell University Press, Ithaca, 1979.
- DE GENNES, P. G. [85]. Kinetics of collapse for a flexible coil. *J. Phys.-Paris (Lettre)*, **46**, L639 (1985).
- DES CLOIZEAUX, J. AND JANNINK, G. [90]. *Polymers in Solution: Their Modeling and Structure*. Clarendon, Oxford, 1990.
- DIJKSTRA, M. AND FRENKEL, D. [94]. Evidence for entropy-driven demixing in hard-core fluids. *Phys. Rev. Lett.*, **72**(2), 298 (1994).
- DIJKSTRA, M., FRENKEL, D., AND HANSEN, J.-P. [94]. Phase separation in binary hard-core mixtures. *J. Chem. Phys.*, **101**(4), 3179 (1994).
- DOI, M. [96]. *Introductions to polymer physics*. Oxford University Press, Oxford, 1996.

- DOI, M. AND EDWARDS, S. F. [86]. *The theory of polymer dynamics*, volume 73 of *International Series of Monographs on Physics*. Oxford University Press, Oxford, 1986.
- DOMB, C. AND HIOE, F. T. [69]. Correlations in a self-avoiding walk. *J. Chem. Phys.*, **51**, 1920 (1969).
- DUAN, Y. AND KOLLMAN, P. A. [98]. Pathways to a protein folding intermediate observed in a 1-microsecond simulation in aqueous solution. *Science*, **282**, 740 (1998).
- DÜNWEG, B. AND KREMER, K. [91]. Microscopic verification of dynamic scaling in dilute polymer solutions: a molecular-dynamics simulation. *Phys. Rev. Lett.*, **66**(23), 2996 (1991).
- ELLIS, T. M. R. [90]. *Fortran 77 programming*. Addison-Wesley Publishing Company, Workingham, England, second edition, 1990.
- ESCOBEDO, F. A. AND PABLO, J. J. D. [96]. Chemical potential and dimensions of chain molecules in athermal environments. *Molec. Phys.*, **89**(6), 1733 (1996).
- EVANS, D. J. AND MORRISS, G. P. [90]. *Statistical mechanics of nonequilibrium liquids*, pages 105–111. Academic Press, San Diego.
- FRENKEL, D. [96]. *Understanding molecular simulations: From algorithms to applications*. Academic Press, San Diego, 1996.
- FRENKEL, D. AND LOUIS, A. A. [92]. Phase separation in binary hard-core mixtures: an exact result. *Phys. Rev. Lett.*, **68**(22), 3363 (1992).
- FUGUGITA, M., LANCASTER, D., AND MITCHARD, M. G. [92]. Energy level structure of two-dimensional self-interacting random chains. *J. Phys. A*, **25**, L121 (1992).
- GAN, H. H. AND EU, B. C. [98]. Influence of the solvent on the conformation of a chain molecule. *J. Chem. Phys.*, **109**(5), 2011 (1998).
- GANAZZOLI, F., FERLA, R. L., AND ALLEGRA, G. [95]. Kinetics of contraction of a stiff chain. *Macromolecules*, **28**, 5285 (1995).
- GO, N. AND ABE, H. [81]. *Biopolymers*, **20**, 991 (1981).

- GOLDENFELD, N. [92]. *Lectures on phase transitions and the renormalization group.* Frontier in Physics. Addison-Wesley Publishing Company, Reading, Massachusetts, 1992.
- GRAYCE, C. J. [97]. The conformation of hard-sphere polymers in hard-sphere solution calculated by single-chain simulation in a many-body solvent influence functional. *J. Chem. Phys.*, **106**(12), 5171 (1997).
- GREST, G. S. AND MURAT, M. [93]. Structure of grafted polymeric brushes in solvents of varying quality: a molecular dynamics study. *Macromolecules*, **26**, 3108 (1993).
- GREST, G. S. AND MURAT, M. [95]. Computer simulations of tethered membranes. In Binder, K., editor, *Monte Carlo and molecular dynamics in polymer science*. Oxford University Press, Oxford.
- GROSBERG, A. Y. AND KHOKHLOV, A. R. [94]. AIP Series in Polymers and Complex Materials. AIP Press, New York, 1994.
- GROSBERG, A. Y., NECHAEV, S. K., AND SHAKHNOVICH, E. I. [88]. The role of topological constraints in the kinetics of collapse of macromolecules. *J. Phys.-Paris (Lettre)*, **49**, 2095 (1988).
- HAILE, J. M. [92]. *Molecular dynamics simulation: Elementary methods*. Wiley-Interscience, New York, 1992.
- HALPERIN, A. AND GOLDBART, P. M. [00]. Early stages of homopolymer collapse. *Phys. Rev. E*, **61**(1), 565 (2000).
- HONEYCUTT, J. AND THIRUMALAI, D. [90]. Metastability of the folded state of globular proteins. *Proc. Natl. Acad. Sci. USA*, **87**, 3526 (1990).
- HONEYCUTT, J. AND THIRUMALAI, D. [92]. The nature of folded states of globular proteins. *Biopolymers*, **32**, 695 (1992).
- HOOVER, W. G. [85]. Canonical dynamics: Equilibrium phase-space distributions. *Phys. Rev. A*, **31**(3), 1695 (1985).
- IBEN, I., BRAUNSTEIN, D., DOSTER, W., FRAUENFELDER, H., HONG, M. K., JOHNSON, J. B., LUCK, S., ORMOS, P., SCHULTE, A., BRAUNSTEIN, D., XIE, A. H., AND

- YOUNG, R. D. [89]. Glassy behavior of a protein. *Phys. Rev. Lett.*, **62**, 1916 (1989).
- IORI, G., MARINARI, E., AND PARISI, G. [91]. Random self-interacting chains: a mechanism for protein folding. *J. Phys. A*, **24**, 5349 (1991).
- IORI, G., MARINARI, E., PARISI, G., AND STRUGLIA, M. V. [92]. Statistical mechanics of heteropolymer folding. *Physica*, **185A**, 98 (1992).
- KHALATUR, P. G., ZHERENKOVA, L. V., AND KHOKHLOV, A. R. [98]. Entropy-driven polymer collapse: application of the hybrid mc/rism method to the study of conformational transitions in macromolecules interacting with hard colloidal particles. *Eur. Phys. J. B*, **5**(4), 881 (1998).
- KHOKHLOV, A. R. AND KHALATUR, P. G. [98]. Protein-like copolymers: computer simulation. *Physica A*, **249**(1-4), 253 (1998).
- KHOKHLOV, A. R. AND KHALATUR, P. G. [99]. Conformation-dependent sequence design (engineering) of ab copolymers. *Phys. Rev. Lett.*, **82**(17), 3456 (1999).
- KIERNAN, A. B. P., GREEN, D., AND DAWSON, K. A. [95]. Kinetics of homopolymer collapse. *J. Chem. Phys.*, **102**(1), 573 (1995).
- KONG, Y., MANKE, C. W., MADDEN, W. G., AND SCHLIJPER, A. G. [97]. Effect of solvent quality on the conformation and relaxation of polymers via dissipative particle dynamics. *J. Chem. Phys.*, **106**(2), 592 (1997).
- KUZNETSOV, Y. A., TIMOSHENKO, E. G., AND DAWSON, K. A. [96a]. Equilibrium and kinetic phenomena in a stiff homopolymer and possible applications to *dna*. *J. Chem. Phys.*, **105**(16), 7116 (1996).
- KUZNETSOV, Y. A., TIMOSHENKO, E. G., AND DAWSON, K. A. [96b]. Kinetic law at the collapse transition of a homopolymer. *J. Chem. Phys.*, **104**(9), 3338 (1996).
- LAI, P.-Y. [95]. Relaxation time spectrum in glassy states. *Chinese J. Phys.*, **33**(3), 271 (1995).
- LAMPORT, L. [94]. *TEX*. Addison-Wesley Publishing Company, Reading, Massachusetts, second edition, 1994.

- LARADJI, M., GUO, H., AND ZUCKERMANN, M. [94]. Off-lattice monte carlo simulation of polymer brushes in good solvents. *Phys. Rev. E*, **49**, 3199 (1994).
- LEVINTHAL, C. [68]. Are there pathways for protein folding? *J. Chim. Phys.*, **65**, 44 (1968).
- LI, H., HELLING, R., TANG, C., AND WINGREEN, N. [96]. Emergence of preferred structures in a simple model of protein folding. *Science*, **273**, 666 (1996).
- LI, H., TANG, C., AND WINGREEN, N. [97]. Nature of driving force for protein folding: a result from analyzing the statistical potential. *Phys. Rev. Lett.*, **79**, 765 (1997).
- LUNA-BÁRCENA, G., BENNETT, G. E., SANCHEZ, I. C., AND JOHNSTON, K. P. [96]. Monte carlo simulation of polymer chain collapse in athermal solvents. *J. Chem. Phys.*, **104**(24), 9971 (1996).
- LUNA-BÁRCENA, G., MEREDITH, J. C., SANCHEZ, I. C., AND JOHNSTON, K. P. [97]. Relationship between polymer chain conformation and phase boundaries in a supercritical fluid. *J. Chem. Phys.*, **107**(24), 10782 (1997).
- MAKHATADZE, G. AND PRIVALOV, P. [96]. Thermodynamic properties of proteins. In Mark, J. E., editor, *Physical properties of polymers handbook*, chapter 8. AIP Press, New York.
- MALEVANETS, A. AND YEOMANS, J. M. [00]. Dynamics of short polymer chains in solution. *Europhys. Lett.*, **52**(2), 231 (2000).
- MARTYNA, G. J., KLEIN, M. L., AND TUCKERMAN, M. [92]. Nosé-hoover chains: The canonical ensemble via continuous dynamics. *J. Chem. Phys.*, **97**, 2635 (1992).
- MARTYNA, G. J., TUCKERMAN, M. E., TOBIAS, D. J., AND KLEIN, M. L. [96]. Explicit reversible integrators for extended systems dynamics. *Molec. Phys.*, **87**(5), 1117 (1996).
- MÉLIN, R., LI, H., WINGREEN, N., AND TANG, C. [99]. Designability, thermodynamic stability, and dynamics in protein folding: A lattice model study. *J. Chem. Phys.*, **110**, 1252 (1999).
- MIAO, L., GUO, H., AND ZUCKERMANN, M. [96]. Conformation of polymer brushes under shear: chain tilting and stretching. *Macromolecules*, **29**, 2289 (1996).

- MIYAZAWA, S. AND JERNIGAN, R. L. [85]. Estimation of effective interresidue contact energies from protein crystal structures: Chemical approximation. *Macromolecules*, **18**, 534 (1985).
- MONOD, J. [71]. *Chance and Necessity: an Essay on the Natural Philosophy of Modern Biology*. Knopf, New York, first american ed. edition, 1971.
- NAKATA, M. AND NAKAGAWA, T. [97]. Coil-globule transition of poly(methyl methacrylate) in isoamyl acetate. *Phys. Rev. E*, **56**, 3338 (1997).
- NOSÉ, S. [84]. A unified formulation of the constant temperature molecular dynamics method. *J. Chem. Phys.*, **81**(1), 511 (1984).
- OSTROVSKI, B. AND BAR-YAM, Y. [94]. Irreversible polymer collapse in 2 and 3 dimensions. *Europhys. Lett.*, **25**(6), 409 (1994).
- OSTROVSKI, B. AND BAR-YAM, Y. [95]. Motion of polymer ends in homopolymer and heteropolymer collapse. *Biophys. J.*, **68**, 1694 (1995).
- PANDE, V. S., GROSBERG, A. Y., JOERG, C., AND TANAKA, T. [96]. Is heteropolymer freezing well described by the random energy model? *Phys. Rev. Lett.*, **76**, 3987 (1996).
- PANDE, V. S., GROSBERG, A. Y., AND TANAKA, T. [00]. Heteropolymer freezing and design: Towards physical models of protein folding. *Rev. Mod. Phys.*, **72**(1), 259 (2000).
- PANDE, V. S., GROSBERG, A. Y., TANAKA, T., AND ROKHSAR, D. S. [98]. Pathways for protein folding: is a new view needed? *Curr. Opin. Struct. Biol.*, **8**, 68 (1998).
- PARRINELLO, M. AND RAHMAN, A. [80]. Crystal structure and pair potentials: A molecular-dynamics study. *Phys. Rev. Lett.*, **45**, 1196 (1980).
- PATHRIA, R. K. [72]. *Statistical Mechanics*, volume 45 of *International Series of Monographs on Physics*. Pergamon Press, Oxford, New York, first edition, 1972.
- PIERLEONI, C. AND RYCKAERT, J.-P. [91]. Relaxation of a single chain molecule in good solvent conditions by molecular-dynamics simulation. *Phys. Rev. Lett.*, **66**(23), 2992 (1991).

- PITARD, E. [99]. Influence of hydrodynamics on the dynamics of a homopolymer. *Eur. Phys. J. B*, **7**(4), 665 (1999).
- POLLACK, L., TATE, M. W., FINNEFROCK, A. C., KALIDAS, C., TROTTER, S., DARNTON, N. C., LURIO, L., AUSTIN, R. H., BATT, C. A., GRUNER, S. M., AND MOCHRIE, S. G. J. [01]. Time resolved collapse of a folding protein observed with small angle x-ray scattering. *Phys. Rev. Lett.*, **86**, 4962 (2001).
- POLSON, J. M. [99]. Entropic collapse transition of a polymer in a solvent with a nonadditive potential. *Phys. Rev. E*, **60**(3), 3429 (1999).
- POLSON, J. M. AND ZUCKERMANN, M. J. [00]. Simulation of heteropolymer collapse with an explicit solvent in two dimensions. *J. Chem. Phys.*, **113**(3), 1283 (2000).
- POLSON, J. M. AND ZUCKERMANN, M. J. [01]. Simulation of short-chain polymer collapse with an explicit solvent. preprint.
- PRESS, W. H., TEUKOLSKY, S. A., VETTERING, W. T., AND FLANNERY, B. P. [92]. *Numerical recipes in fortran*. Cambridge University Press, Cambridge, second edition, 1992.
- PTITSYN, O. B. [95]. Molten globule and protein folding. *Adv. Protein Chem.*, **47**, 83 (1995).
- REEVES, H. [93]. *Malicorne: Earthly reflections of an astrophysicist*. Stoddart Publishing Co. Limited, Toronto, 1993.
- REIF, F. [65]. *Statistical and thermal physics*. McGraw-Hill, New York, 1965.
- SALI, A., SHAKHNOVICH, E., AND KARPLUS, M. [94]. How does a protein fold? *Nature*, **359**, 248 (1994).
- SANCHEZ, I. C. [69]. *Statistical properties of some model macromolecules*. PhD thesis, University of Delaware.
- SEARS, F. W. AND SALINGER, G. L. [75]. *Thermodynamics, kinetic theory, and statistical thermodynamics*. Addison-Wesley Publishing Company, Reading, Massachusetts, third edition, 1975.
- SHAKHNOVICH, E., FARZTDINOV, G., GUTIN, A., AND KARPLUS, M. [91]. Protein folding bottlenecks: a lattice monte carlo simulation. *Phys. Rev. Lett.*, **67**, 1665

- (1991).
- SHAKHNOVICH, E. AND GUTIN, A. [90]. Implications of thermodynamics of protein folding for evolution of primary sequences. *Nature*, **346**, 773 (1990).
- SHANNON, S. R. AND CHOY, T. C. [97]. Dynamical scaling anomaly for a two dimensional polymer chain in solution. *Phys. Rev. Lett.*, **79**(8), 1455 (1997).
- SKOROBOGATYY, M., GUO, H., AND ZUCKERMANN, M. J. [97a]. A deterministic approach to the protein design problem. *Macromolecules*, **30**, 3403 (1997).
- SKOROBOGATYY, M., GUO, H., AND ZUCKERMANN, M. J. [97b]. Relaxation in a perfect funnel. *Phys. Rev. E*, **55**, 7354 (1997).
- SLATER, G. [93a]. Introduction aux simulations numériques en physique. In L. Lewis, J. Lopez, G. S. A.-M. S. T., editor, *Simulations numériques en physique*, volume 1, Sherbrooke. Une école d'été du Centre de Recherche en Physique du Solide, Université de Sherbrooke, 1993.
- SLATER, G. [93b]. Marche aléatoire et diffusion; marches aléatoire auto-évitantes (saw) et polymères. In L. Lewis, J. Lopez, G. S. A.-M. S. T., editor, *Simulations numériques en physique*, volume 2, Sherbrooke. Une école d'été du Centre de Recherche en Physique du Solide, Université de Sherbrooke, 1993.
- SMIT, B. [92]. Phase diagram of lennard-jones fluids. *J. Chem. Phys.*, **96**(11), 8639 (1992).
- SOGA, K., GUO, H., AND ZUCKERMANN, M. [96]. Binary polymer brush in a solvent. *Macromolecules*, **29**, 1998 (1996).
- SOGA, K., ZUCKERMANN, M., AND GUO, H. [95]. Polymer brush in a poor solvent. *Europhys. Lett.*, **29**, 531 (1995).
- STEINBACH, P. J. AND BROOKS, B. R. [94]. Protein simulation below the glass-transition temperature: Dependence on cooling protocol. *Chem. Phys. Letters*, **226**, 447 (1994).
- STRUGLIA, M. V. [95]. Conformational properties of random heteropolymers in the folded phase. *J. Phys. A*, **28**, 1469 (1995).

- SUEN, J. K. C., ESCOBEDO, F. A., AND PABLO, J. J. D. [97]. Monte carlo simulation of polymer chain collapse in an athermal solvent. *J. Chem. Phys.*, **106**(3), 1288 (1997).
- TAKAHASHI, T. AND MUNAKATA, T. [97]. Solvent effects on polymer conformation: Density-functional-theory approach. *Phys. Rev. E*, **56**, 4344 (1997).
- TIMOSHENKO, E. G., KUZNETSOV, Y. A., AND DAWSON, K. A. [95]. Kinetics at the collapse transition gaussian self-consistent approach. *J. Chem. Phys.*, **102**(4), 1816 (1995).
- TIMOSHENKO, E. G., KUZNETSOV, Y. A., AND DAWSON, K. A. [96]. Kinetics of a gaussian random copolymer as a prototype for protein folding. *Phys. Rev. E*, **54**, 4071 (1996).
- TIMOSHENKO, E. G., KUZNETSOV, Y. A., AND DAWSON, K. A. [98]. Conformational transitions of heteropolymers in dilute solutions. *Phys. Rev. E*, **57**(6), 6801 (1998).
- TOXVAERD, S. [93]. Molecular dynamics at constant temperature and pressure. *Phys. Rev. E*, **47**, 343 (1993).
- VAN DER SCHOOT, P. [98]. Protein-induced collapse of polymer chains. *Macromolecules*, **31**(14), 4635 (1998).
- VILLENEUVE, C., GUO, H., AND ZUCKERMANN, M. J. [97]. Relaxational dynamics of a random heteropolymer. *Macromolecules*, **30**, 3066 (1997).
- WITTEN, T. A. AND SCHAFER, L. [78]. Two critical ratios in polymer solutions. *J. Phys. A*, **11**, 1843 (1978).
- WOLFRAM, S. [91]. *Mathematica*. Addison-Wesley Publishing Company, Redwood City, California, second edition, 1991.
- WOLYNES, P., ONUCHIC, J., AND THIRUMALAI, D. [95]. Navigating the folding routes. *Science*, **267**, 1619 (1995).
- WU, C. AND ZHOU, S. [96]. First observation of the molten globule state of a single homopolymer chain. *Phys. Rev. Lett.*, **77**, 3053 (1996).

- XU, P. [96]. Definitions. In Mark, J. E., editor, *Physical properties of polymers handbook*, chapter 51. AIP Press, New York.
- YU, A., KUZNETSOV, Y. A., TIMOSHENKO, E. G., AND DAWSON, K. A. [95]. Kinetics at the collapse transition of homopolymers and random copolymers. *J. Chem. Phys.*, **103**(11), 4807 (1995).
- ZHOU, Y., KARPLUS, M., WICHERT, J. M., AND HALL, C. K. [97]. Equilibrium thermodynamics of homopolymers and clusters: Molecular dynamics and monte carlo simulations of systems with square-well interactions. *J. Chem. Phys.*, **107**, 10691 (1997).
- ZWANZIG, R. [95]. Simple model of protein folding kinetics. *Proc. Natl. Acad. Sci. USA*, **92**, 9801 (1995).